HiSIM 2.8.0 User's Manual

Copyright © 2014
Hiroshima University & STARC
All Rights Reserved

HiSIM 2.8.0 Copyright © 2014 Hiroshima University & STARC

HiSIM28 Developers

Hiroshima University:

M. Miura-Mattausch, H. Kikuchihara, T. Umeda, H. Miyamoto, T. Iizuka, M. Miyake,
U. Feldmann, H. J. Mattausch

Acknowledgement:

CMC HiSIM Subcommittee chair (S. Kumashiro) and members

HiSIM2 Developers of Previous Versions

Hiroshima University:

D. Navarro, N. Sadachika, M. Miyake, M. Yokomichi, A. Yumisaki, A. Oohashi
T. Minami, T. Kajiwara, M. Ando
T. Yoshida, T. Warabino, Y. Mizukane, Y. Takeda, G. Suzuki, N. Nakayama
S. Hosokawa, T. Mizoguchi, O. Matsushima, S. Jinbou, S. Chiba, K. Konno, K. Machida
H. Ueno, K. Matsumoto, T. Ezaki, H. Kikuchihara, U. Feldmann, H. J. Mattausch,
M. Miura-Mattausch

Semiconductor Technology Academic Research Center:

T. Ohguro, T. Iizuka, M. Taguchi, S. Kumashiro, S. Miyamoto, R. Inagaki
S. Hazama, Y. Furui, N. Fudanuki, G. Yokomizo

HiSIM1 Developers

Hiroshima University:

M. Miura-Mattausch, H. Ueno, H. J. Mattausch, K. Hisamitsu, H. Kawano
D. Kitamaru, T. Honda, S. Matsumoto, S. Mitani, D. Miyawaki, H. Nagakura, S. Nara
D. Navarro, M. Nishizawa, T. Okagaki, S. Ohshiro, Y. Shiraga, K. Suematsu
M. Suetake, M. Tanaka, Y. Tatsumi, T. Yamaoka

Semiconductor Technology Academic Research Center:

S. Kumashiro, T. Yamaguchi, K. Yamashita, N. Nakayama, S. Itoh, K. Morikawa

revision : HiSIM 2.80

date : 2014.6.5

Contents

1 Physical Constants Used

Physical constants used in HiSIM2 and their values are summarized in Table 1.

Table 1: Physical constants used in HiSIM2 and their values.

q	elementary charge	1.60218 $\times 10^{-19}$ C
k	Boltzmann constant	1.38066 $\times 10^{-23}$ J/K
ϵ_{Si}	permittivity in silicon	8.85418 $\times 11.9 \times 10^{-14}$ F/cm
ϵ_{ox}	permittivity in oxide	8.85418 $\times 3.9 \times 10^{-14}$ F/cm

2 Model Concept

HiSIM (Hiroshima-university STARC IGFET Model) is the first complete surface-potential-based MOSFET model for circuit simulation based on the drift-diffusion approximation, which was originally developed by Pao and Sah [1]. The most important advantage of the surface-potential-based modeling is the unified description of device characteristics for all bias conditions. The physical reliability of the drift-diffusion approximation has been proved by 2D device simulations with channel lengths even down to below 0.1μm [2]. To obtain analytical solutions for describing device performances, the charge sheet approximation of the inversion layer with zero thickness has been introduced (for example [3]). Together with the gradual-channel approximation all device characteristics are then described analytically by the channel-surface potentials at the source side (ϕ_{S0}) and at the drain side (ϕ_{SL}) (see Fig. 1). These surface potentials are functions of applied voltages on the four MOSFET terminals; the gate voltage V_{g}, the drain voltage V_{d}, the bulk voltage V_{b} and the reference potential of the source V_{s}. This is the long-channel basis of the HiSIM model, and extensions of the model approximations are done for advanced technologies [4]. All newly appearing phenomena such as short-channel and reverse-short-channel effects are included in the surface potential calculations causing modifications resulting from the features of these advanced technologies [5].
Since the surface potentials are implicit functions of the applied voltages, model-internal iteration procedures are introduced in addition to the global iteration of the circuit simulator. By choosing the iterative solution, we preserve the MOSFET physics, which is built into the set of implicit functions. Such an iterative solution is commonly believed to result in an execution time penalty for the model. Therefore, specific attention is directed towards calculating the surface potentials with enough accuracy even with small CPU run-time. The number of HiSIM-internal iteration steps could be reduced in average to two steps. Up to now validity of HiSIM has been tested for channel lengths down to $45nm$ with CMOS fabrication technologies using the pocket-implant technology. Though all descriptions in this manual are given for the n-channel MOSFET, they are also valid for the p-channel case.

The focus of this manual is a description of the bulk MOSFET model HiSIM2 for model users. Extensions of the described concepts and model equations of HiSIM2 are applied for HiSIM-SOI, HiSIM_HV and HiSIM-DG, which are the compact models for SOI-MOSFETs, LDMOS/HV-MOSFETs and Double-Gate

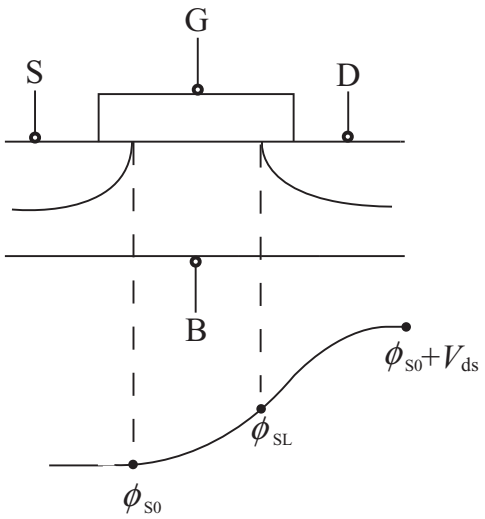

Fig. 1: Schematic of the surface potential distribution in the channel.

MOSFETs in the HiSIM series of compact models for circuit simulation.

3 Definition of Device Size

The effective channel length $L_{\rm eff}$ and width $W_{\rm eff}$ are calculated from the gate length $L_{\rm gate}$ and width $W_{\rm gate}$, where $L_{\rm gate}$ and width $W_{\rm gate}$ deviate from the gate drawn length and width

$$L_{\rm gate} = L_{\rm drawn} + \mathbf{XL} \tag{1}$$

$$W_{\rm gate} = \frac{W_{\rm drawn}}{\mathbf{NF}} + \mathbf{XW} \tag{2}$$

$$L_{\rm poly} = L_{\rm gate} - 2 \cdot \frac{\mathbf{LL}}{(L_{\rm gate} + \mathbf{LLD})^{\mathbf{LLN}}} \tag{3}$$

$$W_{\rm poly} = W_{\rm gate} - 2 \cdot \frac{\mathbf{WL}}{(W_{\rm gate} + \mathbf{WLD})^{\mathbf{WLN}}} \tag{4}$$

$$L_{\rm eff} = L_{\rm poly} - 2 \cdot \mathbf{XLD} \tag{5}$$

$$W_{\rm eff} = W_{\rm poly} - 2 \cdot \mathbf{XWD} \tag{6}$$

where **XL** and **XW** describe the difference between the real and drawn gate length and width, whereas **XLD** and **XWD** account for the overlaps of source/drain contact and the gate oxide as shown in Fig. 2. **LL**, **LLD**, **LLN**, **WL**, **WLD**, and **WLN** are further model parameters for including $L_{\rm gate}$ or $W_{\rm gate}$ dependencies on $L_{\rm eff}$ and $W_{\rm eff}$.

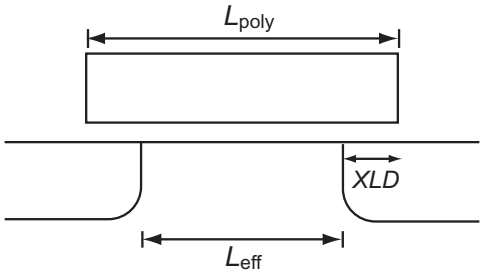

Fig. 2: Cross section of the device.

Table 2: HiSIM model parameters introduced in section 3 of this manual. # indicates an instance parameter.

#NF	number of gate fingers
XL	difference between real and drawn gate length
XW	difference between real and drawn gate width
XLD	gate-overlap in length
XWD	gate-overlap in width
LL	coefficient of gate length modification
LLD	coefficient of gate length modification
LLN	coefficient of gate length modification
WL	coefficient of gate width modification
WLD	coefficient of gate width modification
WLN	coefficient of gate width modification

4 Charges

By applying the Gauss law, the charge density induced in the channel is derived ($Q_{\rm B}$: bulk charge, $Q_{\rm I}$: inversion charge) from the Poisson equation [5]:

$$\begin{aligned} -\left(Q_{\rm b}(y)+Q_{\rm i}(y)\right) &= C_{\rm ox}\left(V'_{\rm G}-\phi_{\rm S}(y)\right) \\ &= \sqrt{\frac{2\epsilon_{\rm Si}qN_{\rm sub}}{\beta}}\Bigg[\exp\left\{-\beta(\phi_{\rm S}(y)-V_{\rm bs})\right\}+\beta(\phi_{\rm S}(y)-V_{\rm bs})-1 \\ &\quad +\frac{n_{\rm p0}}{p_{\rm p0}}\Big\{\exp\big(\beta(\phi_{\rm S}(y)-\phi_{\rm f}(y))\big)-\exp\big(\beta(V_{\rm bs}-\phi_{\rm f}(y))\big)\Big\}\Bigg]^{\frac{1}{2}} \end{aligned} \tag{7}$$

$$C_{\rm ox} = \frac{\epsilon_{\rm ox}}{\mathbf{TOX}} \tag{8}$$

$$V'_{\rm G} = V_{\rm gs}-V_{\rm FB}+\Delta V_{\rm th} \tag{9}$$

$$\beta = \frac{q}{kT} \tag{10}$$

where $V_{\rm FB}$ is the flat-band voltage, **TOX** is the physical gate-oxide thickness, and $\Delta V_{\rm th}$ is the threshold voltage shift in comparison to the threshold voltage of a long-channel transistor (see section 6) [6]. The electron charge is denoted by q, and $\epsilon_{\rm Si}$ and $N_{\rm sub}$ are the silicon permittivity and the substrate impurity concentration, respectively. The Boltzmann constant and the lattice temperature in Kelvin are k and T, respectively. The quasi-Fermi potential $\phi_{\rm f}(y)$ preserves the following relationship:

$$\phi_{\rm f}(L_{\rm eff})-\phi_{\rm f}(0) = V_{\rm ds,eff} \tag{11}$$

$V_{\rm ds,eff}$ is introduced to fit measured transition characteristics of the channel conductance $g_{\rm ds}$ between the linear region and the saturation region to compensate for insufficiencies of the charge-sheet approximation as

$$V_{\rm ds,eff} = \frac{V_{\rm ds}}{\left[1+\left(\frac{V_{\rm ds}}{V_{\rm ds,sat}}\right)^{\Delta}\right]^{\frac{1}{\Delta}}} \tag{12}$$

where

CODDLT=0 :

$$\Delta = \frac{\mathbf{DDLTMAX}\cdot T1}{\mathbf{DDLTMAX}+T1}+1 \tag{13}$$

$$T1 = \mathbf{DDLTSLP}\cdot L_{\rm gate}\cdot 10^6+\mathbf{DDLTICT} \tag{14}$$

CODDLT=1 (defualt) :

$$\Delta = \frac{\mathbf{DDLTMAX}\cdot T1}{\mathbf{DDLTMAX}+T1}+\mathbf{DDLTICT} \tag{15}$$

$$T1 = \mathbf{DDLTSLP}\cdot L_{\rm gate}\cdot 10^6 \tag{16}$$

and $V_{\rm ds,sat}$ is calculated by solving the Poisson equation analytically by neglecting the inversion carrier density [4].

The electron concentration at equilibrium condition $n_{\rm p0}$ is

$$n_{\rm p0} = \frac{n_{\rm i}^2}{p_{\rm p0}} \tag{17}$$

where the intrinsic carrier concentration $n_{\rm i}$ is

$$n_{\rm i} = n_{\rm i0} T^{\frac{3}{2}} \exp\left(-\frac{E_{\rm g}}{2q}\beta\right) \tag{18}$$

$p_{\rm p0}$ is approximated to be $N_{\rm sub}$, and $E_{\rm g}$ describes the temperature dependence of the bandgap (see section 15). The Poisson equation is solved iteratively, where the previous time-step value can be used as the initial value. This is activated by selecting the flag **COPPRV**=1 (default).

Hereafter integrated charges ($Q_{\rm B}$: bulk charge, $Q_{\rm I}$: inversion charge and $Q_{\rm D}$: drain charge) along the channel are considered. Analytical equations for $Q_{\rm B}$ and $Q_{\rm I}$ are derived as a function of $\phi_{\rm S0}$ and $\phi_{\rm SL}$. The final equations for $Q_{\rm B}$, $Q_{\rm I}$, and $Q_{\rm D}$ are given in Eqs. (19)- (21).

$$\begin{aligned}
Q_{\rm B} =& -\frac{\mu(W_{\rm eff}\cdot\mathbf{NF})^2}{I_{\rm ds}}\Bigg[const0\, C_{\rm ox}(V_{\rm G}-V_{\rm FB})\frac{1}{\beta}\frac{2}{3}\Big[\big\{\beta(\phi_{\rm S}-V_{\rm bs})-1\big\}^{\frac{3}{2}}\Big]_{\phi_{\rm S0}}^{\phi_{\rm SL}} \\
&- const0\, C_{\rm ox}\frac{1}{\beta}\frac{2}{3}\Big[\phi_{\rm S}\big\{\beta(\phi_{\rm S}-V_{\rm bs})-1\big\}^{\frac{3}{2}}\Big]_{\phi_{\rm S0}}^{\phi_{\rm SL}} + const0\, C_{\rm ox}\frac{1}{\beta}\frac{2}{3}\frac{1}{\beta}\frac{2}{5}\Big[\big\{\beta(\phi_{\rm S}-V_{\rm bs})-1\big\}^{\frac{5}{2}}\Big]_{\phi_{\rm S0}}^{\phi_{\rm SL}} \\
&- const0^2\frac{1}{\beta}\frac{1}{2}\big[\beta^2(\phi_{\rm SL}-V_{\rm bs})^2-2\beta(\phi_{\rm SL}-V_{\rm bs})+1-\beta^2(\phi_{\rm S0}-V_{\rm bs})^2+2\beta(\phi_{\rm S0}-V_{\rm bs})-1\big]\Bigg] \\
&- \frac{1}{\beta}\frac{\mu(W_{\rm eff}\cdot\mathbf{NF})^2}{I_{\rm ds}}\Big[const0\, C_{\rm ox}\frac{1}{\beta}\frac{2}{3}\big\{\beta(\phi_{\rm S}-V_{\rm bs})-1\big\}^{\frac{3}{2}} + \frac{1}{2}const0^2\beta\phi_{\rm S}\Big]_{\phi_{\rm S0}}^{\phi_{\rm SL}}
\end{aligned} \tag{19}$$

Here $const0$ is defined as

$$const0 = \sqrt{\frac{2\epsilon_{\rm Si} q N_{\rm sub}}{\beta}}$$

while μ and $I_{\rm ds}$ are the carrier mobility and the drain current, respectively [7, 8].

$Q_{\rm I}$ and $Q_{\rm D}$ are written with simple formulas as

$$Q_{\rm I} = -WLC_{\rm ox}(VgVt)\frac{2}{3}\left(\frac{1+\alpha+\alpha^2}{1+\alpha}\right) \tag{20}$$

$$Q_{\rm D} = Q_{\rm I}\left(\frac{3}{5}-\frac{1}{5}\frac{1+2\alpha}{(1+\alpha)(1+\alpha+\alpha^2)}\right) \tag{21}$$

where the surface-potential-based description derives

$$\alpha = 1-\frac{(1+\delta)(\phi_{\rm SL}-\phi_{\rm S0})}{VgVt} \tag{22}$$

$$VgVt = V_{\rm gs}-\left(V_{\rm FB}+\phi_{\rm S0}+\frac{const0}{C_{\rm ox}}BPS0^{\frac{1}{2}}\right) \tag{23}$$

$$\delta = C0Cox\frac{4}{3}\frac{1}{\beta}\frac{(BPSL^{\frac{3}{2}}-BPS0^{\frac{3}{2}})}{(\phi_{\rm SL}-\phi_{\rm S0})} - 2C0Cox\frac{BPS0^{\frac{1}{2}}}{(\phi_{\rm SL}-\phi_{\rm S0})} \tag{24}$$

and

$$\begin{aligned} C0Cox =& \frac{const0}{C_{\rm ox}} \\ BPSL^{\frac{1}{2}} =& \sqrt{\beta(\phi_{\rm SL} - V_{\rm bs}) - 1} \\ BPS0^{\frac{1}{2}} =& \sqrt{\beta(\phi_{\rm S0} - V_{\rm bs}) - 1} \\ BPSL^{\frac{3}{2}} =& (BPSL^{\frac{1}{2}})^3 \\ BPS0^{\frac{3}{2}} =& (BPS0^{\frac{1}{2}})^3 \end{aligned} \tag{25}$$

The HiSIM model parameters introduced in section 4 are summarized in Table 3.

Table 3: HiSIM model parameters introduced in section 4 of this manual. $*$ indicates minor parameters.

TOX	physical gate-oxide thickness
***DDLTMAX**	smoothing coefficient for $V_{\rm ds}$
***DDLTSLP**	$L_{\rm gate}$ dependence of smoothing coefficient
***DDLTICT**	$L_{\rm gate}$ dependence of smoothing coefficient

5 Drain Current

The drift-diffusion approximation describes the drain current $I_{\rm ds}$ as [1]

$$I_{\rm ds} = W_{\rm eff} \cdot \mathbf{NF} \cdot q \cdot \mu \cdot n(y) \cdot \left(-\frac{d\phi_{\rm S}(y)}{dy} + \frac{1}{\beta} \cdot \frac{d \ln n(y)}{dy} \right) \tag{26}$$

where $n(y)$ is the carrier density calculated from the relationship

$$Q_{\rm i}(y) = q \cdot n(y) \; . \tag{27}$$

Under the gradual-channel approximation with further approximations of an idealized gate structure and uniform channel doping, the final equation for $I_{\rm ds}$ is written [3, 5]

$$I_{\rm ds} = \frac{W_{\rm eff} \cdot \mathbf{NF}}{L_{\rm eff}} \cdot \mu \cdot \frac{I_{\rm dd}}{\beta} \tag{28}$$

$$\begin{aligned} I_{\rm dd} = {} & C_{\rm ox}(\beta V'_{\rm G} + 1)(\phi_{\rm SL} - \phi_{\rm S0}) - \frac{\beta}{2} C_{\rm ox}(\phi_{\rm SL}^2 - \phi_{\rm S0}^2) \\ & - \frac{2}{3} const0 \Big[\big\{ \beta(\phi_{\rm SL} - V_{\rm bs}) - 1 \big\}^{\frac{3}{2}} - \big\{ \beta(\phi_{\rm S0} - V_{\rm bs}) - 1 \big\}^{\frac{3}{2}} \Big] \\ & + const0 \Big[\big\{ \beta(\phi_{\rm SL} - V_{\rm bs}) - 1 \big\}^{\frac{1}{2}} - \big\{ \beta(\phi_{\rm S0} - V_{\rm bs}) - 1 \big\}^{\frac{1}{2}} \Big] \end{aligned} \tag{29}$$

The above description includes the further approximation that the mobility μ is independent of position along the channel y. A constant mobility approximation along the channel has been estimated to cause a few % of inaccuracy, which is not severe for the drain current. However, the position dependent mobility has strong influence on phenomena related to distributed effects along the channel. Therefore, the potential distribution along the channel, which is exactly the origin of the position dependence of the mobility, has to be considered to derive analytical equations for phenomena such as noise (see section 21). Here a model parameter **KAPPA** is introduced for $C_{\rm ox} = \epsilon_0 \cdot \mathbf{KAPPA}/\mathbf{TOX}$, where ϵ_0 and **KAPPA** are permittivities in vacuum and in the gate dielectric, respectively. If this is not specified, $\epsilon_{\rm ox} = \epsilon_0 \epsilon_{\rm SiO_2}$ is taken.

By further approximating

$$\phi_{\rm S0} = 2\Phi_{\rm B} \; , \; \Phi_{\rm B} = \frac{2}{\beta} \ln \left(\frac{N_{\rm sub}}{n_{\rm i}} \right) \tag{30}$$

$$\phi_{\rm SL} = 2\Phi_{\rm B} + V_{\rm ds} \tag{31}$$

in Eqs. (28) and (29), the well-known description for the long-channel case [9] is obtained as

$$I_{\rm ds} = \frac{W_{\rm eff} \cdot \mathbf{NF}}{L_{\rm eff}} \mu C_{\rm ox} \left[(V'_{\rm G} - V_{\rm th}) V_{\rm ds} - \left(\frac{1}{2} + \frac{\sqrt{2\epsilon_{\rm Si} q N_{\rm sub}}}{4 C_{\rm ox} \sqrt{2\Phi_{\rm B}}} \right) V_{\rm ds}^2 \right] \tag{32}$$

$$V_{\rm th} = V_{\rm FB} + 2\Phi_{\rm B} + \frac{\sqrt{2\epsilon_{\rm Si} q N_{\rm sub}}}{C_{\rm ox}} \sqrt{2\Phi_{\rm B}} \; . \tag{33}$$

The approximation of Eqs. (30) and (31) for the surface potentials is equivalent to the conventional drift approximation. The models using the drift approximation (e.g. BSIM3 [10] and also BSIM4 [11]) are often called $V_{\rm th}$-based models.

The gradual-channel approximation, being introduced to derive closed-form equations, limits the validity of the model description to the non-saturated condition. As $V_{\rm ds}$ is increased to the saturation condition, the so-called pinch-off region appears at drain side of the channel. However, it is difficult to obtain information about the position where the gradual-channel approximation terminates and where the pinch-off region starts. The $I_{\rm ds}$ equation is extended to include the saturation condition by introducing a steep increase of the surface potential in the pinch-off region, which is mainly controlled by the lateral electric field instead of the vertical one. The modeling details are explained in the channel-length-modulation section (section 11).

The HiSIM model parameters introduced in section 5 are summarized in Table 4.

Table 4: HiSIM model parameters introduced in section 5 of this manual.

KAPPA	dielectric constant of gate dielectric

6 Threshold Voltage Shift

Different from the drift approximation (see for example Eq. (32)), the drift-diffusion approximation does not require a threshold voltage parameter $V_{\rm th}$ for describing device performances. The MOSFET device parameters such as the oxide thickness **TOX** and the substrate doping concentration **NSUBC** determine the complete MOSFET behavior including the subthreshold characteristics automatically and consistently. The measured $V_{\rm th}$ is influenced by various phenomena such as the short-channel effects, which cause a reduction of $V_{\rm th}$ for short-channel transistors in comparison to long-channel transistors as shown in Fig. 3. This so-called $V_{\rm th}$ roll-off is very much dependent on the technology applied for MOSFET fabrication. Therefore, HiSIM can derive many detailed information on the MOSFET fabrication technology, which are relevant for modeling device characteristics, from the $V_{\rm th}$ changes ($\Delta V_{\rm th}$) as a function of gate length ($L_{\rm gate}$). The modeled $\Delta V_{\rm th}$ is incorporated in the $\phi_{\rm S}$ iteration as can be seen in Eq. (9), and can be viewed as consisting of two main effects or components:

(I) the short-channel effect: $\Delta V_{\rm th,SC}$

(II) the reverse-short-channel effect: $\Delta V_{\rm th,R}$ and $\Delta V_{\rm th,P}$

The separation into these two components ($\Delta V_{\rm th} = \Delta V_{\rm th,SC} + \Delta V_{\rm th,R}$ (or $\Delta V_{\rm th,P}$)) is schematically shown in Fig. 3.

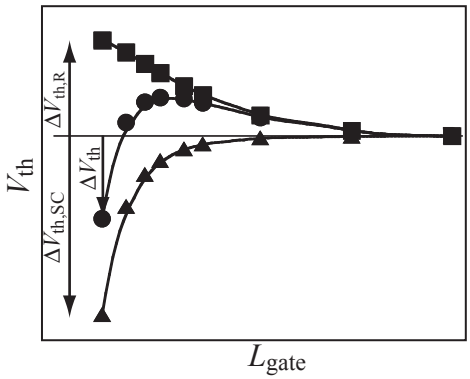

Fig. 3: Schematic plot of the separation of $V_{\rm th}$ into the contributions of the short-channel and the reverse-short-channel effect.

6.1 (I) Short-Channel Effects

As for the short-channel effects four important phenomena are observed: (i) reduction of $V_{\rm th}$ for reduced $L_{\rm gate}$, (ii) $V_{\rm th}$ dependence on $V_{\rm ds}$, (iii) reduction of the body effect, (iv) increase of the subthreshold swing, where (iv) is often not obvious for the normal case of fabrication technologies. Recent advanced technologies utilize aggressive scaling, which induces observable subthreshold degradation. This was modeled with the parameter **PTHROU** up to the HiSIM24 versions. However, the effect is rewritten as puchthrough from the HiSIM250 version. The modeling is described in the next section.

All observed phenomena are caused by the lateral-electric-field contribution in the MOSFET channel, which is important even at threshold condition with small $V_{\rm ds}$. Thus $\Delta V_{\rm th,SC}$ can be written as a function of the lateral electric field E_y by applying the Gauss law. A parabolic potential distribution along the

channel is approximated, which results in a position independent gradient of the lateral electric field $\frac{dE_y}{dy}$ [6]

$$\Delta V_{\mathrm{th,SC}} = \frac{\epsilon_{\mathrm{Si}}}{C_{\mathrm{ox}}} W_{\mathrm{d}} \frac{dE_y}{dy} \tag{34}$$

where W_{d} is the depletion-layer thickness written as

$$W_{\mathrm{d}} = \sqrt{\frac{2\epsilon_{\mathrm{Si}}(2\Phi_{\mathrm{B}} - V_{\mathrm{bs}})}{qN_{\mathrm{sub}}}} \tag{35}$$

$$2\Phi_{\mathrm{B}} = \frac{2}{\beta} \ln\left(\frac{N_{\mathrm{sub}}}{n_{\mathrm{i}}}\right) \tag{36}$$

$\frac{dE_y}{dy}$ is derived with model parameters in the form

$$\begin{aligned}\frac{dE_y}{dy} = \frac{2(\mathbf{VBI} - 2\Phi_{\mathrm{B}})}{(L_{\mathrm{gate}} - \mathbf{PARL2})^2} \Big(& \mathbf{SC1} + \mathbf{SC2} \cdot V_{\mathrm{ds}} + \mathbf{SC3} \cdot \frac{2\Phi_{\mathrm{B}} - V_{\mathrm{bs}}}{L_{\mathrm{gate}}} \\ & + \mathbf{SC4} \cdot V_{\mathrm{ds}} \cdot (2\Phi_{\mathrm{B}} - V_{\mathrm{bs}}) \Big)\end{aligned} \tag{37}$$

VBI and **PARL2** represent the built-in potential and the depletion width of the junction vertical to the channel, respectively. The model parameter **SC1** determines the threshold voltage shift for small V_{ds} and V_{bs}, and is expected to be unity. If measured V_{th} is plotted as a function of V_{ds}, it shows nearly a linear dependence. The gradient is proportional to **SC2**. **SC3** implements a correction of the charge-sheet approximation and is expected to be small. Thus this parameter describes modification of the V_{th} on V_{bs} due to inhomogeneous substrate impurity profile vertical to the channel. It is expected that the impurity concetration converges to a certain value. To consider the impurity-concentration minimum the model parameter **SC3VBS** is introduced, where the value denotes the maximum V_{bs} to be considered. **SC4** is introduced to describe the coupling effect of V_{ds} and V_{bs}.

6.2 (II) Reverse-Short-Channel Effects

The reverse-short-channel effect is categorized into resulting from two physical MOSFET properties:

(i) Impurity concentration inhomogeneity in the direction vertical to the channel (vertical channel inhomogeneity)

(obvious in the retrograded implantation): $\Delta V_{\mathrm{th,R}}$

(ii) Impurity concentration inhomogeneity in the direction parallel to the channel (lateral channel inhomogeneity)

(obvious in the pocket implantation): $\Delta V_{\mathrm{th,P}}$

(i) Impurity concentration inhomogeneity in the direction vertical to the channel (Retrograded Implantation)

The model part described in this subsection is to some extent (i. e. Eq. (40)) not included in HiSIM2, because it is rarely necessary for fitting MOSFET technologies. Furthermore, the above model parameters **SC3** and **SCP3** can be successfully used, if the inhomogeneity is not extremely large.

The substrate impurity pile-up of the retrograded profile at the surface near the source/drain contact is a cause for reverse short channel effects [12]. The impurity profile $N_{\rm sub}(x)$ is modeled by a linear function of the depth x to allow its easy extraction. With the depletion charge $Q_{\rm dep}$, the $V_{\rm th}$ shift in comparison to a long-channel transistor is written [13, 14] as

$$\Delta V_{\rm th,R} = \frac{Q_{\rm dep}}{C_{\rm ox}} - \frac{Q_{\rm dep}({\rm long})}{C_{\rm ox}} \tag{38}$$

$$Q_{\rm dep} = q\int_0^{W_{\rm d}} N_{\rm sub}(x)dx \tag{39}$$

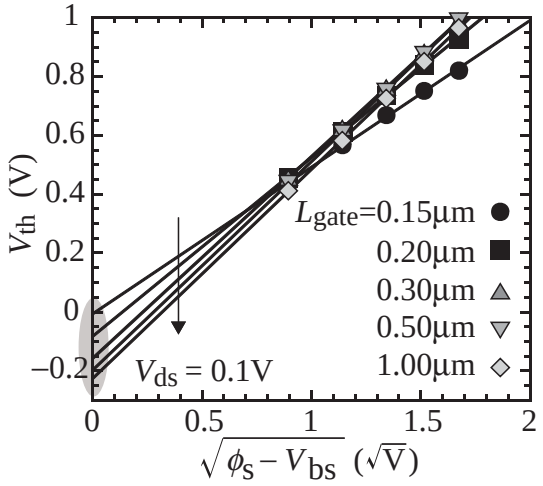

Fig. 4: Simulated $V_{\rm th}$-$\sqrt{\phi_{\rm S} - V_{\rm bs}}$ characteristics. The gradient and the intersect are dependent on the $N_{\rm sub}(x)$ profile.

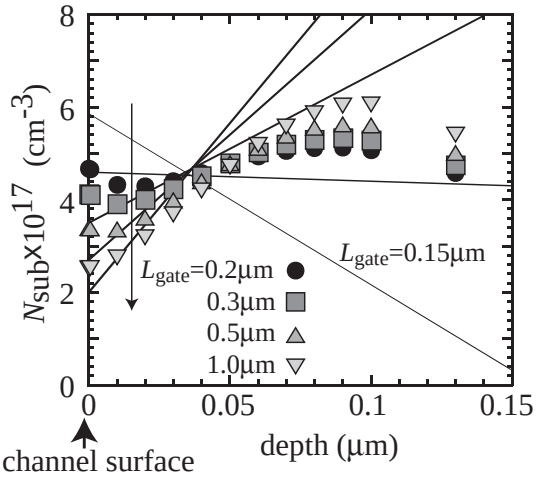

Fig. 5: Symbols are the impurity profiles used for the $V_{\rm th}$ simulation shown in Fig. 4. Lines are extracted profiles.

The impurity profiles are dependent on $L_{\rm gate}$ and are extracted from measured $V_{\rm th}$-$\sqrt{2\Phi_{\rm B} - V_{\rm bs}}$ characteristics as demonstrated in Fig. 4. Here $2\Phi_{\rm B}$ is the surface potential at threshold condition. Since a non-homogeneous impurity profile does not allow to describe $W_{\rm d}$ analytically, Eq. (39) has to be solved numerically. The gradient of $N_{\rm sub}(x)$ and its intersect at $x = 0$ are determined to reproduce measured $V_{\rm th}$-$\sqrt{\phi_{\rm S} - V_{\rm bs}}$ characteristics. Fig. 5 compares the extracted impurity profiles with the 2D process simulation results [15]. Fig. 6 compares simulated and measured $V_{\rm th}$ values as a function of $L_{\rm gate}$. The integrated $Q_{\rm dep}$, represented by a polynomial function of $L_{\rm gate}$, is implemented into the circuit-simulation model to eliminate the integration procedure

$$Q_{\rm dep} = \mathbf{QDEPCC} + \frac{\mathbf{QDEPCL}}{L_{\rm gate}^{\mathbf{QDEPCS}}} + \left(\mathbf{QDEPBC} + \frac{\mathbf{QDEPBL}}{L_{\rm gate}^{\mathbf{QDEPBS}}}\right)\sqrt{2\Phi_{\rm B} - V_{\rm bs}} \tag{40}$$

QDEPCC, **QDEPCL**, **QDEPCS**, **QDEPBC**, **QDEPBL**, and **QDEPBS** are the final model parameters. The impurity concentration used for the surface-potential calculations is the value at the surface, $N_{\rm sub}(0)$. The reason is that the inversion charge density $Q_{\rm i}$, which mostly determines the MOSFET characteristics, extends only in a few nm into the vertical direction.

Although Eq. (40) is not implemented in the present version of HiSIM2, this could be easily done, if the necessity should arise.

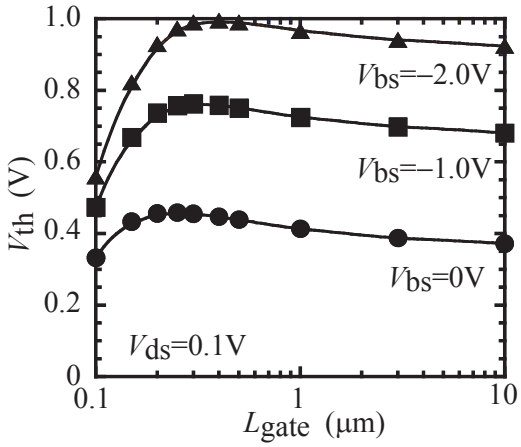

Fig. 6: Comparison of measured $V_{\rm th}$ (solid symbols) with model results (solid lines).

Fig. 7 shows the $V_{\rm th}$ dependence as a function of $\sqrt{2\Phi_{\rm B} - V_{\rm bs}}$ for two different impurity profiles along the vertical direction. For cases where the inhomogeneity is large or where positive $V_{\rm bs}$ is applied, deviation from the linearity of $V_{\rm th}$ as a function of $\sqrt{2\Phi_{\rm B} - V_{\rm bs}}$ is modeled with two fitting parameters **BS1** and **BS2** as

$$Q_{\rm Bmod} = \sqrt{2q \cdot N_{\rm sub} \cdot \epsilon_{Si} \cdot \left(2\Phi_{\rm B} - V_{\rm bs} - \frac{\mathbf{BS1}}{\mathbf{BS2} - V_{\rm bs}}\right)} \tag{41}$$

where **BS1** represents the strength of the deviation and **BS2** is the starting value of $V_{\rm bs}$ where the deviation becomes visible.

(ii) Impurity concentration inhomogeneity in the lateral direction parallel to the channel (Pocket Implantation)

The pocket-implant technology causes an inhomogeneity along the channel. Two obvious features are: (1) the $V_{\rm th}$ increase starts already from relative long $L_{\rm gate}$ and (2) the short-channel effects such as the $V_{\rm ds}$ dependence on $V_{\rm th}$ appear also even for long-channel transistors [16]. This is modeled by developing a new definition for the threshold voltage based on the idea that the threshold condition is determined by the inversion carrier densities in both the non-pocket region and in the pocket region [17] as shown in Fig. 8. The gate voltage inducing a certain amount of total carrier density in the two regions is defined as $V_{\rm th}$. Two model parameters (**LP**: length of the pocket extension into the channel; **NSUBP**: peak of the pocket impurity concentration) are introduced as shown in Fig. 9. The impurity concentration in the substrate is distinguished with **NSUBC** from **NSUBP**. The final model equation requires an iteration procedure for finding the surface potential value, which gives the determined threshold condition.

To eliminate this iteration for model application in circuit simulation, a simplification of the pocket-implantation model is introduced, which nevertheless keeps the key features of the developed concept [18]. The resulting model equations for the $V_{\rm th}$ shift due to the pocket implant are:

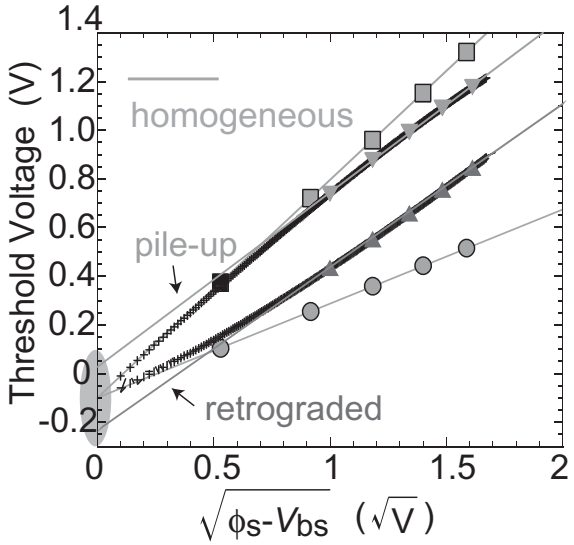

Fig. 7: Threshold voltage as a function of $\sqrt{\phi_{\rm S} - V_{\rm bs}}$ for pile-up and retrograded impurity profiles in the channel, where $\phi_{\rm S}$ is fixed to $2\phi_{\rm B}$. The deviation from linearity for small $V_{\rm bs}$ is modeled with the parameters **BS1** and **BS2**.

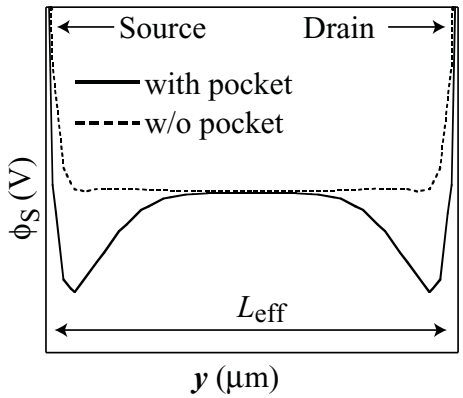

Fig. 8: Surface potential distribution along the channel simulated with a 2D simulator.

$$\Delta V_{\rm th,P} = (V_{\rm th,R} - V_{\rm th0})\frac{\epsilon_{\rm Si}}{C_{\rm ox}} W_{\rm d} \frac{dE_{y,\rm P}}{dy} + dqb \tag{42}$$

$$V_{\rm th,R} = V_{\rm FB} + 2\Phi_{\rm B} + \frac{Q_{\rm B0}}{C_{\rm ox}} + \frac{1}{\beta}\log\left(\frac{N_{\rm subb}}{\mathbf{NSUBC}}\right) \tag{43}$$

$$Q_{\rm B0} = \sqrt{2q \cdot N_{\rm sub} \cdot \epsilon_{Si} \cdot (2\Phi_{\rm B} - V_{\rm bs})} \tag{44}$$

$$V_{\rm th0} = V_{\rm FB} + 2\Phi_{\rm BC} + \frac{\sqrt{2q\mathbf{NSUBC}\epsilon_{\rm Si}(2\Phi_{\rm BC} - V_{\rm bs})}}{C_{\rm ox}} \tag{45}$$

$$\frac{dE_{y,\rm P}}{dy} = \frac{2(\mathbf{VBI} - 2\Phi_{\rm B})}{\mathbf{LP}^2}\left(\mathbf{SCP1} + \mathbf{SCP2} \cdot V_{\rm ds} + \mathbf{SCP3} \cdot \frac{2\Phi_{\rm B} - V_{\rm bs}}{\mathbf{LP}}\right) \tag{46}$$

$$N_{\rm subb} = \begin{cases} 2 \cdot N_{\rm subp} - \frac{(N_{\rm subp} - \mathbf{NSUBC}) \cdot L_{\rm gate}}{\mathbf{LP}} - \mathbf{NSUBC} & (L_{\rm gate} \le 2 \cdot \mathbf{LP}) \\ 0 & (L_{\rm gate} > 2 \cdot \mathbf{LP}) \end{cases} \tag{47}$$

$$dqb = \frac{Q_{\rm B0} - Q_{\rm Bmod}}{C_{\rm ox}} \tag{48}$$

The parameters **SCP1** - **SCP3** describe the short-channel effect caused by the potential minimum at the higher impurity concentration of the pocket. $2\Phi_{\rm BC}$ is the potential giving threshold condition with **NSUBC** and $2\Phi_{\rm B}$ is the equivalent potential with $N_{\rm sub}$

$$\Phi_{\rm BC} = \frac{2}{\beta} \ln\left(\frac{\mathbf{NSUBC}}{n_{\rm i}}\right) \tag{49}$$

$$\Phi_{\rm B} = \frac{2}{\beta} \ln\left(\frac{N_{\rm sub}}{n_{\rm i}}\right) \tag{50}$$

$$N_{\rm sub} = \frac{\mathbf{NSUBC}(L_{\rm gate} - \mathbf{LP}) + \mathbf{NSUBP} \cdot \mathbf{LP}}{L_{\rm gate}} \tag{51}$$

As defined in Eq. (51), $N_{\rm sub}$ is replaced to the averaged impurity concentration in the channel and $N_{\rm subb}$ is introduced, beginning from channel lengths where pockets at source and drain start to overlap.

As $V_{\rm ds}$ approaches zero, the $V_{\rm th}$ dependence on $V_{\rm ds}$ deviates from linearity and $V_{\rm th}$ increases drastically as shown schematically in Fig. 10. This is modeled with two model parameters **SCP21** and **SCP22** as

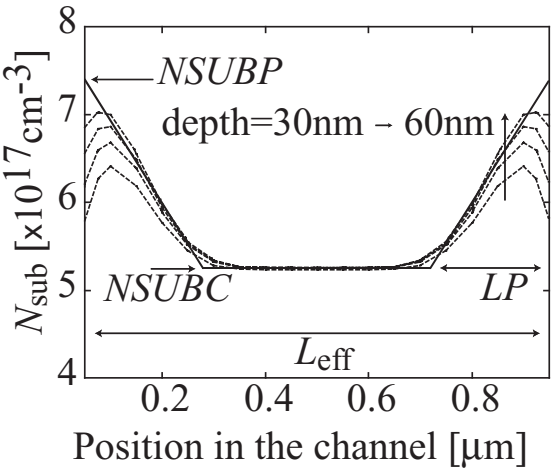

Fig. 9: The dashed curves are simulated impurity profiles by the 2D-process simulator TSUPREM at various depths. The extracted pocket profile with the model is depicted by a solid line.

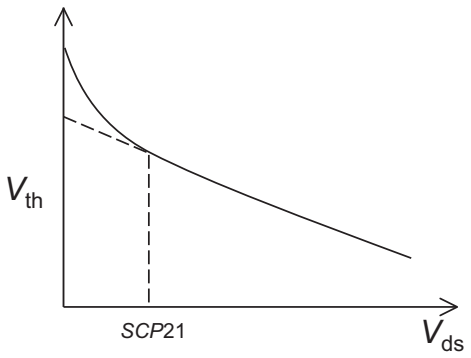

Fig. 10: Threshold voltage as a function of $V_{\rm ds}$. The deviation from linearity for small $V_{\rm ds}$ is modeled with parameters **SCP21** and **SCP22**.

$$\Delta V_{\rm th,P} = \Delta V_{\rm th,P} - \frac{\mathbf{SCP22}}{(\mathbf{SCP21} + V_{\rm ds})^2} \tag{52}$$

where **SCP21** determines the $V_{\rm ds}$ value at which $V_{\rm th}$ starts to deviate from linearity as a function of $V_{\rm ds}$. The parameter **SCP22** determines the gradient of this deviation.

$V_{\rm th,R}$ and $V_{\rm th0}$, defined in Eqs. (43) and (45), are the threshold voltages for the cases with and without pocket-implant, respectively. The overlap start of source and drain pockets causes a steep increase of $V_{\rm th}$ as a function of decreasing $L_{\rm gate}$. This effect enables to extract **LP** from measurements. Fig. 11 compares the $V_{\rm th}$-$L_{\rm gate}$ characteristics of the developed pocket-implant model with and without inclusion of the short-channel effects (SCE). The steep increase at $L_{\rm gate}$=0.1μm in Fig. 11a means the starting of the pocket overlap, where **LP**=0.05μm.

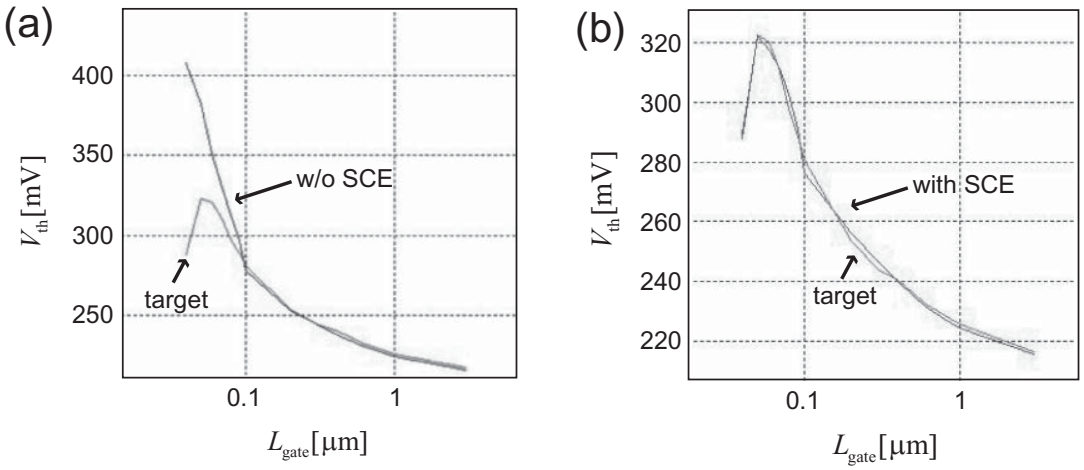

Fig. 11: Comparison of measurements and pocket-implant model for $V_{\rm th}$ as a function of $L_{\rm gate}$. Results (a) with and (b) without short-channel effects (SCE) are shown.

In some cases the pocket profile cannot be described by the single linearly decreasing form, but provides extensive tails as schematically shown in Fig. 12. Therefore, two model parameters **NPEXT** and **LPEXT** are introduced to model the pocket tails as

$$N_{\rm sub} = N_{\rm sub} + \frac{N_{\rm PEXT} - N_{\rm subc}}{\left(\frac{1}{\mathbf{xx}} + \frac{1}{\mathbf{LPEXT}}\right) L_{\rm gate}}$$
$$N_{\rm PEXT} = \mathbf{NPEXT} \tag{53}$$

where

$$\mathbf{xx} = 0.5 \cdot L_{\rm gate} - \mathbf{LP} \ . \tag{54}$$

NPEXT is the maximum concentration of the pocket tail and **LPEXT** describes the tail extension characteristics. Usually strong pocket implantation induces a vertical impurity distribution at the same time. For fitting the measured results in such cases it is recommended to use the parameter **SCP3** together with parameters **BS1** and **BS2**.

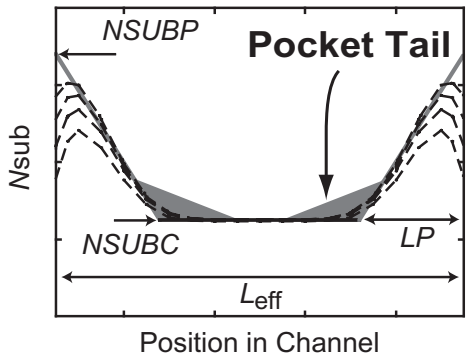

Fig. 12: Modeled pocket tail with **NPEXT** and **LPEXT**.

6.3 CORECIP = 1 for Accurate Reciprocal Capacitance Calculation

The model flag **CORECIP** has been introduced for accurate calculation of the capacitacne reciprocity (**CORECIP**=1: default). If **CORECIP** = 1 is selected, the potential value for describing the short-channel effect is no more pinned to $2\Phi_{\rm B}$ but is treated as bias dependent, namely $\phi_{\rm S}$, for example

$$W_{\rm d} = \sqrt{\frac{2\epsilon_{\rm Si}(2\phi_{\rm S} - V_{\rm bs})}{qN_{\rm sub}}}$$

except $2\Phi_{\rm B}$ in

$$(\mathbf{VBI} - 2\Phi_{\rm B})$$

In this case the $V_{\rm ds}$ dependence is moved to the puchthrough model described in the next section (see section 7). Accordingly, model parameters **SC2**, **SC4**, **SCP2** must be set to zero, and **PT2** and **PT4** must be activated, if it is necessary.

The HiSIM model parameters introduced in section 6 are summarized in Table 5.

Table 5: HiSIM model parameters introduced in section 6 of this manual. $*$ indicates minor parameters, and $**$ indicates a more minor parameter.

VBI	built-in potential
PARL2	depletion width of channel/contact junction
SC1	magnitude of short-channel effect
SC2	$V_{\rm ds}$ dependence of short-channel effect
$*$**SC3**	$V_{\rm bs}$ dependence of short-channel effect
$**$ **SC4**	coupling of $V_{\rm ds}$ and $V_{\rm bs}$ dependence
NSUBC	substrate-impurity concentration
NSUBP	maximum pocket concentration
LP	pocket penetration length
$*$**BS1**	body-coefficient modification due to impurity profile
$*$**BS2**	body-coefficient modification due to impurity profile
SCP1	magnitude of short-channel effect due to pocket
SCP2	$V_{\rm ds}$ dependence of short-channel due to pocket
$*$**SCP3**	$V_{\rm bs}$ dependence of short-channel effect due to pocket
$*$**SCP21**	short-channel-effect modification for small $V_{\rm ds}$
$*$**SCP22**	short-channel-effect modification for small $V_{\rm ds}$
$*$**NPEXT**	maximum concentration of pocket tail
$*$**LPEXT**	extension length of pocket tail
$*$**SC3VBS**	for diminishing of impurity gradient

7 Short-Channel Effects

7.1 Punchthrough Effect

The origin of the punchthrough effect is the bipolar effect through source, substrate, and drain.The effect is described by a power function of the potential difference instead of the exponential function as

$$POTENTIAL = (\mathbf{VBI} - \phi_{\mathrm{S0}})^{\mathbf{PTP}} \tag{55}$$

The final drain current I_{ds} is written

$$\begin{aligned} I_{\mathrm{ds}} &= I_{\mathrm{ds}} + PUNCH \\ PUNCH &= \frac{W_{\mathrm{eff}} \cdot \mathbf{NF}}{L_{\mathrm{eff}}} \frac{\mu}{\beta} \cdot (\phi_{\mathrm{SL}} - \phi_{\mathrm{S0}}) \\ &\quad \left\{ C_{\mathrm{ox}} \cdot \beta \frac{\mathbf{PTL}}{(L_{\mathrm{gate}} \cdot 10^6)^{\mathbf{PTLP}}} \cdot POTENTIAL \cdot \left(1 + \mathbf{PT2} \cdot V_{\mathrm{ds}} + \frac{\mathbf{PT4} \cdot (\phi_{\mathrm{S0}} - V_{\mathrm{bs}})}{(L_{\mathrm{gate}} \cdot 10^6)^{\mathbf{PT4P}}} \right) \right\} \end{aligned} \tag{56}$$

where model parameters $\mathbf{PTL}, \mathbf{PTLP}, \mathbf{PT2}$, $\mathbf{PT4}$, and $\mathbf{PT4P}$ are introduced.

7.2 Channel Conductance

The high field under the saturation condition causes the pinch-off region and the current flows away from the surface. This effect is considered as the lateral-field-induced charge for the capacitacne (see section 17). The simplified formulation is applied to consider the effect as

$$\begin{aligned} I_{\mathrm{ds}} &= I_{\mathrm{ds}} + \frac{W_{\mathrm{eff}} \cdot \mathbf{NF}}{L_{\mathrm{eff}}} \frac{\mu}{\beta} \cdot (\phi_{\mathrm{SL}} - \phi_{\mathrm{S0}}) \cdot CONDUCTANCE \\ CONDUCTANCE &= C_{\mathrm{ox}} \cdot \beta \frac{\mathbf{GDL}}{(L_{\mathrm{gate}} \cdot 10^6 + \mathbf{GDLD} \cdot 10^6)^{\mathbf{GDLP}}} \cdot V_{\mathrm{ds}} \end{aligned} \tag{57}$$

7.3 Pocket-Impurity-Concentration Reduction

If the gate length becomes shorter, the pocket-impurity concentration may become lower than for long channels. This effect is modeled as

$$N_{\mathrm{subp,0}} = \mathbf{NSUBP} \cdot \left(\frac{2 \cdot (1 - \mathbf{NSUBPFAC})}{\mathbf{NSUBPL}} \cdot L_{\mathrm{gate}} \cdot 10^6 + 2 \cdot \mathbf{NSUBPFAC} - 1 \right) \tag{58}$$

where $N_{\mathrm{subp,0}}$ becomes lower than $\mathbf{NSUBP}$ by selecting $0.2 \leq \mathbf{NSUBPFAC} < 1$ and $\mathbf{NSUBPL}$ determines the starting channel length of $N_{\mathrm{subp,0}}$ reduction. To obtain smooth change of $N_{\mathrm{subp,0}}$ as a function of L_{gate} between upper boundary $\mathbf{NSUBP}$ and lower boundary $\mathbf{NSUBPFAC} \cdot \mathbf{NSUBP}$, a smoothing function with the model parameter $\mathbf{NSUBPDLT}$ is introduced, which is usually treated as a fixed value. By selecting $\mathbf{NSUBPDLT}$ small/large, steep/gentle deviation of $N_{\mathrm{subp,0}}$ from $\mathbf{NSUBP}$ at small L_{gate} around $\mathbf{NSUBPL}$ is achieved. $\mathbf{NSUBPFAC} = 1$ refers to a constant $\mathbf{NSUBP}$ independent of L_{gate}.

7.4 Flat-Band Voltage Shift due to Stress

It is known that the stress induced on the gate changes the work function, which causes the flat-band shift. This effect is introduced as

$$V_{\rm fb} = \mathbf{VFBC} \cdot \left(1 + \frac{\mathbf{VFBCL}}{(L_{\rm gate} \cdot 10^6)^{\mathbf{VFBCLP}}}\right) \tag{59}$$

The HiSIM model parameters introduced in section 7 are summarized in Table 6.

Table 6: HiSIM model parameters introduced in section 7 of this manual. $*$ indicates minor parameters.

$*$**PTL**	strength of punchthrough effect
$*$**PTLP**	channel-length dependence of punchthrough effect
$*$**PTP**	strength of punchthrough effect
$*$**PT2**	$V_{\rm ds}$ dependence of punchthrough effect
$*$**PT4**	$V_{\rm bs}$ dependence of punchthrough effect
$*$**PT4P**	$V_{\rm bs}$ dependence of punchthrough effect
$*$**GDL**	strength of high-field effect
$*$**GDLP**	channel-length dependence of high-field effect
$*$**GDLD**	channel-length dependence of high-field effect
$*$**NSUBPL**	starting channel length of **NSUBP** reduction
$*$**NSUBPFAC**	minimun factor of reduction
$*$**NSUBPDLT**	delta for smoothness of the **NSUBPFAC** model
VFBC	flat-band voltage
$*$**VFBCL**	channel length dependence of flat-band voltage
$*$**VFBCLP**	channel length dependence of flat-band voltage

8 Depletion Effect of the Gate Poly-Si

Carrier depletion in the gate poly-Si occurs due to the relatively low impurity concentration of the poly-Si in the region above the gate-oxide. Nevertheless, this concentration is usually much higher than the impurity concentration in the substrate. Therefore, carrier depletion in the poly-Si near the gate-oxide interface starts after the formation of the inversion layer in the substrate as shown in Fig. 13. For modeling the gate poly-Si depletion a physical model parameter, namely the impurity concentration in the gate poly-Si ($N_{\rm pg}$), is introduced. The Poisson equation has to be solved in the substrate and in the gate poly-Si simultaneously by iteration [19], which results in

$$V'_{\rm G} - \phi_{\rm S} - \phi_{\rm Spg} = -\frac{Q_{\rm SP}}{C_{\rm ox}} = \frac{\epsilon_{\rm Si} E_{\rm Si}}{C_{\rm ox}} \tag{60}$$

where $E_{\rm Si}$ is the vertical electric field at the substrate surface. The electric field $E_{\rm pg}$ in the poly-Si at the gate oxide interface is written as

$$E_{\rm pg} = qN_{\rm pg}L_{\rm D,pg}\sqrt{2}\left[\left\{\exp(-\beta\phi_{\rm Spg}) + \beta\phi_{\rm Spg} - 1\right\} + \frac{n_{\rm p0,pg}}{p_{\rm p0,pg}}\left\{\exp(\beta\phi_{\rm Spg}) - \beta\phi_{\rm Spg} - 1\right\}\right]^{\frac{1}{2}} \tag{61}$$

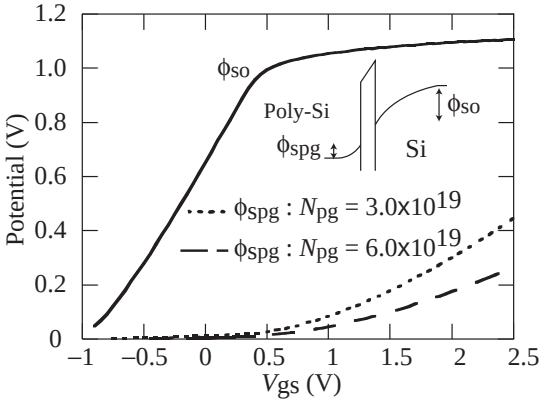

Fig. 13: Simulated surface potential at the source side ($\phi_{\rm S0}$) as a function of $V_{\rm gs}$. The poly-depletion potential is also shown for two doping concentrations $N_{\rm pg}$ in the poly-Si.

where $L_{\rm D,pg}$, $n_{\rm p0,pg}$ and $p_{\rm p0,pg}$ are the Debye length, the intrinsic carrier concentration for electrons and the intrinsic carrier concentration for holes in the poly-Si, respectively. A further reasonable approximation is that $\phi_{\rm Spg}$ never enters the inversion region under normal operation conditions, and thus Eq. (61) can be simplified as

$$E_{\rm pg} = qN_{\rm pg}L_{\rm D,pg}\sqrt{2}(\beta\phi_{\rm Spg} - 1)^{\frac{1}{2}} \tag{62}$$

Eqs. (60) and (62) are solved iteratively under the boundary condition of $E_{\rm Si} = E_{\rm pg}$. Fig. 13 shows calculation results of $\phi_{\rm Spg}$ together with $\phi_{\rm S0}$ as a function of $V_{\rm gs}$.

To eliminate the necessary iteration procedure for the circuit-simulation application, $\phi_{\rm Spg}$ is further approximated as a function of $V_{\rm gs}$ and $V_{\rm ds}$ by the simple formula of Eq. (63), and is included in the $\Delta V_{\rm th}$ calculation as a potential drop of $V_{\rm gs}$.

$$\phi_{\mathrm{Spg}} = \mathbf{PGD1}\left(1 + \frac{1}{L_{\mathrm{gate}} \cdot 10^6}\right)^{\mathbf{PGD4}} \exp\left(\frac{V_{\mathrm{gs}} - \mathbf{PGD2}}{V}\right) \tag{63}$$

where previous versions describe the **PGD4** term with the impurity concentration ratio as

$$\left(\frac{N_{\mathrm{sub}}}{\mathbf{NSUBC}}\right) \tag{64}$$

In Eq. (63), **PGD1** describes the strength of the poly-depletion, **PGD2** represents the threshold voltage of the poly-depletion. The reason for adopting an exponential function for the V_{gs} dependence is the exponential ϕ_{Spg}-V_{gs} characteristic obtained when solving Eqs. (60) and (62) iteratively. It has to be noticed, however, that the function of Eq. (63) has to be smoothed so that ϕ_{Spg} does not exceed ϕ_{S0} for very large V_{gs}. A further parameter **PGD4** has been introduced to represent the channel length dependence of the gate poly-depletion effect. V in the exp term is introduced just to delete dimension. The HiSIM model parameters introduced in section 8 are summarized in Table 7.

Table 7: HiSIM model parameters introduced in section 8 of this manual. $*$ indicates a minor parameter.

PGD1	strength of poly depletion
PGD2	threshold voltage of poly depletion
$*$**PGD4**	L_{gate} dependence of poly depletion

9 Quantum-Mechanical Effects

The main quantum-mechanical phenomenon, which has to be included into a MOSFET model for circuit simulation, is the repulsion of the channel's carrier-density peak into the substrate away from the surface. This can be described phenomenologically by an increased effective oxide thickness $T_{\rm ox}$. Two major approximations are introduced to derive a simple set of equations for $T_{\rm ox}$: First, a triangular potential perpendicular to the channel is approximated and second, carriers are assumed to occupy only the lowest quantized energy level. The resulting effective oxide thickness $T_{\rm ox}$ can be written as [20, 21]

$$\begin{aligned} T_{\rm ox} &= \mathbf{TOX} + \Delta T_{\rm OX} \\ &= \mathbf{TOX} + Q_{\rm ealp}\left(Q_{\rm b} + \frac{11}{32}Q_{\rm i}\right)^{-\frac{1}{3}} \\ Q_{\rm ealp} &= \left(\frac{48\pi m_{\rm e} q}{\epsilon_{\rm Si}\hbar^2}\right)^{-\frac{1}{3}} = 3.5\cdot 10^{-10}[\mathrm{C\,cm}]^{\frac{1}{3}} \end{aligned} \tag{65}$$

The coefficient $Q_{\rm ealp}$, originally calculated quantum mechanically under the above mentioned approximations, is used for fitting purposes. From measured $C_{\rm gate}$-$V_{\rm gs}$ characteristics $Q_{\rm ealp}$ can be extracted (e. g. Fig. 14). The extraction is performed at $V_{\rm ds} = 0$ and results in position independent values for $Q_{\rm b}$ and $Q_{\rm i}$. However, as can be seen from the above $T_{\rm ox}$ in Eq. (65), $Q_{\rm b}$ and $Q_{\rm i}$ are required to calculate $T_{\rm ox}$. On the other hand, the $Q_{\rm b}$ and $Q_{\rm i}$ calculations require the previous knowledge of $T_{\rm ox}$. Therefore, the $T_{\rm ox}$ extraction procedure has to be carried out iteratively. From the iteratively calculated $\Delta T_{\rm ox}$-$V_{\rm gb}$ characteristics, shown in Fig. 15, it is concluded that the $\Delta T_{\rm ox}$ dependence on $V_{\rm gb}$ can be described by the simple equation

$$\Delta T_{\rm ox} = \frac{a}{V_{\rm gb} - V_{\rm th} + b} + c \tag{66}$$

where a, b, and c are fitting parameters and

$$V_{\rm th} = 2\Phi_{\rm B} + V_{\rm FB} + \frac{T_{\rm ox} + \Delta T_{\rm ox}}{\epsilon_{\rm ox}} q N_{\rm sub} W_{\rm d} \tag{67}$$

Here the $V_{\rm th}$ calculation requires again the previous knowledge of $\Delta T_{\rm ox}$. By substituting Eq. (67) into Eq. (66), $\Delta T_{\rm ox}$ is obtained analytically after some simplifications

$$\Delta T_{\rm ox} = \frac{\mathbf{QME1}}{V_{\rm gb} - V_{\rm th}(T_{\rm ox} = \mathbf{TOX}) + \mathbf{QME2}} + \mathbf{QME3} \tag{68}$$

where **QME1**, **QME2**, and **QME3** are the quantum-effect model parameters. A limiting function is introduced in the source code to avoid unreasonable $\Delta T_{\rm ox}$ increase below the threshold voltage. Final equations implemented into HiSIM for the reproduction of quantum mechanical effects are:

$$T_{\rm ox} = \mathbf{TOX} + \Delta T_{\rm ox} \tag{69}$$

The HiSIM model parameters introduced in section 9 are summarized in Table 8.

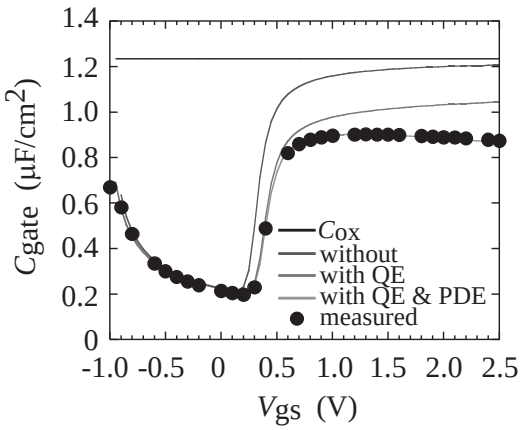

Fig. 14: Comparison of measured C-V characteristics with simulation results for different model complexities with and without quantum effect (QE) or poly-Si depletion effect (PDE).

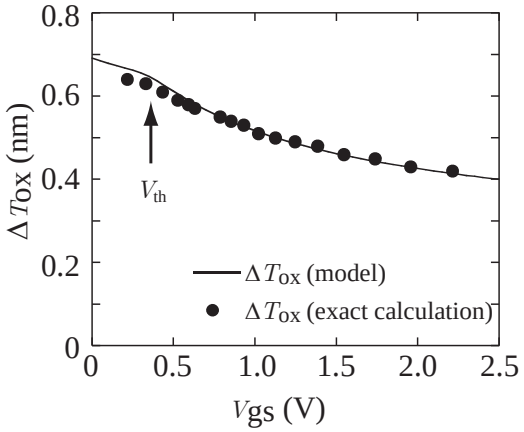

Fig. 15: Calculated $T_{\rm ox}$ increase by the quantum mechanical effect. The solid line shows model results with Eqs. (69). Symbols are exact calculation results by solving the Poisson equation and the Schrödinger equation simultaneously.

Table 8: HiSIM model parameters introduced in section 9 of this manual.

QME1	$V_{\rm gb}$ dependence
QME2	$V_{\rm gb}$ dependence
QME3	minimum $T_{\rm ox}$ modification

10 Mobility Model

The low-field mobility is described with the following expressions and includes the three independent mechanisms of Coulomb, phonon and surface-roughness scattering [22]:

$$\frac{1}{\mu_0} = \frac{1}{\mu_{\rm CB}} + \frac{1}{\mu_{\rm PH}} + \frac{1}{\mu_{\rm SR}} \tag{70}$$

$$\mu_{\rm CB}({\rm Coulomb}) = M_{\rm Coulomb0} + M_{\rm Coulomb1}\frac{Q_{\rm i}}{q\cdot 10^{11}} \tag{71}$$

$$\mu_{\rm PH}({\rm phonon}) = \frac{M_{\rm uephonon}}{E_{\rm eff}^{\mathbf{MUEPH0}}} \tag{72}$$

$$\mu_{\rm SR}({\rm surface\ roughness}) = \frac{\mathbf{MUESR1}}{E_{\rm eff}^{M_{\rm uesurface}}} \tag{73}$$

where $\mu_{\rm PH}$(phonon) is temperature dependent as modeled in section 15.

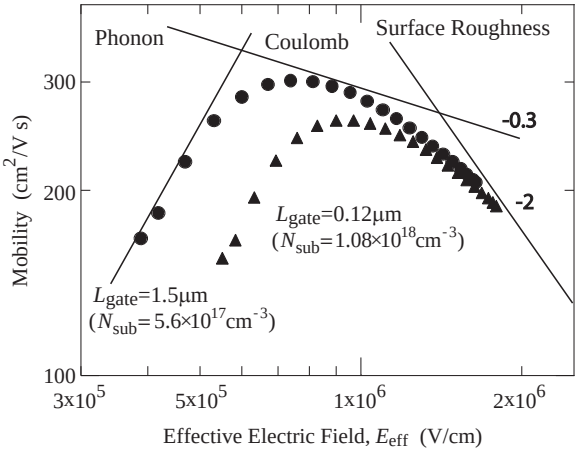

Fig. 16: Calculated mobility as a function of effective field for different MOSFET devices.

Here $E_{\rm eff}$ is the effective field normal to the surface. The field are written as

$$E_{\rm eff} = \frac{1}{\epsilon_{\rm Si}}\left(N_{\rm dep}\cdot Q_{\rm b} + \mathbf{NINV}\cdot Q_{\rm i}\right)\cdot f(\phi_{\rm S}) \tag{74}$$

$$f(\phi_{\rm S}) = \frac{1}{1+(\phi_{\rm SL}-\phi_{\rm S0})\cdot N_{\rm invd}} \tag{75}$$

where $N_{\rm dep}$ and $N_{\rm invd}$ considers the gate length dependence with two model parameters **NDEPL** and **NDEPLP** as

$$N_{\rm dep} = \mathbf{NDEP}\frac{(L_{\rm gate}\cdot 10^6)^{\mathbf{NDEPLP}}}{\mathbf{NDEPL}+(L_{\rm gate}\cdot 10^6)^{\mathbf{NDEPLP}}} \tag{76}$$

$$N_{\rm invd} = \mathbf{NINVD}\left(1+\frac{\mathbf{NINVDL}}{(L_{\rm gate}\cdot 10^6)^{\mathbf{NINVDLP}}}\right) \tag{77}$$

The mobility universality preserves following conditions [23, 24]

$$\mathbf{MUEPH0} \simeq 0.3 \tag{78}$$

$$M_{\mathrm{uesurface}} = 2.0 \tag{79}$$

$$\mathbf{NDEP} = 1.0 \tag{80}$$

$$\mathbf{NINV} = 0.5 \tag{81}$$

independent of technology variations, as illustrated in Fig. 16. However, these parameters can be used for fitting purposes [25], if it is necessary.

The channel length dependence of the screening effect of the Coulomb scattering is introduced as

$$M_{\mathrm{Coulomb0}} = \mathbf{MUECB0} \cdot \left(\frac{L_{\mathrm{gate}} \cdot 10^6}{1\mu m} \right)^{\mathbf{MUECB0LP}} \tag{82}$$

$$M_{\mathrm{Coulomb1}} = \mathbf{MUECB1} \cdot \left(\frac{L_{\mathrm{gate}} \cdot 10^6}{1\mu m} \right)^{\mathbf{MUECB1LP}} \tag{83}$$

Due to the carrier flow at increasing distance from the surface with reducing L_{gate}, the electric field experienced by the carriers is different from the field in the long L_{gate} case. This results in a modification of M_{uephonon}, which is modeled as

$$M_{\mathrm{uephonon}} = \mathbf{MUEPH1} \cdot \left(1 + \frac{\mathbf{MUEPHL}}{(L_{\mathrm{gate}} \cdot 10^6 + \mathbf{MUEPLD} \cdot 10^6)^{\mathbf{MUEPLP}}} \right) \cdot \left(1 + \frac{\mathbf{MUEPHL2}}{(L_{\mathrm{gate}} \cdot 10^6)^{\mathbf{MUEPLP2}}} \right) \tag{84}$$

The surface-roughness coefficient $M_{\mathrm{uesurface}}$ is modeled to have a similar channel length dependence written as

$$M_{\mathrm{uesurface}} = \mathbf{MUESR0} \cdot \left(1 + \frac{\mathbf{MUESRL}}{(L_{\mathrm{gate}} \cdot 10^6)^{\mathbf{MUESLP}}} \right) \tag{85}$$

because the same physical reasoning as for the M_{uephonon} dependence on L_{gate} applies.

The high-field mobility is modeled as [26]

$$\mu = \frac{\mu_0}{\left(1 + \left(\frac{\mu_0 E_{\mathrm{y}}}{V_{\mathrm{max}}} \right)^{\mathbf{BB}} \right)^{\frac{1}{\mathbf{BB}}}} \tag{86}$$

where the maximum velocity V_{max} is temperature dependent modeled, as described in section 15. **BB** is usually fixed to 2 for electrons and 1 for holes, which preserves symmetry for device characteristics at $V_{\mathrm{ds}} = 0$ even for odd numbers different from the argument given in [27]. E_y is derived from calculated ϕ_{S} values. The maximum velocity V_{max} should be the maximum electron-saturation velocity ($\simeq 1 \cdot 10^7 \mathrm{cm/s}$), which is however exceeded at reduced L_{gate}. This phenomenon, called velocity overshoot, is included in the mobility model in the following manner

$$V_{\mathrm{max}} = \mathbf{VMAX} \cdot \left(1 + \frac{\mathbf{VOVER}}{(L_{\mathrm{gate}} \cdot 10^6)^{\mathbf{VOVERP}}} \right) \tag{87}$$

The HiSIM model parameters introduced in section 10 are summarized in Table 9.

Table 9: HiSIM model parameters introduced in section 10 of this manual. ∗ indicates minor parameters. ∗∗ indicates minor parameters for special cases.

MUECB0	Coulomb scattering
MUECB0LP	length dependence of Coulomb scattering
MUECB1	Coulomb scattering
MUECB1LP	length dependence of Coulomb scattering
MUEPH0	phonon scattering
MUEPH1	phonon scattering
∗**MUEPHL**	length dependence of phonon mobility reduction
∗**MUEPLP**	length dependence of phonon mobility reduction
∗**MUEPLD**	length dependence of phonon mobility reduction
∗∗ **MUEPHL2**	length dependence of phonon mobility reduction
∗∗ **MUEPLP2**	length dependence of phonon mobility reduction
MUESR0	surface-roughness scattering
MUESR1	surface-roughness scattering
∗**MUESRL**	length dependence of surface roughness mobility reduction
∗**MUESLP**	length dependence of surface roughness mobility reduction
NDEP	depletion charge contribution on effective-electric field
∗**NDEPL**	modification of $Q_{\rm B}$ contribution for short-channel case
∗**NDEPLP**	modification of $Q_{\rm B}$ contribution for short-channel case
NINV	inversion charge contribution on effective-electric field
∗**NINVD**	reduced resistance effect for small $V_{\rm ds}$
∗**NINVDL**	$L_{\rm gate}$ reduced resistance effect for small $V_{\rm ds}$
∗**NINVDLP**	$L_{\rm gate}$ reduced resistance effect for small $V_{\rm ds}$
BB	high-field-mobility degradation
VMAX	maximum saturation velocity
VOVER	velocity overshoot effect
VOVERP	$L_{\rm eff}$ dependence of velocity overshoot

11 Channel-Length Modulation

The gradual-channel approximation is applied to derive analytical equations for describing device characteristics. However, this approximation is not valid for large $V_{\rm ds}$ causing the pinch-off phenomenon in the channel. Without taking into account the pinch-off phenomenon, the calculated channel conductance $g_{\rm ds}$ enters abruptly into the saturation condition. To include the pinch-off phenomenon in HiSIM, we apply the conventional method of modeling the pinch-off region (ΔL) separately from the rest of the channel as depicted in Fig. 17 [28].

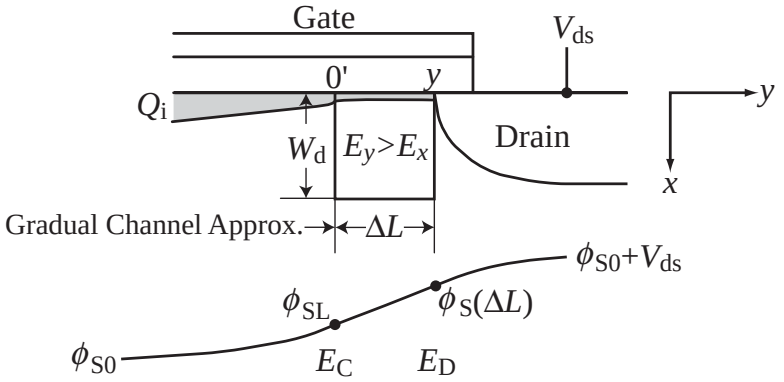

Fig. 17: Schematic showing the correlation among physical quantities in the pinch-off region.

The position $y = 0'$ corresponds to the end point of the gradual-channel approximation, where the surface potential is $\phi_{\rm SL}$. The length from $y = 0'$ to the drain contact is called ΔL. The surface potential at the drain junction is referred to by $\phi_{\rm S}(\Delta L)$. After integrating the Poisson equation in the ΔL region under neglect of the vertical electric field E_x, we obtain [29]

$$\Delta L = \epsilon_{\rm Si} \frac{E_{\rm D} - E_{\rm C}}{qN_{\rm sub} + Q_{\rm i}/W_{\rm d}} \tag{88}$$

where

$$E_{\rm D}^2 = E_{\rm C}^2 + \frac{2qN_{\rm sub}}{\epsilon_{\rm Si}} \left(\phi_{\rm S}(\Delta L) - \phi_{\rm SL}\right) \tag{89}$$

and $E_{\rm C}$ is the electric field at $y = 0'$.

The validity of the gradual-channel approximation at $y = 0'$ is exploited to obtain

$$E_{\rm C} = \frac{I_{\rm dd}}{\beta(L_{\rm eff} - \Delta L)Q_{\rm i}} \tag{90}$$

Though $E_{\rm C}$ is dependent on ΔL, this dependence may be neglected to simplify Eq. (90) as

$$E_{\rm C} = \frac{I_{\rm dd}}{\beta L_{\rm eff} Q_{\rm i}} \tag{91}$$

For simple parameter extraction $Q_{\rm i}$ at the source side is used in (91). The final potential value at the end of the channel ($\phi_{\rm S}(\Delta L)$) lies between $\phi_{\rm SL}$ and $\phi_{\rm S0} + V_{\rm ds}$. The exact value is dependent on the junction

profile between the channel and the drain contact. This dependence is modeled with the parameter **CLM1** as

$$\phi_{\rm S}(\Delta L) = (1 - \mathbf{CLM1}) \cdot \phi_{\rm SL} + \mathbf{CLM1} \cdot (\phi_{\rm S0} + V_{\rm ds}) \tag{92}$$

where **CLM1** can be interpreted to represent the hardness of the junction and must be in the range $0 \leq \mathbf{CLM1} \leq 1$. Here $\mathbf{CLM1} = 1$ means that the contact profile is abrupt and the complete potential increase occurs in the ΔL region, whereas $\mathbf{CLM1} = 0$ corresponds to the opposite condition and there is no potential increase in the ΔL region.

Starting from the HiSIM2.2.0 model version, ΔL is calculated by solving Eqs. (88), (89) and (90), simultaneously. The dependence of E_c on ΔL, which becomes more significant for sub-100nm devices, is consistently included in the calculation. The equation describing ΔL is

$$\Delta L^2 + \frac{1}{L_{eff}}\left(2\frac{I_{\rm dd}}{\beta Q_{\rm i}}z + 2\frac{N_{\rm sub}}{\epsilon_{Si}}(\phi_S(\Delta L) - \phi_{SL})z^2 + E_0 z^2\right)\Delta L - \left(2\frac{N_{\rm sub}}{\epsilon_{Si}}(\phi_S(\Delta L) - \phi_{SL})z^2 + E_0 z^2\right) = 0 \tag{93}$$

by taking into account only up to quadratic terms. The final ΔL is derived as

$$\begin{aligned}\Delta L = \frac{1}{2}\Bigg[&-\frac{1}{L_{eff}}\left(2\frac{I_{\rm dd}}{\beta Q_{\rm i}}z + 2\frac{N_{\rm sub}}{\epsilon_{Si}}(\phi_s(\Delta L) - \phi_{SL})z^2 + E_0 z^2\right) \\ &+ \sqrt{\frac{1}{L_{eff}^2}\left(2\frac{I_{\rm dd}}{\beta Q_{\rm i}}z + 2\frac{N_{\rm sub}}{\epsilon_{Si}}(\phi_s(\Delta L) - \phi_{SL})z^2 + E_0 z^2\right)^2 + 4\left(2\frac{N_{\rm sub}}{\epsilon_{Si}}(\phi_s(\Delta L) - \phi_{SL})z^2 + E_0 z^2\right)}\Bigg]\end{aligned} \tag{94}$$

where E_0 is fixed to 10^5 and

$$z = \frac{\epsilon_{Si}}{\mathbf{CLM2} \cdot Q_b + \mathbf{CLM3} \cdot Q_i} \tag{95}$$

Two model parameters **CLM2** and **CLM3** are introduced to consider the uncertainty of $Q_{\rm i}$ in the pinch-off region and to counterbalance the two contributions from $Q_{\rm b}$ ($= qN_{\rm sub}W_{\rm d}$) and $Q_{\rm i}$. It has to be notified that ΔL is equal to zero, when **CLM1**=0.

Though ΔL is determined mostly by $\phi_{\rm S}(\Delta L)$, the combination between **CLM2** and **CLM3** influences the lateral-field-induced capacitance C_{Q_y} described in section 17.

Occasionally it happens that the channel conductance $g_{\rm ds}$ is not smooth as a function of $V_{\rm ds}$ but shows wiggles. To eliminate the problem smoothing parameter **CLM4** was introduced in the HiSIM2.3.1 version. This is removed in HiSIM2.4.0, and $V_{\rm ds,eff}$ is introduced for the smoothing (see section 4).

For the pocket implantation the lateral field increase is observed even for long-channel transistors. The effect is modeled by the threshold voltage shift. However, the degradation of the channel conductance under the saturation condition is much stronger than that described by the threshold voltage shift alone. This additional pocket effect is modeled as

$$\Delta L = \Delta L \left(1 + \mathbf{CLM6} \cdot (L_{\rm gate} \cdot 10^6)^{\mathbf{CLM5}}\right) \tag{96}$$

It can be happen that $L_{\text{eff}} - \Delta L$ becomes negative, if extracted **CLM5** and **CLM6** values are out of acceptable ranges. In this case HiSIM gives "warning" and fixes $L_{\text{eff}} - \Delta L$ to $1nm$.

The HiSIM model parameters introduced in section 11 are summarized in Table 10.

Table 10: HiSIM model parameters introduced in section 11 of this manual. $*$ indicates minor parameters.

CLM1	hardness coefficient of channel/contact junction
CLM2	coefficient for Q_{B} contribution
CLM3	coefficient for Q_{I} contribution
***CLM4**	no more used
***CLM5**	effect of pocket implantation
***CLM6**	effect of pocket implantation

12 Narrow-Channel Effects

12.1 Threshold Voltage Modification

The shallow-trench-isolation technology induces a $V_{\rm th}$ reduction for reduced channel width ($W_{\rm gate}$). This phenomenon is modeled under inclusion of the edge-fringing capacitances $C_{\rm ef}$ at the edge of the trench [8] as

$$\Delta V_{\rm th,W} = \left(\frac{1}{C_{\rm ox}} - \frac{1}{C_{\rm ox} + 2C_{\rm ef}/(L_{\rm eff} W_{\rm eff})} \right) qN_{\rm sub} W_{\rm d} + \frac{\mathbf{WVTH0}}{W_{\rm gate} \cdot 10^6} \tag{97}$$

where **WVTH0** is the parameter for including the basic width dependence and

$$C_{\rm ef} = \frac{2\epsilon_{\rm ox}}{\pi} L_{\rm eff} \ln \left(\frac{2T_{\rm fox}}{T_{\rm ox}} \right) = \frac{\mathbf{WFC}}{2} L_{\rm eff} \tag{98}$$

Here, $T_{\rm fox}$ is the thickness of the oxide at the trench edge, and **WFC** is the model parameter for including the edge-fringing-capacitance effects. The final $\Delta V_{\rm th}$ of Eq. (9), under inclusion of the shallow-trench-isolation effects, becomes:

$$\Delta V_{\rm th} = \Delta V_{\rm th,SC} + \Delta V_{\rm th,R} + \Delta V_{\rm th,P} + \Delta V_{\rm th,W} - \phi_{\rm Spg} \tag{99}$$

Fig. 18 shows the schematic $V_{\rm th}$ dependence on $W_{\rm gate}$ for two gate lengths, $L_{\rm gate}$. Enhancement of the $V_{\rm th}$ reduction with decreasing $W_{\rm gate}$ is often measured when $L_{\rm gate}$ is also small. This effect becomes obvious for the pocket technology and is modeled by a modification of the pocket impurity concentration as

$$N_{\rm subp,1} = N_{\rm subp,0} \cdot \left(1 + \frac{\mathbf{NSUBPW}}{(W_{\rm gate} \cdot 10^6)^{\mathbf{NSUBPWP}}} \right) \tag{100}$$

The pocket extension includes also the width dependence as

$$N_{\rm pext} = \mathbf{NPEXT} \cdot \left(1 + \frac{\mathbf{NPEXTW}}{(W_{\rm gate} \cdot 10^6)^{\mathbf{NPEXTWP}}} \right) \tag{101}$$

The width dependence of the substrate impurity concentration $N_{\rm SUBC}$ is also considered as

$$N_{\rm subc} = \mathbf{NSUBC} \cdot \left(1 + \frac{\mathbf{NSUBCW}}{(W_{\rm gate} \cdot 10^6)^{\mathbf{NSUBCWP}}} \right) \cdot \left(1 + \frac{\mathbf{NSUBCW2}}{(W_{\rm gate} \cdot 10^6)^{\mathbf{NSUBCWP2}}} \right) \tag{102}$$

$$N_{\rm subc} \leq \mathbf{NSUBCMAX} \tag{103}$$

where **NSUBCMAX** determines the maximum **NSUBC** value.

12.2 Mobility Change

Fig. 19 shows a schematic of the measured saturation current as a function of $W_{\rm gate}$. It is known that the trench isolation induces mechanical stress in the channel, which results in a degradation of the mobility [30], and causes a reduction of $I_{\rm ds,sat}$ with reduced $W_{\rm gate}$ as indicated by curve C1. This effect is modeled by a decreasing phonon mobility with three model parameters **MUEPHW**, **MUEPWP**, and **MUEPWD** as

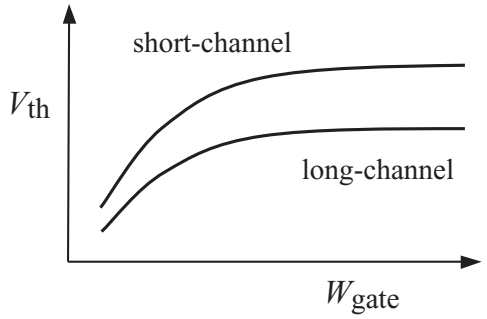

Fig. 18: Schematic of the $V_{\rm th}$ characteristic as a function of the gate width $W_{\rm gate}$ for two different gate lengths, $L_{\rm gate}$.

$$M_{\rm uephonon} = M_{\rm uephonon} \cdot \left(1 + \frac{\mathbf{MUEPHW}}{(W_{\rm gate} \cdot 10^6 + \mathbf{MUEPWP} \cdot 10^6)^{\mathbf{MUEPWP}}}\right) \cdot \left(1 + \frac{\mathbf{MUEPHW2}}{(W_{\rm gate} \cdot 10^6)^{\mathbf{MUEPWP2}}}\right) \tag{104}$$

However, the $I_{\rm ds}$-$W_{\rm gate}$ characteristic does not show monotonous decrease but starts to increase for narrower $W_{\rm gate}$ as denoted by curve C2. This effect is modeled as a change of the surface-roughness contribution caused by a carrier flow in increasing distance from the surface as

$$M_{\rm uesurface} = M_{\rm uesurface} \cdot \left(1 + \frac{\mathbf{MUESRW}}{(W_{\rm gate} \cdot 10^6)^{\mathbf{MUESWP}}}\right) \tag{105}$$

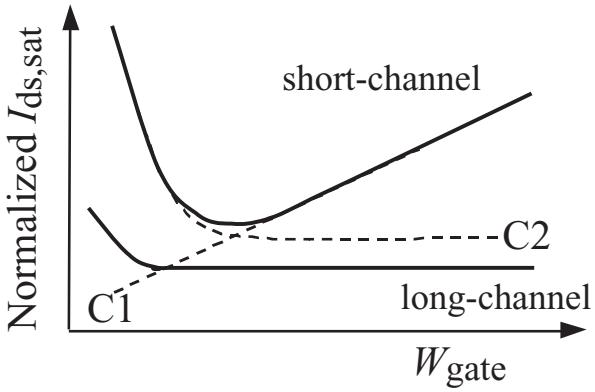

Fig. 19: Schematic of the normalized saturation current $I_{\rm ds,sat}$ as a function of the gate width $W_{\rm gate}$ for two different gate lengths $L_{\rm gate}$.

The universal mobility includes the width dependence as

$$N_{\rm dep} = N_{\rm dep} \frac{(W_{\rm gate} \cdot 10^6)^{\mathbf{NDEPWP}}}{\mathbf{NDEPW} + (W_{\rm gate} \cdot 10^6)^{\mathbf{NDEPWP}}} \tag{106}$$

12.3 Transistor Leakage due to Shallow Trench Isolation (STI): Hump in $I_{\rm ds}$

The shallow trench isolation induces also an undesired hump in the subthreshold region of the $I_{\rm ds}$-$V_{\rm gs}$ characteristics. This is due to an increased electric field at the edge of the trench. At this trench edge

the impurity concentration as well as the oxide thickness are different from the MOSFET middle position along the width direction. Therefore, the surface potential values are expected to be different at the trench edge and are found to cause a $V_{\rm th}$ reduction there. Thus a MOSFET leakage current occurs at these edges, which is smaller than the main MOSFET current, and only important for modeling of the subthreshold characteristics of the MOSFET. The surface potential of the leakage regions at the trench edges can be derived analytically as [31]

$$\phi_{\rm S,STI} = V'_{\rm gs,STI} + \frac{\epsilon_{\rm Si} Q_{\rm N,STI}}{C'^{\,2}_{\rm ox}} \left[1 - \sqrt{1 + \frac{2C'^{\,2}_{\rm ox}}{\epsilon_{\rm Si} Q_{\rm N,STI}} \left(V'_{\rm gs,STI} - V_{\rm bs} - \frac{1}{\beta} \right)} \right] \tag{107}$$

where

$$\begin{aligned} Q_{\rm N,STI} &= q \cdot N_{\rm STI} \\ N_{\rm STI} &= \mathbf{NSTI} \cdot \left(1 + \frac{\mathbf{NSTIL}}{(L_{\rm gate} \cdot 10^6)^{\mathbf{NSTILP}}} \right) \end{aligned}$$

$$V'_{\rm gs,STI} = V_{\rm gs} - V_{\rm FB} + V_{\rm thSTI} + \Delta V_{\rm th,SCSTI} \tag{108}$$

where

$$V_{\rm thSTI} = \mathbf{VTHSTI} - \mathbf{VDSTI} \cdot V_{\rm ds} \tag{109}$$

and

$$\Delta V_{\rm th,SCSTI} = \frac{\epsilon_{\rm Si}}{C_{\rm ox}} W_{\rm d,STI} \frac{dE_y}{dy} \tag{110}$$

The threshold voltage for the STI effect **VTHSTI** describes STI specific features, which are different from the substrate. The depletion-layer thickness $W_{\rm d,STI}$ is written as

$$W_{\rm d,STI} = \sqrt{\frac{2\epsilon_{\rm Si}(2\Phi_{\rm B,STI} - V_{\rm bs})}{qN_{\rm STI}}}. \tag{111}$$

$\dfrac{dE_y}{dy}$ is described with model parameters in the same form as in section 6.1 on short-channel effects

$$\frac{dE_y}{dy} = \frac{2(\mathbf{VBI} - 2\Phi_{\rm B,STI})}{(L_{\rm gate,sm} - \mathbf{PARL2})^2} \left(\mathbf{SCSTI1} + \mathbf{SCSTI2} \cdot V_{\rm ds} \right) \tag{112}$$

where

$$L_{\rm gate,sm} = L_{\rm gate} + \frac{\mathbf{WL1}}{wl^{\mathbf{WL1P}}} \tag{113}$$

$$wl = (W_{\rm gate} \cdot 10^6) \cdot (L_{\rm gate} \cdot 10^6) \tag{114}$$

The model parameter **SCSTI3** is deleted from the HiSIM2.4.0 version.

The modeling of the transistor leakage for STI technologies is based on the idea that the current in the subthreshold region is governed only by the diffusion term. The carrier concentration $Q_{\rm i,STI}$ is

calculated analytically by the Poisson equation in the form shown in Eq. (7) with the substrate-impurity concentration **NSTI** different from **NSUBC** and **NSUBP**. The final leakage current equation is written as

$$I_{\mathrm{ds,STI}} = 2\frac{W_{\mathrm{STI}}}{L_{\mathrm{eff}} - \Delta L}\mu\frac{Q_{\mathrm{i,STI}}}{\beta}\left[1 - \exp(-\beta V_{\mathrm{ds}})\right] \tag{115}$$

where W_{STI} determines the width of the high-field region. The gate length dependence of W_{STI} is included as

$$W_{\mathrm{STI}} = \mathbf{WSTI}\left(1 + \frac{\mathbf{WSTIL}}{(L_{\mathrm{gate,sm}} \cdot 10^6)^{\mathbf{WSTILP}}}\right)\left(1 + \frac{\mathbf{WSTIW}}{(W_{\mathrm{gate}} \cdot 10^6)^{\mathbf{WSTIWP}}}\right) \tag{116}$$

Calculated $I_{\mathrm{ds,STI}}$ is compared in Fig. 20 with measurements.

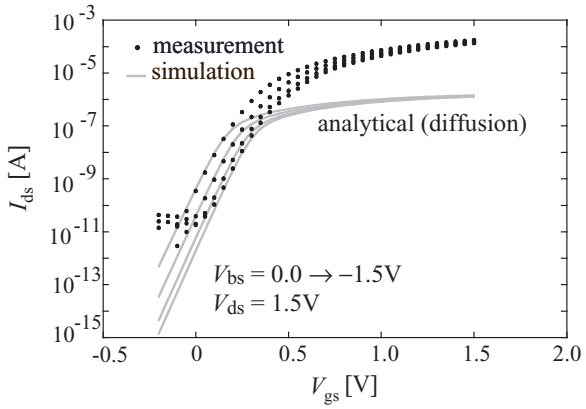

Fig. 20: Comparison of measured I_{ds}-V_{gs} (solid circles) and simulated results (lines). The simulation accounts only for the leakage at the transistor edges.

To consider the current caused by the STI effect, the flag **COISTI** must be set to 1, where the default is set to zero.

12.4 Small Geometry

Small size devices do not show the same scaling characteristic as long-channel or wide-channel devices, but rather deviate significantly. The reason is mainly due to the resolution inaccuracy of the lithography. The small geometry effects are modeled first as the threshold voltage shift

$$\Delta V_{\mathrm{th}} = \Delta V_{\mathrm{th,SC}} + \Delta V_{\mathrm{th,R}} + \Delta V_{\mathrm{th,P}} + \Delta V_{\mathrm{th,W}} + \Delta V_{\mathrm{th,sm}} - \phi_{\mathrm{Spg}} \tag{117}$$

where

$$\Delta V_{\mathrm{th,sm}} = \frac{\mathbf{WL2}}{wl^{\mathbf{WL2P}}} \tag{118}$$

The mobility modification due to the small device geometry is also modeled in the phonon scattering as

$$M_{\mathrm{uephonon}} = M_{\mathrm{uephonon}} \cdot \left(1 + \frac{\mathbf{MUEPHS}}{wl^{\mathbf{MUEPSP}}}\right) \tag{119}$$

$$V_{\max} = V_{\max} \cdot \left(1 + \frac{\mathbf{VOVERS}}{wl^{\mathbf{VOVERSP}}}\right) \tag{120}$$

The HiSIM model parameters introduced in section 12 are summarized in Table 11.

Table 11: HiSIM model parameters introduced in section 12 of this manual. $*$ indicates minor parameters. $**$ indicates minor parameters for special cases.

WFC	threshold voltage change due to capacitance change
$*$**WVTH0**	threshold voltage shift
$*$**NSUBPW**	modification of pocket concentration for narrow width
$*$**NSUBPWP**	modification of pocket concentration for narrow width
$**$ **NSUBCW**	modification of substrate concentration for narrow width
$**$ **NSUBCWP**	modification of substrate concentration for narrow width
$**$ **NSUBCW2**	modification of substrate concentration for narrow width
$**$ **NSUBCWP2**	modification of substrate concentration for narrow width
$**$ **NSUBCMAX**	upper limit of substrate concentration for narrow width
$*$**NPEXTW**	modification of expension concentration for narrow width
$*$**NPEXTWP**	modification of expension concentration for narrow width
$*$**MUEPHW**	phonon related mobility reduction
$*$**MUEPWP**	phonon related mobility reduction
$*$**MUEPWD**	width dependence of phonon mobility reduction
$**$ **MUEPHW2**	phonon related mobility reduction
$**$ **MUEPWP2**	phonon related mobility reduction
$*$**MUESRW**	change of surface roughness related mobility
$*$**MUESWP**	change of surface roughness related mobility
$*$**NDEPW**	modification of expension concentration for narrow width
$*$**NDEPWP**	modification of expension concentration for narrow width
$*$**VTHSTI**	threshold voltage shift due to STI
$*$**VDSTI**	$V_{\rm ds}$ dependence of threshold voltage shift due to STI
$*$**SCSTI1**	the same effect as **SC1** but at STI edge
$*$**SCSTI2**	the same effect as **SC2** but at STI edge
NSTI	substrate-impurity concentration at the STI edge
$**$**NSTIL**	length dependence of STI impurity concentration
$**$**NSTILP**	length dependence of STI impurity concentration
WSTI	width of the high-field region at STI edge
$*$**WSTIL**	channel-length dependence of **WSTI**
$*$**WSTILP**	channel-length dependence of **WSTI**
$*$**WSTIW**	channel-width dependence of **WSTI**
$*$**WSTIWP**	channel-width dependence of **WSTI**
WL1	threshold voltage shift of STI leakage due to small size effect
WL1P	threshold voltage shift of STI leakage due to small size effect
WL2	threshold voltage shift due to small size effect
WL2P	threshold voltage shift due to small size effect
$*$**MUEPHS**	mobility modification due to small size
$*$**MUEPSP**	mobility modification due to small size
$*$**VOVERS**	modification of maximum velocity due to small size
$*$**VOVERSP**	modification of maximum velocity due to small size

13 Well-Proximity Effect

Impurity concentration of the channel region within the well (**NSUBC**, **NSUBP**, **NPEXT**) is dependent on the distance between the well edge and the gate edge. The channel length is also a factor to modify the impurity concentration. This becomes obvious as the distance reduces. To charactersize the layout features, three specific factors are determined by CMC; **SCA**, **SCB**, **SCC** [32]. The use of these factors the well-proximity effect is model as

$$\mathbf{NSUBC} = \mathbf{NSUBC} + \mathbf{NSUBCWPE} \cdot (\mathbf{SCA} + \mathbf{WEB} \cdot \mathbf{SCB} + \mathbf{WEC} \cdot \mathbf{SCC}) \tag{121}$$

$$\mathbf{NSUBP} = \mathbf{NSUBP} + \mathbf{NSUBPWPE} \cdot (\mathbf{SCA} + \mathbf{WEB} \cdot \mathbf{SCB} + \mathbf{WEC} \cdot \mathbf{SCC}) \tag{122}$$

$$\mathbf{NPEXT} = \mathbf{NPEXT} + \mathbf{NPEXTWPE} \cdot (\mathbf{SCA} + \mathbf{WEB} \cdot \mathbf{SCB} + \mathbf{WEC} \cdot \mathbf{SCC}) \tag{123}$$

where **SCA**, **SCB**, and **SCC** are instance parameters determined from the layout, and **NSUBCWPE**, **NSUBPWPE**, **NPEXTWPE**, **WEB**, and **WEC** are model parameters.

The HiSIM model parameters introduced in section 13 are summarized in Table 12.

Table 12: HiSIM model parameters introduced in section 13 of this manual. # indicates instance parameters.

#SCA	layout characterization factor
#SCB	layout characterization factor
#SCC	layout characterization factor
NSUBCWPE	channel concentration change due to WPE
NSUBPWPE	pocket concentration change due to WPE
NPEXTWPE	pocket-tail concentration change due to WPE
WEB	modification of layout characterization factor
WEC	modification of layout characterization factor

14 Effects of the Source/Drain Diffusion Length for Shallow Trench Isolation (STI) Technologies

The diffusion length, $L_{\rm od}$ between MOSFET gate and STI edge affects the MOSFET characteristics. The influence is observed mainly in $V_{\rm th}$ and in the saturation current. The $V_{\rm th}$ change is attributed to a change of the pocket impurity concentration and modeled as

$$N_{\rm substi} = \frac{1 + T1 \cdot T2}{1 + T1 \cdot T3} \tag{124}$$

where

$$\begin{aligned} T1 &= \frac{1}{1 + \mathbf{NSUBCSTI2}} \\ T2 &= \left(\frac{\mathbf{NSUBCSTI1}}{L_{\rm od\_half}} \right)^{\mathbf{NSUBCSTI3}} \\ T3 &= \left(\frac{\mathbf{NSUBCSTI1}}{L_{\rm od\_half\_ref}} \right)^{\mathbf{NSUBCSTI3}} \end{aligned} \tag{125}$$

which is used to modify the pocket concentration $N_{\rm subc}$ as

$$N_{\rm subc} = N_{\rm subc} \cdot N_{\rm substi}. \tag{126}$$

$$N_{\rm substi} = \frac{1 + T1 \cdot T2}{1 + T1 \cdot T3} \tag{127}$$

where

$$\begin{aligned} T1 &= \frac{1}{1 + \mathbf{NSUBPSTI2}} \\ T2 &= \left(\frac{\mathbf{NSUBPSTI1}}{L_{\rm od\_half}} \right)^{\mathbf{NSUBPSTI3}} \\ T3 &= \left(\frac{\mathbf{NSUBPSTI1}}{L_{\rm od\_half\_ref}} \right)^{\mathbf{NSUBPSTI3}} \end{aligned} \tag{128}$$

which is also used to modify the pocket concentration $N_{\rm subp}$ as

$$N_{\rm subp} = N_{\rm subp,1} \cdot N_{\rm substi}. \tag{129}$$

The saturation-current change is attributed to a change of the mobility and modeled as

$$M_{\rm uesti} = \frac{1 + T1 \cdot T2}{1 + T1 \cdot T3} \tag{130}$$

where

$$\begin{aligned} T1 &= \frac{1}{1 + \mathbf{MUESTI2}} \\ T2 &= \left(\frac{\mathbf{MUESTI1}}{L_{\rm od\_half}} \right)^{\mathbf{MUESTI3}} \\ T3 &= \left(\frac{\mathbf{MUESTI1}}{L_{\rm od\_half\_eff}} \right)^{\mathbf{MUESTI3}} \end{aligned} \tag{131}$$

which is used to modify the phonon mobility parameter $M_{\rm uephonon}$ as

$$M_{\rm uephonon} = M_{\rm uephonon} \cdot M_{\rm uesti} \tag{132}$$

where $L_{\rm od\_half}$ and $L_{\rm od\_half\_eff}$ are determined with model parameters **SAREF** and **SBREF** and instance parameters **SA**, **SB**, and **SD** in the same way as BSIM4.6.0 [32] in section 13.1.3 and 13.2

$$L_{\rm od\_half} = 2 \cdot \mathbf{NF} \left\{ \sum_{i=0}^{\mathbf{NF}-1} \frac{1}{SAD} + \sum_{i=0}^{\mathbf{NF}-1} \frac{1}{SBD} \right\}^{-1} \tag{133}$$

$$L_{\rm od\_half\_ref} = 2 \left\{ \frac{1}{\mathbf{SAREF} + 0.5 \cdot L_{\rm drawn}} + \frac{1}{\mathbf{SBREF} + 0.5 \cdot L_{\rm drawn}} \right\}^{-1} \tag{134}$$

$$SAD = \mathbf{SA} + 0.5 \cdot L_{\rm drawn} + i(\mathbf{SD} + L_{\rm drawn}) \tag{135}$$

$$SBD = \mathbf{SB} + 0.5 \cdot L_{\rm drawn} + i(\mathbf{SD} + L_{\rm drawn}) \tag{136}$$

The HiSIM model parameters introduced in section 14 are summarized in Table 13.

Table 13: HiSIM model parameters introduced in section 14 of this manual. # indicates instance parameters.

NSUBCSTI1	channel concentration change due to diffusion-region length between gate and STI
NSUBCSTI2	channel concentration change due to diffusion-region length between gate and STI
NSUBCSTI3	channel concentration change due to diffusion-region length between gate and STI
NSUBPSTI1	pocket concentration change due to diffusion-region length between gate and STI
NSUBPSTI2	pocket concentration change due to diffusion-region length between gate and STI
NSUBPSTI3	pocket concentration change due to diffusion-region length between gate and STI
MUESTI1	mobility change due to diffusion-region length between gate and STI
MUESTI2	mobility change due to diffusion-region length between gate and STI
MUESTI3	mobility change due to diffusion-region length between gate and STI
SAREF	reference length of diffusion between gate and STI
SBREF	reference length of diffusion between gate and STI
#SA	length of diffusion between gate and STI
#SB	length of diffusion between gate and STI
#SD	length of diffusion between gate and gate

15 Temperature Dependence

If **TEMP** is treated as a simulator-option parameter as well as an instance parameter, temperature T is determined as

$$T = \mathbf{TEMP} + DTEMP \tag{137}$$

where $DTEMP$ is the temperature increase by self-heating. $DTEMP$ can also be an instance parameter **DTEMP**. If **TEMP** is treated as an instance parameter, T is determined as

$$T = \mathbf{TEMP} \tag{138}$$

The temperature dependence is included automatically in the surface potentials through β, which is the inverse of the thermal voltage. Additionally the bandgap, the intrinsic carrier concentration, the carrier mobility, and the carrier saturation velocity are also temperature dependent. The temperature dependence of the bandgap determines the temperature dependence of $V_{\rm th}$ [33] and is modeled as

$$E_{\rm g} = E_{\rm g,TNOM} - \mathbf{BGTMP1} \cdot (T - \mathbf{TNOM}) - \mathbf{BGTMP2} \cdot (T^2 - \mathbf{TNOM}^2) \tag{139}$$

where T is the given temperature, and

$$E_{\rm g,TNOM} = \mathbf{EG0} - 90.25 \times 10^{-6} \cdot \mathbf{TNOM} - 1.0 \times 10^{-7} \cdot \mathbf{TNOM}^2 \tag{140}$$

The temperature dependence of the intrinsic carrier concentration is given by

$$n_{\rm i} = n_{\rm i0} \cdot T^{\frac{3}{2}} \cdot \exp\left(-\frac{E_{\rm g}}{2q}\beta\right) \tag{141}$$

The temperature dependence of the mobility and the temperature dependence of the saturation velocity have a major influence on the temperature dependence of the $I_{\rm ds}$-$V_{\rm ds}$ characteristics under the on-current condition. They are modeled as [26]:

$$\mu_{\rm PH}({\rm phonon}) = \frac{M_{\rm uephonon}}{(T/\mathbf{TNOM})^{\mathbf{MUETMP}} \times E_{\rm eff}^{\mathbf{MUEPH0}}} \tag{142}$$

$$V_{\rm max} = \frac{\mathbf{VMAX}}{1.8 + 0.4(T/\mathbf{TNOM}) + 0.1(T/\mathbf{TNOM})^2 - \mathbf{VTMP} \times (1 - T/\mathbf{TNOM})} \tag{143}$$

The temperature dependence of the gate current is modeled by modifying the bandgap specific for the gate current as

$$E_{\rm gp} = E_{\rm g,TNOM} + \mathbf{EGIG} + \mathbf{IGTEMP2}\left(\frac{1}{T} - \frac{1}{\mathbf{TNOM}}\right) + \mathbf{IGTEMP3}\left(\frac{1}{T^2} - \frac{1}{\mathbf{TNOM}^2}\right) \tag{144}$$

Junction Capacitance at Drain Side:

$$C_{\rm J} = \mathbf{CJ} \cdot (1 + \mathbf{TCJBD} \cdot (T - \mathbf{TNOM})) \tag{145}$$

$$C_{\rm JSW} = \mathbf{CJSW} \cdot (1 + \mathbf{TCJBDSW} \cdot (T - \mathbf{TNOM})) \tag{146}$$

$$C_{\rm JSWG} = \mathbf{CJSWG} \cdot (1 + \mathbf{TCJBDSWG} \cdot (T - \mathbf{TNOM})) \tag{147}$$

Junction Capacitance at Source Side:

$$C_{\rm J} = \mathbf{CJ} \cdot (1 + \mathbf{TCJBS} \cdot (T - \mathbf{TNOM})) \tag{148}$$

$$C_{\rm JSW} = \mathbf{CJSW} \cdot (1 + \mathbf{TCJBSSW} \cdot (T - \mathbf{TNOM})) \tag{149}$$

$$C_{\rm JSWG} = \mathbf{CJSWG} \cdot (1 + \mathbf{TCJBSSWG} \cdot (T - \mathbf{TNOM})) \tag{150}$$

The HiSIM model parameters introduced in section 15 are summarized in Table 14.

Table 14: HiSIM model parameters introduced in section 15 of this manual. $*$ indicates minor parameters. # indicates instance parameters.

EG0	bandgap
BGTMP1	temperature dependence of bandgap
BGTMP2	temperature dependence of bandgap
MUETMP	temperature dependence of phonon scattering
TNOM	temperature selected as nominal temperature value
$*$**VTMP**	temperature dependence of saturation velocity
EGIG	bandgap of gate current
IGTEMP2	temperature dependence of gate current
IGTEMP3	temperature dependence of gate current
TCJBD	temperature dependence of drain-side diode capacitance
TCJBDSW	temperature dependence of drain-side diode capacitance
TCJBDSWG	temperature dependence of drain-side diode capacitance
TCJBS	temperature dependence of source-side diode capacitance
TCJBSSW	temperature dependence of source-side diode capacitance
TCJBSSWG	temperature dependence of source-side diode capacitance
TEMP	given temperature
#**TEMP**	given also as an instance parameter
#**DTEMP**	additional temperature increase

16 Resistances

The source and the drain resistances $R_{\rm s}$ and $R_{\rm d}$ are considered by voltage drops on each terminal as:

$$V_{\rm gs,eff} = V_{\rm gs} - I_{\rm ds} \cdot R_{\rm s} \tag{151}$$

$$V_{\rm ds,eff} = V_{\rm ds} - I_{\rm ds} \cdot (R_{\rm s} + R_{\rm d}) \tag{152}$$

$$V_{\rm bs,eff} = V_{\rm bs} - I_{\rm ds} \cdot R_{\rm s} \tag{153}$$

where

$$R_{\rm s} = \frac{\mathbf{RS}}{W_{\rm eff} \cdot \mathbf{NF}} + \mathbf{NRS} \cdot \mathbf{RSH} \tag{154}$$

$$R_{\rm d} = \frac{\mathbf{RD}}{W_{\rm eff} \cdot \mathbf{NF}} + \mathbf{NRD} \cdot \mathbf{RSH} \tag{155}$$

The first terms of the right hand sides consider the resistance in the LDD region and the second terms are the those in the diffusion regions, which are layout dependent. These voltage drops are calculated iteratively for given voltages to keep consistency among all device performances. However, $R_{\rm s}$ and $R_{\rm d}$ can be also treated as extrinsic resistances, and can be included in the equivalent circuit. The flag **COIPREV** is introduced to use the previous time-step solution by setting to 1 (default). The parasitic source and drain resistances, $R_{\rm s}$ and $R_{\rm d}$, can be included by two optional approaches. The first approach is to include them as external resistances of HiSIM, so that the circuit simulator has to find the iterative solution for the source/drain-resistance contributions. The second approach is to include them as internal resistances of HiSIM, so that HiSIM has to solve for the resistance contributions iteratively. The flag **CORSRD** is provided for the selection of one of the possible approaches. **CORSRD** = 0 refers to no contact resistance. **CORSRD** =1, 2, -1 means "internal", "analytical", and "external" source/drain resistances, respectively. **CORSRD** = 0 is the default. **CORSRD**=2 is introduced to avoid simulation time penalty with an analytical description of the resistance effect as

$$I_{\rm ds} = \frac{I_{\rm ds0}}{1 + I_{\rm ds0} \frac{R_{\rm d}}{V_{\rm ds}}} \tag{156}$$

where $I_{\rm ds0}$ is the drain current without the resistance effect.

The approach with external source/drain resistances leads to shorter simulation times for circuits with small to medium transistor numbers, while the approach with internal source/drain resistances leads to shorter simulation times for circuits with very large transistor numbers. The transistor number, for which both approaches result in approximately equal simulation times (the switching point for the choice between the 2 approximations) is normally between 10000 and 50000 transistors.

The gate resistance becomes large as the gate width becomes large, which is the case for RF circuits. The equation for the gate-resistance calculation is taken from BSIM4 [11] description as

$$R_{\rm g} = \frac{\mathbf{RSHG} \cdot \left(\mathbf{XGW} + \frac{W_{\rm eff}}{3 \cdot \mathbf{NGCON}}\right)}{\mathbf{NGCON} \cdot (L_{\rm drawn} - \mathbf{XGL}) \cdot \mathbf{NF}} \tag{157}$$

where **RSHG** is the gate sheet resistance, and others are instance parameters dependent on layout. The flag **CORG** is provided for the inclusion of gate resistance. **CORG** = 0,1 means "no", "external" gate resistance, respectively.

Model parameters for the same substrate resistance network as BSIM4 (treated also as an instance **RBPB**, **RBPD**, **RBPS**, **RBDB**, **RBSB**) are included in the model parameter list.

The HiSIM model parameters introduced in section 16 are summarized in Table 15.

Table 15: HiSIM model parameters introduced in section 16 of this manual. # indicates instance parameters.

RS	source-contact resistance of LDD region
RD	drain-contact resistance of LDD region
RSH	source/drain sheet resistance of diffusion region
RSHG	gate sheet resistance
# **RBPB**	substrate resistance network treated also as an instance p.
# **RBPD**	substrate resistance network treated also as an instance p.
# **RBPS**	substrate resistance network treated also as an instance p.
# **RBDB**	substrate resistance network treated also as an instance p.
# **RBSB**	substrate resistance network treated also as an instance p.
# **NRS**	number of source squares
# **NRD**	number of drain squares
# **XGW**	distance from the gate contact to the channel edge
# **XGL**	offset of the gate length
# **NF**	number of fingers
# **NGCON**	number of gate contacts

17 Capacitances

17.1 Intrinsic Capacitances

The intrinsic capacitances are derivatives of the node charges determined as

$$\begin{aligned} C_{jk} &= \delta \frac{\partial Q_j}{\partial V_k} \\ \delta = -1 \quad &\text{for} \quad j \neq k \\ \delta = \quad 1 \quad &\text{for} \quad j = k \end{aligned} \tag{158}$$

HiSIM uses analytical solutions for all 9 independent intrinsic capacitances, derived from the charges given in Eqs. (19) – (21) as explicit functions of the surface potentials. Therefore, there are no extra model parameters for the intrinsic capacitances.

The lateral electric field along the channel induces a capacitance C_{Q_y} which significantly affects the gate capacitance in saturation [34]. The induced charge associated with C_{Q_y} is described with the surface potential values as

$$Q_y = \epsilon_{\rm Si} W_{\rm eff} \cdot \mathbf{NF} W_{\rm d} \left(\frac{\phi_{\rm S0} + V_{\rm ds} - \phi_{\rm S}(\Delta L)}{\mathbf{XQY}} \right) + \frac{\mathbf{XQY1} \cdot W_{\rm eff} \times 10^6 \cdot \mathbf{NF}}{(L_{\rm gate} \times 10^6)^{\mathbf{XQY2}}} V_{\rm bs} \tag{159}$$

introducing **XQY**, a parameter determining the maximum field at the channel/drain junction independent of $L_{\rm gate}$. To compensate the enhanced short-channel effect, determined by the current characteristics, two model parameters **XQY1** and **XQY2** are introduced.

This charge is added to the drain and the source charges with the partitioning ratio **QYRAT**. Under the saturation condition, C_{Q_y} together with the overlap capacitance dominates the gate-drain capacitance $C_{\rm gd}$. This effect is more visibly observed as the gate-length reduces. Therefore, in the $C_{\rm gd}$ modeling, C_{Q_y} is added to the intrinsic components as depicted in Fig. 21, which has the similar meaning as the so-called inner-fringing field effect conventionally applied [35]. To activate $Q_{\rm y}$ the model parameter **CLM1** must be smaller than unity with the model flag **COQY** = 1.

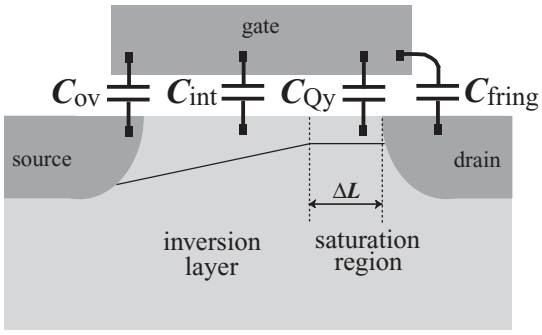

Fig. 21: Modeling of the gate-drain capacitance with C_{Q_y} added to the conventional components.

17.2 Overlap Capacitances

To consider the overlap capacitance the flag **COADOV** must be selected to 1, which is the default. The overlap capacitance includes three options as summarized in Fig. 22, where the drain side and the source side are treated as identical. If Flag **COOVLP**=0, the overlap capacitances are treated to be constant. If **CGSO** and **CGDO** are determined, these values are taken. If they are not determined, the values are calculated with the overlap length and oxide capacitance.

If Flags **COOVLP**=1, the bias dependent overlap capacitances are considered. Here two models are provided: One is the surface-potential-based model and the other describes with a simple $V_{\rm gs}$ dependence. In addition to the bias dependent capacitances, **CGSO** and **CGDO** can be also added, if they are determined.

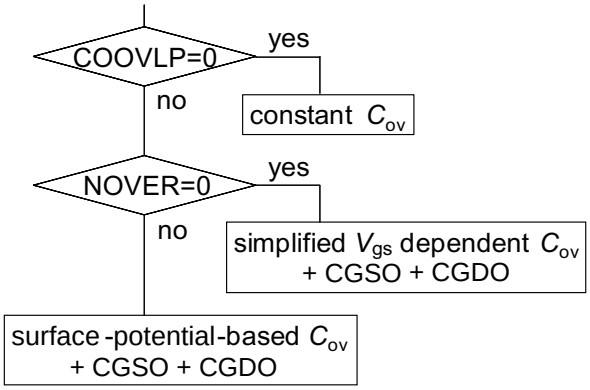

Fig. 22: Model options of the overlap capacitance at the drain side are summarized.

The description is focussed on the drain side. For the source side the same calculation is performed with $V_{\rm ds}$=0.

i) Surface-Potential-Based Model

The surface potential $\phi_{\rm S}$ is calculated in the same manner as in the channel region, and only the polarity is inverted from the channel. The final overlap charge equation is written with the calculated $\phi_{\rm S}$

a) under the depletion and the accumulation conditions

$$Q_{\rm over} = W_{\rm eff} \cdot \mathbf{NF} \cdot \mathbf{LOVER} \left(\sqrt{\frac{2\epsilon_{\rm Si} q \mathbf{NOVER}}{\beta}} \sqrt{\beta(\phi_{\rm S} + V_{\rm ds}) - 1} \right) \tag{160}$$

b) under the inversion condition

$$Q_{\rm over} = W_{\rm eff} \cdot \mathbf{NF} \cdot \mathbf{LOVER} \cdot C_{\rm ox}(V_{\rm gs} - \mathbf{VFBOVER} - \phi_{\rm S}) \tag{161}$$

where **LOVER** is the length of the overlap region of the gate over drain, **NOVER** is the impurity concentration in the drift region, and **VFBOVER** is the flat-band voltage in the overlap region. This model is selected, if **NOVER** is not equal to zero.

Three options are provided to calculate ϕ_s, which is selected by the flag **COQOVSM**:

COQOVSM=0: with an analytical equation excluding inversion charge

COQOVSM=1: with iterative procedure (default)

COQOVSM=2: with an analytical equation including inversion charge

ii) Simplified Bias-Dependent Model

If **NOVER**=0 and **LOVER** > 0 and the flag **COOVLP** $= 1$, the overlap charge is modeled as

$$Q_{\rm god} = W_{\rm eff} \cdot \mathbf{NF} \cdot C_{\rm ox} \left[(V_{\rm gs} - V_{\rm ds}) \mathbf{LOVER} - \mathbf{OVSLP} \cdot (1.2 - (\phi_{\rm SL} - V_{\rm ds})) \cdot (\mathbf{OVMAG} + (V_{\rm gs} - V_{\rm ds})) \right] \tag{162}$$

The overlap capacitance Flags (**COOVLP** $= 0$) calculates bias-independent overlap capacitances. User-defined values can be specified using the input parameters **CGDO** and **CGSO**. If these values are not specified, the overlap capacitances are calculated using

$$C_{\rm ov} = -\frac{\epsilon_{\rm ox}}{\mathbf{TOX}} \mathbf{LOVER} \cdot W_{\rm eff} \cdot \mathbf{NF} \tag{163}$$

The gate-to-bulk overlap capacitance $C_{\rm gbo\_loc}$ is calculated only with a user-defined value **CGBO** using

$$C_{\rm gbo\_loc} = -\mathbf{CGBO} \cdot L_{\rm gate} \tag{164}$$

independent of the model Flag **COOVLP**.

17.3 Extrinsic Capacitances

The outer fringing capacitance is modeled as [36]

$$C_{\rm f} = \frac{\epsilon_{\rm ox}}{\pi/2} W_{\rm gate} \cdot \mathbf{NF} \cdot \ln \left(1 + \frac{\mathbf{TPOLY}}{T_{\rm ox}} \right) \tag{165}$$

where **TPOLY** is the gate-poly thickness. This capacitance is bias independent.

The HiSIM model parameters introduced in section 17 are summarized in Table 16.

Table 16: HiSIM model parameters introduced in section 17 of this manual.

XQY	distance from drain junction to maximum electric field point
***XQY1**	$V_{\rm bs}$ dependence of $Q_{\rm y}$
***XQY2**	$L_{\rm gate}$ dependence of $Q_{\rm y}$
QYRAT	partitioning ratio of $Q_{\rm y}$ between source and drain
LOVER	overlap length
NOVER	impurity concentration in overlap region
VFBOVER	flat-band voltage in overlap region
OVSLP	coefficient for overlap capacitance
OVMAG	coefficient for overlap capacitance
CGSO	gate-to-source overlap capacitance
CGDO	gate-to-drain overlap capacitance
CGBO	gate-to-bulk overlap capacitance
TPOLY	height of the gate poly-Si

18 Leakage Currents

18.1 Substrate Current

The substrate current $I_{\rm sub}$ is generated by impact ionization in the depletion region at the drain junction (see Fig. 23). Thus $I_{\rm sub}$ is represented by

$$I_{\rm sub} = \alpha I_{\rm ds} \delta L \tag{166}$$

where δL is the length where the impact ionization occurs. This δL region is not necessarily restricted to the channel, namely to the same ΔL determined in the channel-length-modulation modeling, but can extend into the drain region. The coefficient α is the ionization coefficient. α is written as a function of the lateral electric field E_y with fitting parameters C_1 and C_2

$$\alpha = C_1 \exp\left(-\frac{C_2}{E_y}\right) \tag{167}$$

Since α is a function of the electric field, and the field is dependent on the position in the pinch-off region, Eq. (166) has to be integrated along the pinch-off region and beyond

$$I_{\rm sub} = \int_0^{\delta L} I_{\rm ds} C_1 \exp\left(-\frac{C_2}{E_y}\right) dy. \tag{168}$$

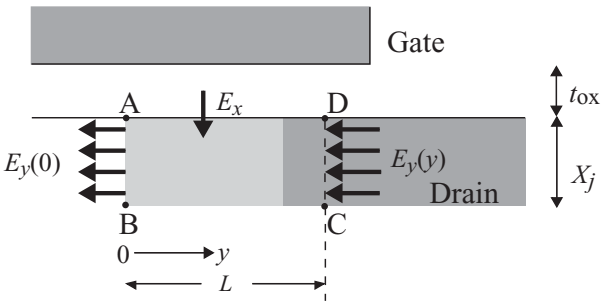

Fig. 23: Schematic of the high field region.

After some simplification we derive the well-known equation [37]

$$I_{\rm sub} = \frac{C_1}{C_2}\big(\phi(y) - \phi(0)\big) I_{\rm ds} \exp\left(-\frac{\lambda C_2}{\phi(y) - \phi(0)}\right) \tag{169}$$

where

$$\lambda^2 = \frac{\epsilon_{\rm Si} X_{\rm j} T_{\rm ox}}{\epsilon_{\rm ox}} \tag{170}$$

and $X_{\rm j}$ is the junction depth.

The basic equation of Eq. (169) is modified so that measurements for all device sizes can be reproduced.

$$I_{\rm sub} = X_{\rm sub1} \cdot P_{\rm sisubsat} \cdot I_{\rm ds} \cdot \exp\left(-\frac{X_{\rm sub2}}{P_{\rm sisubsat}}\right) \tag{171}$$

where

$$X_{\rm sub1} = \mathbf{SUB1} \cdot \left(1 + \frac{\mathbf{SUB1L}}{L_{\rm gate}^{\mathbf{SUB1LP}}}\right) \tag{172}$$

$$X_{\rm sub2} = \mathbf{SUB2} \cdot \left(1 + \frac{\mathbf{SUB2L}}{L_{\rm gate}}\right) \tag{173}$$

$$P_{\rm sisubsat} = \mathbf{SVDS} \cdot V_{\rm ds} + \phi_{\rm S0} - \frac{L_{\rm gate} \cdot P_{\rm sislsat}}{X_{\rm gate} + L_{\rm gate}} \tag{174}$$

$$X_{\rm gate} = \mathbf{SLG} \cdot \left(1 + \frac{\mathbf{SLGL}}{L_{\rm gate}^{\mathbf{SLGLP}}}\right) \tag{175}$$

$$P_{\rm sislsat} = V_{\rm g2} + \frac{q \cdot \epsilon_{\rm Si} \cdot N_{\rm sub}}{C_{\rm ox}^2} \cdot \left\{1 - \sqrt{1 + \frac{2C_{\rm ox}^2}{q \cdot \epsilon_{\rm Si} \cdot N_{\rm sub}} \cdot \left(V_{\rm g2} - \frac{1}{\beta} - X_{\rm vbs} \cdot V_{\rm bs}\right)}\right\} \tag{176}$$

$$X_{\rm vbs} = \mathbf{SVBS} \cdot \left(1 + \frac{\mathbf{SVBSL}}{L_{\rm gate}^{\mathbf{SVBSLP}}}\right) \tag{177}$$

$$V_{\rm g2} = \mathbf{SVGS} \cdot \left(1 + \frac{\mathbf{SVGSL}}{L_{\rm gate}^{\mathbf{SVGSLP}}}\right) \cdot \frac{W_{\rm gate}^{\mathbf{SVGSWP}}}{W_{\rm gate}^{\mathbf{SVGSWP}} + \mathbf{SVGSW}} \cdot V_{\rm gp} \tag{178}$$

Impact-Ionization Induced Bulk Potential Change

The impact ionization induces electron and hole pairs, which is the origin of the substrate current. However, not only the leakage current but also the charge distribution in the bulk is changed. This induced charge redistribution affects as the bulk potential change. This is modeled in a simple way as

$$\begin{aligned}\Delta I_{\rm ds} = \frac{2}{3}\sqrt{\frac{2\epsilon_{\rm Si} q N_{\rm sub}}{\beta}} \Big[\big\{\beta(\phi_{\rm SL} - V_{\rm bs}) - 1\big\}^{\frac{3}{2}} \frac{3}{2} \frac{\beta \Delta V_{\rm bulk}}{\beta(\phi_{\rm SL} - V_{\rm bs}) - 1} \\ - \big\{\beta(\phi_{\rm S0} - V_{\rm bs}) - 1\big\}^{\frac{3}{2}} \frac{3}{2} \frac{\beta \Delta V_{\rm bulk}}{\beta(\phi_{\rm S0} - V_{\rm bs}) - 1} \Big] \\ - \sqrt{\frac{2\epsilon_{\rm Si} q N_{\rm sub}}{\beta}} \Big[\big\{\beta(\phi_{\rm SL} - V_{\rm bs}) - 1\big\}^{\frac{1}{2}} \frac{1}{2} \frac{\beta \Delta V_{\rm bulk}}{\beta(\phi_{\rm SL} - V_{\rm bs}) - 1} \\ - \big\{\beta(\phi_{\rm S0} - V_{\rm bs}) - 1\big\}^{\frac{1}{2}} \frac{1}{2} \frac{\beta \Delta V_{\rm bulk}}{\beta(\phi_{\rm S0} - V_{\rm bs}) - 1} \Big]\end{aligned} \tag{179}$$

where

$$\Delta V_{\rm bulk} = \mathbf{IBPC1}(1 + \mathbf{IBPC2} \cdot \Delta V_{\rm th}) \cdot I_{\rm sub} \tag{180}$$

IBPC1 and **IBPC2** are model parameters.

18.2 Gate Current

All possible gate leakage currents are schematically shown in Fig. 24 [32].

(i) Between Gate and Channel, $I_{\rm gate}$

As for the current between gate and channel, ($I_{\rm gate}$) the direct-tunneling mechanism is considered [38]. Since measured $I_{\rm gate}$ shows nearly linear $L_{\rm gate}$ dependence, the tunneling is assumed to occur along the

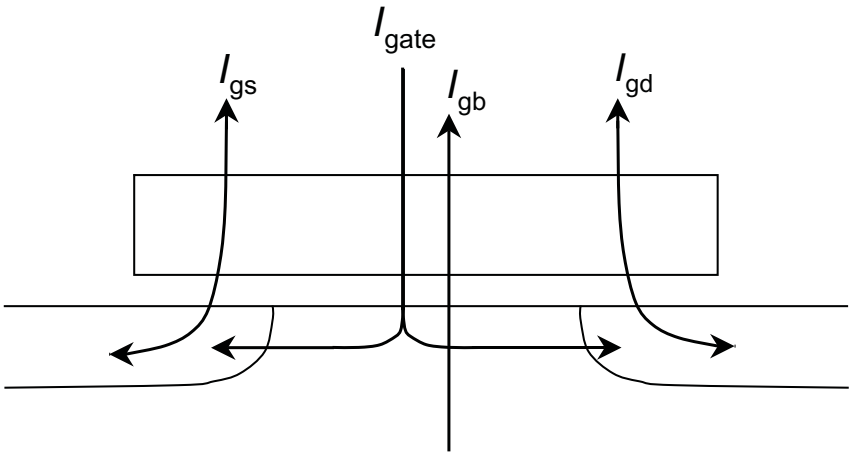

Fig. 24: Gate leakage currents considered.

whole channel length. Thus the final description implemented in HiSIM is [39, 40]

$$I_{\rm gate} = q \cdot \mathbf{GLEAK1} \cdot \frac{E^2}{E_{\rm gp}^{\frac{1}{2}}} \cdot \exp\left(-\frac{E_{\rm gp}^{\frac{3}{2}} \times \mathbf{GLEAK2}}{E}\right) \cdot \sqrt{\frac{Q_{\rm i}}{const0}} \cdot W_{\rm eff} \cdot \mathbf{NF} \cdot L_{\rm eff} \cdot \frac{\mathbf{GLEAK6}}{\mathbf{GLEAK6} + V_{\rm ds}} \cdot \frac{\mathbf{GLEAK7}}{\mathbf{GLEAK7} + W_{\rm eff} \cdot L_{\rm eff}} \tag{181}$$

where

$$E = \frac{V_{\rm G} - \mathbf{GLEAK3} \times \phi_{\rm S}(\Delta L)}{T_{\rm ox}} \cdot \left(1 + \frac{E_{\rm y}}{\mathbf{GLEAK5}}\right) \tag{182}$$

$$V_{\rm G} = V_{\rm gs} - V_{\rm FB} + \mathbf{GLEAK4} \cdot \Delta V_{\rm th} \cdot L_{\rm eff} \tag{183}$$

$$\Delta V_{\rm th} = \Delta V_{\rm th,SC} + \Delta V_{\rm th,P} + \Delta V_{\rm th,W} - \phi_{\rm Spg} \tag{184}$$

GLEAK1 – 7 are model parameters, and $E_{\rm gp}$ describes the temperature dependent bandgap for the gate current (see section 15). The gate-channel current $I_{\rm gate}$ is partitioned into two terminal currents with one model parameter in the following manner.

$$I_{\rm gate} = I_{\rm gate,s} + I_{\rm gate,d} \tag{185}$$

where

$$I_{\rm gate,s} = (1 - P_{\rm artition}) \cdot I_{\rm gate} \tag{186}$$

$$I_{\rm gate,d} = P_{\rm artition} \cdot I_{\rm gate} \tag{187}$$

where analytical description of $P_{\rm artition}$ is obtained by integrating the following equation in the same manner as the drain charge given in Eq. (21)

$$I_{\rm gate,d} = \int_0^{L_{\rm eff}} \frac{y}{L_{\rm eff}} I_{\rm gate}(y) dy = P_{\rm artition} I_{\rm gate} \tag{188}$$

The straightforward simulation result is shown in Fig. 25. However, the derived equation requires long simulation time and has to be simplified.

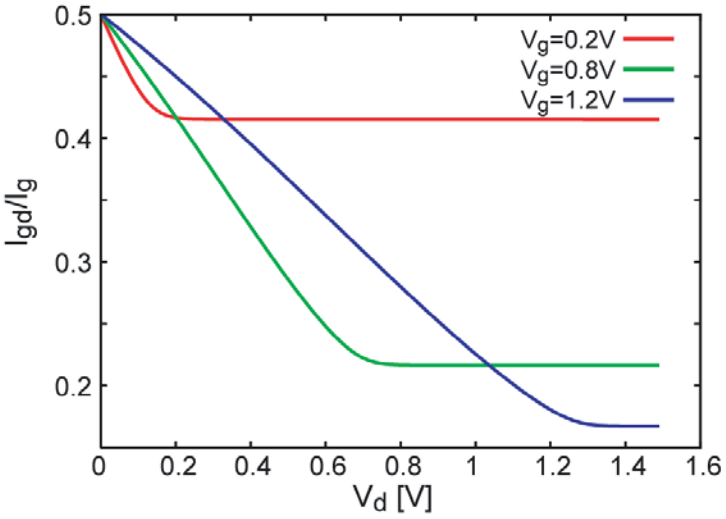

Fig. 25: Exact results of gate partitioning.

(ii) Between Gate and Bulk, $I_{\rm gb}$

The $I_{\rm gb}$ current under the accumulation condition is modeled as

$$I_{\rm gb} = \mathbf{GLKB1} \cdot E_{\rm gb}^2 \cdot \exp\left(-\frac{\mathbf{GLKB2}}{E_{\rm gb}}\right) W_{\rm eff} \cdot \mathbf{NF} \cdot L_{\rm eff} \tag{189}$$

$$E_{\rm gb} = -\frac{V_{\rm gb} - V_{\rm FB} + \mathbf{GLKB3}}{T_{\rm ox}} \tag{190}$$

(iii) Between Gate and Source/Drain, $I_{\rm gs}/I_{\rm gd}$

The tunneling current between the gate and the source/drain overlap region is modeled as

$$I_{\rm gs} = sign\mathbf{GLKSD1} \cdot E_{\rm gs}^2 \exp\left(T_{\rm ox}(-\mathbf{GLKSD2} \cdot V_{\rm gs} + \mathbf{GLKSD3})\right) W_{\rm eff} \cdot \mathbf{NF} \tag{191}$$

$$E_{\rm gs} = \frac{V_{\rm gs}}{T_{\rm ox}} \tag{192}$$

$$I_{\rm gd} = sign\mathbf{GLKSD1} \cdot E_{\rm gd}^2 \exp\left(T_{\rm ox}(\mathbf{GLKSD2} \cdot (-V_{\rm gs} + V_{\rm ds}) + \mathbf{GLKSD3})\right) W_{\rm eff} \cdot \mathbf{NF} \tag{193}$$

$$E_{\rm gd} = \frac{V_{\rm gs} - V_{\rm ds}}{T_{\rm ox}} \tag{194}$$

$$sign = +1 \quad \text{for} \quad E \le 0$$

$$sign = -1 \quad \text{for} \quad E \ge 0$$

18.3 GIDL (Gate-Induced Drain Leakage)

The GIDL current is generated at the drain junction under the accumulation condition. The $V_{\rm ds}$ increase induces a very narrow potential well in the drain just under the gate, causing carrier generation. Therefore, the GIDL current is strongly dependent on $V_{\rm ds}$. At further reduced $V_{\rm gs}$ values the direct gate tunneling starts to dominate the $I_{\rm GIDL}$ measurements, resulting in $V_{\rm ds}$ independence. The $V_{\rm ds}$ dependent $I_{\rm GIDL}$ is modeled here. The generation mechanism is considered to be the direct tunneling between the above mentioned narrow potential well of length ΔY and the ordinary drain region.

$$I_{\rm GIDL} = \alpha I_{\rm ds} \Delta Y \tag{195}$$

The generation occurs only in this ΔY region at the drain. The final equation is

$$I_{\rm GIDL} = q \cdot \mathbf{GIDL1} \cdot \frac{E^2}{E_{\rm g}^{\frac{1}{2}}} \cdot \exp\left(-\mathbf{GIDL2} \cdot \frac{E_{\rm g}^{\frac{3}{2}}}{E_0}\right) \cdot W_{\rm eff} \cdot \mathbf{NF} \cdot \frac{V_{\rm db}^3}{V_{\rm db}^3 + small} \tag{196}$$

where

$$E = \frac{\mathbf{GIDL3} \cdot (V_{\rm ds} + \mathbf{GIDL4}) - V'_{\rm G} - Q_{\rm box}}{T_{\rm ox}} \tag{197}$$

$$E_0 = E^{\mathbf{GIDL7}} \tag{198}$$

and

$$Q_{\rm box} = \mathbf{GIDL6} \cdot \frac{\sqrt{2qN_{\rm sub}\epsilon_{\rm Si} \cdot (2\Phi_{\rm B} - V_{\rm sub})}}{C_{\rm ox}} \tag{199}$$

$$V'_{\rm G} = V_{\rm gs} + \Delta V_{\rm th} \cdot \mathbf{GIDL5} \tag{200}$$

$$V_{\rm db} = V_{\rm ds} - V_{\rm bs} \tag{201}$$

$$small = 0.5 \tag{202}$$

The last term in the right-hand side of Eq. (196) is introduced to preserve $I_{\rm GIDL}$ at $V_{\rm gs} = V_{\rm ds}$=0 [32].The above $I_{\rm GIDL}$ equation is valid for $V_{\rm db} > 0$, and $I_{\rm GIDL} = 0$ for $V_{\rm db} \leq 0$. It is recommended not to use **GIDL4** for certain applications, because $I_{\rm GIDL}$ dose not approach zero even under the condition of $V_{\rm gs} = V_{\rm ds}$=0.
Here $\Delta V_{\rm th}$ is defined as

$$\Delta V_{\rm th} = \Delta V_{\rm th,SC} + \Delta V_{\rm th,P} \tag{203}$$

The GISL current is calculated with the same equation as the GIDL current described above. The selection either $I_{\rm GIDL}$ or $I_{\rm GISL}$ is done by the polarity of the current flow.

The HiSIM model parameters introduced in section 18 are summarized in Table 17.

Table 17: HiSIM model parameters introduced in section 18 of this manual. $*$ indicates minor parameters.

SUB1	substrate current coefficient of magnitude
SUB1L	L_{gate} dependence **SUB1**
SUB1LP	L_{gate} dependence **SUB1**
SUB2	substrate current coefficient of exponential term
SUB2L	L_{gate} dependence of **SUB2**
SVDS	substrate current dependence on V_{ds}
SLG	substrate current dependence on L_{gate}
SLGL	substrate current dependence on L_{gate}
SLGLP	substrate current dependence on L_{gate}
SVBS	substrate current dependence on V_{bs}
SVBSL	L_{gate} dependence of **SVBS**
SVBSLP	L_{gate} dependence of **SVBS**
SVGS	substrate current dependence on V_{gs}
SVGSL	L_{gate} dependence of **SVGS**
SVGSLP	L_{gate} dependence of **SVGS**
SVGSW	W_{gate} dependence of **SVGS**
SVGSWP	W_{gate} dependence of **SVGS**
IBPC1	impact-ionization induced bulk potential change
IBPC2	impact-ionization induced bulk potential change
GLEAK1	gate to channel current coefficient
GLEAK2	gate to channel current coefficient
GLEAK3	gate to channel current coefficient
GLEAK4	gate to channel current coefficient
$*$**GLEAK5**	gate to channel current coefficient (short channel correction)
$*$**GLEAK6**	gate to channel current coefficient (V_{ds} dependence correction)
$*$**GLEAK7**	gate to channel current coefficient (gate length and width dependence correction)
GLKB1	gate to bulk current coefficient
GLKB2	gate to bulk current coefficient
GLKB3	flat-band shift for gate to bulk current
GLKSD1	gate to source/drain current coefficient
GLKSD2	gate to source/drain current coefficient
GLKSD3	gate to source/drain current coefficient
GIDL1	magnitude of the GIDL
GIDL2	field dependence of the GIDL
GIDL3	V_{ds} dependence of the GIDL
$*$**GIDL4**	threshold of V_{ds} dependence
$*$**GIDL5**	correction of high-field contribution
$*$**GIDL6**	V_{bs} dependence of the GIDL
$*$**GIDL7**	correction of high-field contribution

Table 18: HiSIM flags introduced in section 18 of this manual for selecting different options.

COISUB	0: no (default); 1: yes
COIIGS	0: no (default); 1: yes
COGIDL	0: no (default); 1: yes

19 Conservation of Symmetry at $V_{\rm ds} = 0$

HiSIM preserves the symmetry at $V_{\rm ds} = 0$ automatically due to the drift-diffusion approximation as demonstrated in Fig. 26. However, modeling of observed phenomena induces a small wiggle, which is obvious in higher derivatives. To eliminate the wiggle caused by the artifacts of the modeling written as a function of $V_{\rm ds}$, a damping of the modeled effects is done as $V_{\rm ds}$ approaches zero. In HiSIM the damping is done by a mathematical function with two parameters: **VZADD0** and **PZADD0** [41]. The values of these parameters are fixed, and it is recommended not to change them. However, if smoothness at $V_{\rm ds}$=0 is disturbed, it is recommended to increase **VZADD0** until the non-smoothness disappears.

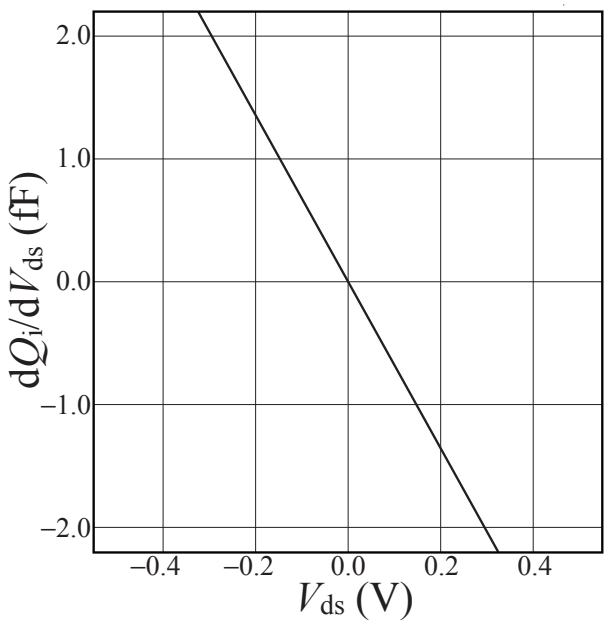

Fig. 26: Symmetry test at $V_{\rm ds} = 0$ for $L_{\rm gate} = 10\mu$m and $V_{\rm gs} = 3$V.

The HiSIM model parameters introduced in section 19 are summarized in Table 19.

Table 19: HiSIM model parameters introduced in section 19 of this manual.

VZADD0	symmetry conservation coefficient
PZADD0	symmetry conservation coefficient

20 Source/Bulk and Drain/Bulk Diode Models

20.1 Diode Current

The model equations for the source/bulk and drain/bulk diode currents are based on the concepts of BSIM3v3 [10], but include a number of modifications.

The two regions denoted (a) and (b) in the schematic diagram of Fig. 27, correspond to the forward-bias current saturation and the backward-bias region, respectively. These regions are distinguished in the modeling and are treated separately according to their origins.

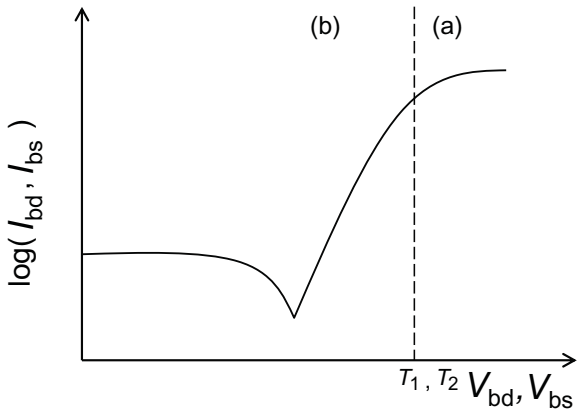

Fig. 27: The two $I_{\rm diode}$ currents ($I_{\rm bd}$ and $I_{\rm bs}$) are modeled separately in the two different operating regions (a) and (b).

The models for forward-biased current densities, describing the area and sidewall components of the source/drain regions, are given in Eqs. (205) and (206), respectively. The corresponding backward-biased current densities are given in Eqs. (207) and (208).

$$T_{\rm tnom} = \frac{T}{\mathbf{TNOM}} \tag{204}$$

$$j_{\rm s} = \mathbf{JS0} \exp\left\{\frac{(E_{\rm g}(T=\mathbf{TNOM})\cdot\beta(T=\mathbf{TNOM}) - E_{\rm g}\beta + \mathbf{XTI}\cdot\log(T_{\rm tnom}))}{\mathbf{NJ}}\right\} \tag{205}$$

$$j_{\rm ssw} = \mathbf{JS0SW} \exp\left\{\frac{(E_{\rm g}(T=\mathbf{TNOM})\cdot\beta(T=\mathbf{TNOM}) - E_{\rm g}\beta + \mathbf{XTI}\cdot\log(T_{\rm tnom}))}{\mathbf{NJSW}}\right\} \tag{206}$$

$$j_{\rm s2} = \mathbf{JS0} \exp\left\{\frac{(E_{\rm g}(T=\mathbf{TNOM})\cdot\beta(T=\mathbf{TNOM}) - E_{\rm g}\beta + \mathbf{XTI2}\cdot\log(T_{\rm tnom}))}{\mathbf{NJ}}\right\} \tag{207}$$

$$j_{\rm ssw2} = \mathbf{JS0SW} \exp\left\{\frac{(E_{\rm g}(T=\mathbf{TNOM})\cdot\beta(T=\mathbf{TNOM}) - E_{\rm g}\beta + \mathbf{XTI2}\cdot\log(T_{\rm tnom}))}{\mathbf{NJSW}}\right\} \tag{208}$$

$$N_{\rm vtm} = \frac{\mathbf{NJ}}{\beta} \tag{209}$$

(i) Between Drain and Bulk

With these current densities and the area parameter AD and the perimeter parameter PD of the drain region, the forward and backward currents between drain and bulk are calculated as

$$I_{\rm sbd} = AD \cdot j_{\rm s} + PD \cdot j_{\rm ssw} \tag{210}$$

$$I_{\rm sbd2} = AD \cdot j_{\rm s2} + PD \cdot j_{\rm ssw2} \tag{211}$$

The resulting drain-bulk current equations in the 2 operating regions (a) and (b) are derived as follows.

a) $V_{\rm bd} \geq T_1$

$$\begin{aligned} I_{\rm bd} =& I_{\rm sbd}\left\{\exp\left(\frac{T_1}{N_{\rm vtm}}\right)-1\right\} + \frac{I_{\rm sbd}}{N_{\rm vtm}}\exp\left(\frac{T_1}{N_{\rm vtm}}\right)(V_{\rm bd}-T_1) \\ &+ I_{\rm sbd2}\cdot\mathbf{CISB}\left\{\exp\left(-\frac{V_{\rm bd}\mathbf{CVBK}}{N_{\rm vtm}}\right)-1\right\}\exp\left\{(T_{\rm tnom}-1)\mathbf{CTEMP}\right\} \\ &+ \mathbf{CISBK}\left\{\exp\left(-\frac{V_{\rm bd}\mathbf{CVBK}}{N_{\rm vtm}}\right)-1\right\} \end{aligned} \tag{212}$$

b) $T_1 \geq V_{\rm bd}$

$$\begin{aligned} I_{\rm bd} =& I_{\rm sbd}\left\{\exp\left(\frac{V_{\rm bd}}{N_{\rm vtm}}\right)-1\right\} \\ &+ I_{\rm sbd2}\cdot\mathbf{CISB}\cdot\left\{\exp\left(-\frac{V_{\rm bd}\cdot\mathbf{CVB}}{N_{\rm vtm}}\right)-1\right\}\exp\left\{(T_{\rm tnom}-1)\mathbf{CTEMP}\right\} \\ &+ \mathbf{CISBK}\cdot\left\{\exp\left(-\frac{V_{\rm bd}\cdot\mathbf{CVBK}}{N_{\rm vtm}}\right)-1\right\} \end{aligned} \tag{213}$$

$$T_1 = N_{\rm vtm}\cdot\log\left\{\frac{\mathbf{VDIFFJ}}{I_{\rm sbd}}\cdot(T_{\rm tnom})^2+1\right\} \tag{214}$$

$$I_{\rm bd} = I_{\rm bd} + \mathbf{DIVX}\cdot I_{\rm sbd2}\cdot V_{\rm bd} \tag{215}$$

(ii) Between Source and Bulk

The area parameter AS and the perimeter parameter PS of the source region are used to calculate the forward and backward currents between source and bulk.

$$I_{\rm sbs} = AS \cdot j_{\rm s} + PS \cdot j_{\rm ssw} \tag{216}$$

$$I_{\rm sbs2} = AS \cdot j_{\rm s2} + PS \cdot j_{\rm ssw2} \tag{217}$$

This leads to the following source-bulk current equations in the 3 operating regions (a), (b) and (c).

a) $V_{\rm bs} \geq T_2$

$$\begin{aligned} I_{\rm bs} =& I_{\rm sbs}\left\{\exp\left(\frac{T_2}{N_{\rm vtm}}\right)-1\right\} + \frac{I_{\rm sbs}}{N_{\rm vtm}}\exp\left(\frac{T_2}{N_{\rm vtm}}\right)(V_{\rm bs}-T_2) \\ &+ I_{\rm sbs2}\cdot\mathbf{CISB}\left\{\exp\left(-\frac{V_{\rm bs}\mathbf{CVBK}}{N_{\rm vtm}}\right)-1\right\}\exp\left\{(T_{\rm tnom}-1)\mathbf{CTEMP}\right\} \\ &+ \mathbf{CISBK}\left\{\exp\left(-\frac{V_{\rm bs}\mathbf{CVBK}}{N_{\rm vtm}}\right)-1\right\} \end{aligned} \tag{218}$$

b) $T_2 \geq V_{\rm bs}$

$$\begin{aligned} I_{\rm bs} =& I_{\rm sbs} \cdot \left\{ \exp\left(\frac{V_{\rm bs}}{N_{\rm vtm}} \right) - 1 \right\} \\ &+ I_{\rm sbs2} \cdot \mathbf{CISB} \cdot \left\{ \exp\left(-\frac{V_{\rm bs} \cdot \mathbf{CVB}}{N_{\rm vtm}} \right) - 1 \right\} \cdot \exp\left\{ (T_{\rm tnom} - 1) \cdot \mathbf{CTEMP} \right\} \\ &+ \mathbf{CISBK} \cdot \left\{ \exp\left(-\frac{V_{\rm bs} \cdot \mathbf{CVBK}}{N_{\rm vtm}} \right) - 1 \right\} \end{aligned} \tag{219}$$

$$T_2 = N_{\rm vtm} \cdot \log\left\{ \frac{\mathbf{VDIFFJ}}{I_{\rm sbs}} \cdot \left\{ T_{\rm tnom} \right)^2 + 1 \right\} \tag{220}$$

$$I_{\rm bs} = I_{\rm bs} + \mathbf{DIVX} \cdot Isbs2 \cdot V_{\rm bs} \tag{221}$$

The hard-breakdown model of the diode will be implemented in a future version of HiSIM.

20.2 Diode Capacitance

The diode capacitances of the source/bulk junction $C_{\rm apbs}$ and of the drain/bulk junction $C_{\rm apbd}$ are given by the following equations. These equations have the same basis as those used in BSIM3v3 [10], but include a number of minor modifications.

The notations $\Theta = S,\ \theta = s$ (for source/bulk junction) and
$\Theta = D,\ \theta = d$ (for drain/bulk junction) apply.

$$c_{{\rm zb}\theta} = \mathbf{CJ} \cdot A\Theta \tag{222}$$

(I) $P\Theta > W_{\rm eff}$

$$c_{{\rm zb}\theta{\rm sw}} = \mathbf{CJSW}(P\Theta - W_{\rm eff} \cdot \mathbf{NF}) \tag{223}$$

$$c_{{\rm zb}\theta{\rm swg}} = \mathbf{CJSWG} \cdot W_{\rm eff} \cdot \mathbf{NF} \tag{224}$$

(i) $V_{{\rm b}\theta} = 0$

$$Q_{{\rm b}\theta} = 0 \tag{225}$$

$$C_{{\rm apb}\theta} = c_{{\rm zb}\theta} + c_{{\rm zb}\theta{\rm sw}} + c_{{\rm zb}\theta{\rm swg}} \tag{226}$$

(ii) $V_{{\rm b}\theta} < 0$

a-1) $c_{{\rm zb}\theta} > 0$

$$arg = 1 - \frac{V_{{\rm b}\theta}}{\mathbf{PB}} \tag{227}$$

α) $\mathbf{MJ} = 0.5$

$$sarg = \frac{1}{\sqrt{arg}} \tag{228}$$

β) $\mathbf{MJ} \neq 0.5$

$$sarg = \exp(-\mathbf{MJ} \cdot \log(arg)) \tag{229}$$

$$Q_{{\rm b}\theta} = \frac{\mathbf{PB} \cdot c_{{\rm zb}\theta}(1 - arg \cdot sarg)}{1 - \mathbf{MJ}} \tag{230}$$

$$C_{{\rm apb}\theta} = c_{{\rm zb}\theta} \cdot sarg \tag{231}$$

a-2) $c_{\mathrm{zb}\theta} \leq 0$

$$Q_{\mathrm{b}\theta} = 0 \tag{232}$$

$$C_{\mathrm{apb}\theta} = 0 \tag{233}$$

b) $c_{\mathrm{zb}\theta\mathrm{sw}} > 0$

$$arg = 1 - \frac{V_{\mathrm{b}\theta}}{\mathbf{PBSW}} \tag{234}$$

α) $\mathbf{MJSW} = 0.5$

$$sarg = \frac{1}{\sqrt{arg}} \tag{235}$$

β) $\mathbf{MJSW} \neq 0.5$

$$sarg = \exp(-\mathbf{MJSW} \cdot \log(arg)) \tag{236}$$

$$Q_{\mathrm{b}\theta} += \frac{\mathbf{PBSW} \cdot c_{\mathrm{zb}\theta\mathrm{sw}}(1 - arg \cdot sarg)}{1.0 - \mathbf{MJSW}} \tag{237}$$

$$C_{\mathrm{apb}\theta} += c_{\mathrm{zb}\theta\mathrm{sw}} \cdot sarg \tag{238}$$

c) $c_{\mathrm{zb}\theta\mathrm{swg}} > 0$

$$arg = 1 - \frac{V_{\mathrm{b}\theta}}{\mathbf{PBSWG}} \tag{239}$$

α) $\mathbf{MJSWG} = 0.5$

$$sarg = \frac{1}{\sqrt{arg}} \tag{240}$$

β) $\mathbf{MJSWG} \neq 0.5$

$$sarg = \exp(-\mathbf{MJSWG} \cdot \log(arg)) \tag{241}$$

$$Q_{\mathrm{b}\theta} += \frac{\mathbf{PBSWG} \cdot c_{\mathrm{zb}\theta\mathrm{swg}}(1 - arg \cdot sarg)}{1 - \mathbf{MJSWG}} \tag{242}$$

$$C_{\mathrm{apb}\theta} += c_{\mathrm{zb}\theta\mathrm{swg}} \cdot sarg \tag{243}$$

(iii) $V_{\mathrm{b}\theta} > 0$

$$\begin{aligned} Q_{\mathrm{b}\theta} &= V_{\mathrm{b}\theta}(c_{\mathrm{zb}\theta} + c_{\mathrm{zb}\theta\mathrm{sw}} + c_{\mathrm{zb}\theta\mathrm{swg}}) \\ &\quad + V_{\mathrm{b}\theta}^2 \left(\frac{1}{2} \frac{c_{\mathrm{zb}\theta} \cdot \mathbf{MJ}}{\mathbf{PB}} + \frac{1}{2} \frac{c_{\mathrm{zb}\theta\mathrm{sw}} \cdot \mathbf{MJSW}}{\mathbf{PBSW}} + \frac{1}{2} \frac{c_{\mathrm{zb}\theta\mathrm{swg}} \cdot \mathbf{MJSWG}}{\mathbf{PBSWG}} \right) \end{aligned} \tag{244}$$

$$\begin{aligned} C_{\mathrm{apb}\theta} &= c_{\mathrm{zb}\theta} + c_{\mathrm{zb}\theta\mathrm{sw}} + c_{\mathrm{zb}\theta\mathrm{swg}} \\ &\quad + V_{\mathrm{b}\theta} \left(\frac{c_{\mathrm{zb}\theta} \cdot \mathbf{MJ}}{\mathbf{PB}} + \frac{c_{\mathrm{zb}\theta\mathrm{sw}} \cdot \mathbf{MJSW}}{\mathbf{PBSW}} + \frac{c_{\mathrm{zb}\theta\mathrm{swg}} \cdot \mathbf{MJSWG}}{\mathbf{PBSWG}} \right) \end{aligned} \tag{245}$$

(II) $P\Theta \leq W_{\mathrm{eff}}$

$$c_{\mathrm{zb}\theta\mathrm{swg}} = \mathbf{CJSWG} \cdot P\Theta \tag{246}$$

(i) $V_{\mathrm{b}\theta} = 0$

$$Q_{\mathrm{b}\theta} = 0 \tag{247}$$

$$C_{\mathrm{apb}\theta} = c_{\mathrm{zb}\theta} + c_{\mathrm{zb}\theta\mathrm{swg}} \tag{248}$$

(ii) $V_{\mathrm{b}\theta} < 0$

a-1) $c_{\mathrm{zb}\theta} > 0$

$$arg = 1 - \frac{V_{\mathrm{b}\theta}}{\mathbf{PB}} \tag{249}$$

α) $\mathbf{MJ} = 0.5$

$$sarg = \frac{1}{\sqrt{arg}} \tag{250}$$

β) $\mathbf{MJ} \neq 0.5$

$$sarg = \exp(-\mathbf{MJ} \cdot \log(arg)) \tag{251}$$

$$Q_{\mathrm{b}\theta} = \frac{\mathbf{PB} \cdot c_{\mathrm{zb}\theta}(1 - arg \cdot sarg)}{1 - \mathbf{MJ}} \tag{252}$$

$$C_{\mathrm{apb}\theta} = c_{\mathrm{zb}\theta} \cdot sarg \tag{253}$$

a-2) $c_{\mathrm{zb}\theta} \leq 0$

$$Q_{\mathrm{b}\theta} = 0 \tag{254}$$

$$C_{\mathrm{apb}\theta} = 0 \tag{255}$$

b) $c_{\mathrm{zb}\theta\mathrm{swg}} > 0$

$$arg = 1 - \frac{V_{\mathrm{b}\theta}}{\mathbf{PBSWG}} \tag{256}$$

α) $\mathbf{MJSWG} = 0.5$

$$sarg = \frac{1}{\sqrt{arg}} \tag{257}$$

β) $\mathbf{MJSWG} \neq 0.5$

$$sarg = \exp(-\mathbf{MJSWG} \cdot \log(arg)) \tag{258}$$

$$Q_{\mathrm{b}\theta} \mathrel{+}= \mathbf{PBSWG} \cdot c_{\mathrm{zb}\theta\mathrm{swg}} \cdot \frac{1 - arg \cdot sarg}{1 - \mathbf{MJSWG}} \tag{259}$$

$$C_{\mathrm{apb}\theta} \mathrel{+}= c_{\mathrm{zb}\theta\mathrm{swg}} \cdot sarg \tag{260}$$

(iii) $V_{\mathrm{b}\theta} > 0$

$$\begin{aligned} Q_{\mathrm{b}\theta} &= V_{\mathrm{b}\theta} \cdot (c_{\mathrm{zb}\theta} + c_{\mathrm{zb}\theta\mathrm{swg}}) \\ &\quad + V_{\mathrm{b}\theta}^2 \left(\frac{1}{2} \frac{c_{\mathrm{zb}\theta} \cdot \mathbf{MJ}}{\mathbf{PB}} + \frac{1}{2} \frac{c_{\mathrm{zb}\theta\mathrm{swg}} \cdot \mathbf{MJSWG}}{\mathbf{PBSWG}} \right) \end{aligned} \tag{261}$$

$$\begin{aligned} C_{\mathrm{apb}\theta} &= c_{\mathrm{zb}\theta} + c_{\mathrm{zb}\theta\mathrm{swg}} \\ &\quad + V_{\mathrm{b}\theta} \left(\frac{c_{\mathrm{zb}\theta} \cdot \mathbf{MJ}}{\mathbf{PB}} + \frac{c_{\mathrm{zb}\theta\mathrm{swg}} \cdot \mathbf{MJSWG}}{\mathbf{PBSWG}} \right) \end{aligned} \tag{262}$$

The HiSIM model parameters introduced in section 20 are summarized in Table 20.

Table 20: HiSIM model parameters introduced in section 20 of this manual. # indicates instance parameters.

JS0	saturation current density
JS0SW	sidewall saturation current density
NJ	emission coefficient
NJSW	sidewall emission coefficient
XTI	temperature coefficient for forward-current densities
XTI2	temperature coefficient for reverse-current densities
DIVX	reverse current coefficient
CISB	reverse biased saturation current
CVB	bias dependence coefficient of **CISB**
CTEMP	temperature coefficient of reverse currents
CISBK	reverse biased saturation current (at low temperature)
CVBK	bias dependence coefficient of **CISB** (at low temperature)
CJ	bottom junction capacitance per unit area at zero bias
CJSW	source/drain sidewall junction cap. grading coefficient per unit length at zero bias
CJSWG	source/drain sidewall junction capacitance per unit length at zero bias
MJ	bottom junction capacitance grading coefficient
MJSW	source/drain sidewall junction capacitance grading coefficient
MJSWG	source/drain gate sidewall junction capacitance grading coefficient
PB	bottom junction build-in potential
PBSW	source/drain sidewall junction build-in potential
PBSWG	source/drain gate sidewall junction build-in potential
VDIFFJ	diode threshold voltage between source/drain and substrate
#AD	junction area of the drain contact
#PD	junction periphery of the drain contact
#AS	junction area of the source contact
#PS	junction periphery of the source contact

21 Noise Models

21.1 1/f Noise Model

The $1/f$ noise is caused by both the carrier fluctuation and the mobility fluctuation. The final description for the drift-diffusion model is [42]

$$S_{I_{\rm ds}} = \frac{I_{\rm ds}^2 \mathbf{NFTRP}}{\beta f (L_{\rm eff} - \Delta L) W_{\rm eff} \cdot \mathbf{NF}} \cdot \left[\frac{1}{(N_0 + N^*)(N_L + N^*)} + \frac{2\mu E_y \mathbf{NFALP}}{N_L - N_0} \ln\left(\frac{N_L + N^*}{N_0 + N^*}\right) + (\mu E_y \mathbf{NFALP})^2 \right] \tag{263}$$

where the parameters **NFALP** and **NFTRP** represent the contribution of the mobility fluctuation and the ratio of trap density to attenuation coefficient, respectively. N_0 and N_L are carrier densities at source side and drain side or pinch-off point, respectively, as calculated in HiSIM. N^* is written as

$$N^* = \frac{C_{\rm ox} + C_{\rm dep} + \mathbf{CIT}}{q\beta} \tag{264}$$

where $C_{\rm dep}$ is the depletion capacitance calculated with $\phi_{\rm S}$. **CIT** is the capacitance caused by the interface-trapped carriers and is normally fixed to be zero.

$$N_{\rm flick} = S_{I_{\rm ds}} \cdot f^{\mathbf{FALPH}} \tag{265}$$

is calculated in HiSIM, where **FALPH** has been introduced to model the derivation from the exact $1/f$ characteristics.

21.2 Thermal Noise Model

Van der Ziel derived the equation for the spectral density of the thermal drain-noise current at temperature T by integrating the transconductance along the channel direction y based on the Nyquist theorem [43]

$$S_{\rm id} = \frac{4kT}{L_{\rm eff}^2} \int g_{\rm ds}(y) dy = 4kT g_{\rm ds0} \gamma \tag{266}$$

Here k, $I_{\rm ds}$, $g_{\rm ds}(y)$, $g_{\rm ds0}$, γ are Boltzmann's constant, drain current, position-dependent channel conductance, channel conductance at $V_{\rm ds} = 0$, and drain-noise coefficient, respectively. In HiSIM the integration is performed with the surface potential $\phi_{\rm s}$ instead of the channel position as [44, 45]

$$S_{\rm id} = \frac{4kT}{L_{\rm eff}^2 I_{\rm ds}} \int g_{\rm ds}^2(\phi_{\rm s}) d\phi_{\rm s} \tag{267}$$

$$g_{\rm ds}(\phi_{\rm s}) = \frac{W_{\rm eff} \cdot \mathbf{NF}}{L_{\rm eff}} \beta \frac{d(\mu(\phi_{\rm s}) f(\phi_{\rm s}))}{d\phi_{\rm s}} \tag{268}$$

Here $f(\phi_{\rm s})$ is a characteristic function of HiSIM related to the carrier concentration [46]. The final equations for $S_{\rm id}$ in our compact-modeling approach, obtained after solving the integral of Eq. (267), become functions of the self-consistent surface potentials as well as the surface-potential derivatives at source and drain.

$$S_{\rm id} = 4kT \frac{W_{\rm eff} \cdot \mathbf{NF} C_{\rm ox}\ V_{\rm g} V_{\rm t}\ \mu}{(L_{\rm eff} - \Delta L)} \frac{(1 + 3\eta + 6\eta^2)\mu_{\rm d}^2 + (3 + 4\eta + 3\eta^2)\mu_{\rm d}\mu_{\rm s} + (6 + 3\eta + \eta^2)\mu_{\rm s}}{15(1 + \eta)\mu_{\rm av}^2} \tag{269}$$

where $\mu_{\rm s}$, $\mu_{\rm d}$ and $\mu_{\rm av}$ are carrier mobilities at the source side, the drain side, and averaged, respectively.

$$\eta = 1 - \frac{(\phi_{\rm SL} - \phi_{\rm S0}) + \chi(\phi_{\rm SL} - \phi_{\rm S0})}{V_{\rm g}V_{\rm t}} \tag{270}$$

$$\chi = 2\frac{cnst0}{C_{\rm ox}}\left[\left[\frac{2}{3}\frac{1}{\beta}\frac{\{\beta(\phi_{\rm SL} - V_{\rm bs}) - 1\}^{\frac{3}{2}} - \{\beta(\phi_{\rm S0} - V_{\rm bs}) - 1\}^{\frac{3}{2}}}{\phi_{\rm SL} - \phi_{\rm S0}}\right] - \sqrt{\beta(\phi_{\rm S0} - V_{\rm bs}) - 1}\right] \tag{271}$$

$V_{\rm g}V_{\rm t}$ is equal to the carrier density at the source side divided by the oxide capacitance.
Thus no additional model parameters are required for the thermal noise model.

$$N_{\rm thrml} = S_{\rm id}/4kT \tag{272}$$

is calculated in HiSIM.

21.3 Induced Gate Noise Model

No additional model parameters are required for the induced gate noise model.

$$N_{\rm igate} = S_{\rm igate}/f^2 \tag{273}$$

is calculated in HiSIM. Explicit model equation is shown in [47].

21.4 Coupling Noise Model

No additional model parameters are required for the coupling noise model.

$$N_{\rm cross} = \frac{S_{\rm igid}}{\sqrt{S_{\rm igate} \cdot S_{\rm id}}} \tag{274}$$

is calculated in HiSIM. Explicit model equation is shown in [47].

The HiSIM model parameters introduced in section 21 are summarized in Table 21.

Table 21: HiSIM model parameters introduced in section 21 of this manual. $*$ indicates a minor parameter.

NFTRP	ratio of trap density to attenuation coefficient
NFALP	contribution of the mobility fluctuation
$*$**CIT**	capacitance caused by the interface trapped carriers
FALPH	power of f describing deviation of $1/f$

22 Non-Quasi-Static (NQS) Model

22.1 Carrier Formation

Carriers in the channel take time to build-up as opposed to the Quasi-Static (QS) approximation. The Non-Quasi-Static effect is switched on by selecting the flag **CONQS**=1, where the defalt is set to zero. To consider this phenomenon in HiSIM, the carrier formation is modeled as [48, 49, 50, 51]

$$q(t_{\rm i}) = \frac{q(t_{\rm i-1}) + \frac{\Delta t}{\tau} Q(t_{\rm i})}{1 + \frac{\Delta t}{\tau}} \tag{275}$$

where $q(t_{\rm i})$ and $Q(t_{\rm i})$ represent the non-quasi-static and the quasi-static carrier density at time $t_{\rm i}$, respectively, and $\Delta t = t_{\rm i} - t_{\rm i-1}$ is valid. Eq. (275) implies that the formation of carriers under the NQS approximation is always delayed in comparison to the QS approximation, which is the basic origin of the NQS effect. The delay is determined by the carrier transit delay τ and the time interval in the circuit simulation Δt.

22.2 Delay Mechanisms

Up to weak inversion, carriers diffuse to the channel and the transit delay is approximated by

$$\tau_{\rm diff} = \mathbf{DLY1} \tag{276}$$

At strong inversion, there is already conduction due to field-driven carriers. The transit delay due to the flow of such conductive carriers is

$$\tau_{\rm cond} = \mathbf{DLY2} \cdot \frac{Q_{\rm i}}{I_{\rm ds}} \tag{277}$$

where **DLY2** is a constant coefficient. These two delay mechanisms (diffusion and conduction) are combined using the Matthiessen rule

$$\frac{1}{\tau} = \frac{1}{\tau_{\rm diff}} + \frac{1}{\tau_{\rm cond}} \tag{278}$$

Carrier delay mechanisms in a MOSFET switch-on operation with a gate-voltage rise time $t_{\rm r}$ of 20ps are illustrated in Fig. 28.

Applying the same approach for the formation of bulk carriers, leads to the approximation of the bulk carrier delay as an RC delay in the form

$$\tau_{\rm B} = \mathbf{DLY3} \cdot C_{\rm ox} \tag{279}$$

where **DLY3** is a constant coefficient and $C_{\rm ox}$ is the oxide capacitance.

22.3 Time-Domain Analysis

The total drain/source/bulk terminal currents are derived from the superposition of the transport current and the charging current. The transport current is a function of the instantaneous terminal voltages and is approximated by the steady-state solution. The source/drain/bulk charging currents are the time derivatives of the associated non-quasi-static charges, $q_{\rm S}$, $q_{\rm D}$, and $q_{\rm B}$, respectively.

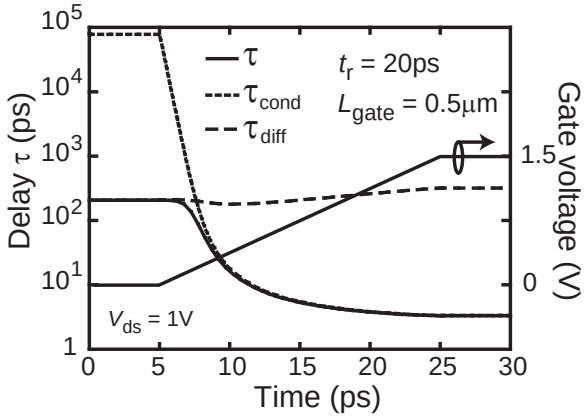

Fig. 28: Example of the dynamically calculated transit delay times, as incorporated in the NQS model of HiSIM, in a MOSFET switch-on simulation.

22.4 AC Analysis

The standard approach is used to for the static part of the NQS AC matrix, and the capacitance matrix is obtained by the first order Taylor expansion with respect to

$$v = v_0 + Ve^{i\omega t} \tag{280}$$

at $v = v_0$, where $v = v_0$ is the DC operating point solution. Since Eq. (275) is just an Euler discretization of

$$\frac{dq}{dt} + \frac{q - Q}{\tau} = 0 \tag{281}$$

resulting in

$$\left(i\omega\frac{\partial q_I}{\partial v} + \frac{1}{\tau}\left(\frac{\partial q_I}{\partial v} - \frac{\partial Q_I}{\partial v}\right)\right)\Bigg|_{v=v_0} \cdot Ve^{i\omega t} = 0 \tag{282}$$

$$\left(i\omega\frac{\partial q_B}{\partial v} + \frac{1}{\tau_B}\left(\frac{\partial q_B}{\partial v} - \frac{\partial Q_B}{\partial v}\right)\right)\Bigg|_{v=v_0} \cdot Ve^{i\omega t} = 0 \tag{283}$$

from which the partial derivatives of q_I, q_B can be calculated

$$\begin{aligned}\frac{\partial q_I}{\partial v} &= \frac{1}{1 + i\omega\tau}\frac{\partial Q_I}{\partial v} \\ \frac{\partial q_B}{\partial v} &= \frac{1}{1 + i\omega\tau_B}\frac{\partial Q_B}{\partial v}\end{aligned}$$

Note that the capacitances are complex and frequency dependent. For $\tau = \tau_B = 0$ the QS capacitances are obtained.

The HiSIM model parameters introduced in section 22 are summarized in Table 22.

Table 22: HiSIM model parameters introduced in section 22 of this manual.

DLY1	coefficient for delay due to diffusion of carriers
DLY2	coefficient for delay due to conduction of carriers
DLY3	coefficient for RC delay of bulk carriers

23 Multiplication Factor

For the case of a multiple device construction the multiple factor **M** is introduced as an instance parameter. All device features such as currents and capacitances are multipled by **M**. Noises are also multiplied by **M**.

The HiSIM model parameters introduced in section 23 are summarized in Table 23.

Table 23: HiSIM model parameters introduced in section 23 of this manual. # indicates an instance parameter.

# **M**	multiplication factor

24 DFM Model

To support design for manufacturability (DFM) HiSIM introduces an option for considering the variation of device parameters.

Accurate prediction of device performance for a wide range of the substrate-impurity-concentration variations is secured by introducing an impurity concentration dependent mobility due to the phonon scattering as

$$M_{\rm uephonon} = \mathbf{MUEPH1}\,[\mathbf{MPHDFM}\{\ln(\mathbf{NSUBCDFM}) - \ln(\mathbf{NSUBC})\} + 1]$$

$$\mathbf{NSUBP} = \mathbf{NSUBP} + (\mathbf{NSUBCDFM} - \mathbf{NSUBC}) \tag{284}$$

$$\mathbf{NPEXT} = \mathbf{NPEXT} + (\mathbf{NSUBCDFM} - \mathbf{NSUBC}) \tag{285}$$

where **NSUBCDFM** is an instance parameter and **MPHDFM** is a model parameter describing the mobility reduction due to the increase of the substrate impurity concentration. This model is activated if the model flag **CODFM** = 1, and **NSUBCDFM** is also given.

The HiSIM model parameters introduced in section 24 are summarized in Table 24.

Table 24: HiSIM model parameters introduced in section 24 of this manual. # indicates an instance parameter and ## indicates a parameter treated both as a model parameter and an isntance parameter.

#NSUBCDFM	substrate impurity concentration
##MPHDFM	mobility dependence of **NSUBC** due to $\mu_{\rm phonon}$

25 Depletion Mode Model Option

To support depletion mode MOSFET devices, an option for considering the new structure is introduced in HiSIM.

In the depletion mode MOSFET, an N^- layer is constructed at the channel surface of conventional MOSFET devices as shown Fig. 29.

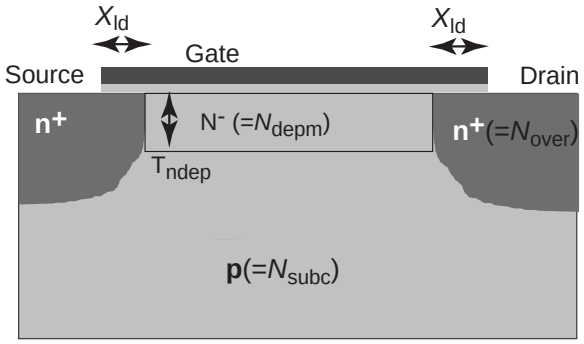

Fig. 29: Schematic of the typical depletion mode MOSFET structure and device parameters.

where $N_{\rm depm}$ denotes the impurity concentration of the N^- Layer, and $T_{\rm ndep}$ denotes the thickness of the N^- layer. This model is activated if the model flag **CODEP** = 1(default = 0).

Fig. 30 shows the potential and the electron carrier density distribution along the channel cross section of a depletion mode MOSFET.

In such a depletion mode MOSFET device, the electron carriers in the N^- layer strongly influence both, the current and capacitance characteristics. Therefore, the Poisson equation is solved for majority carrier under the consideration of the P/N junction depletion charge in the depletion mode model.

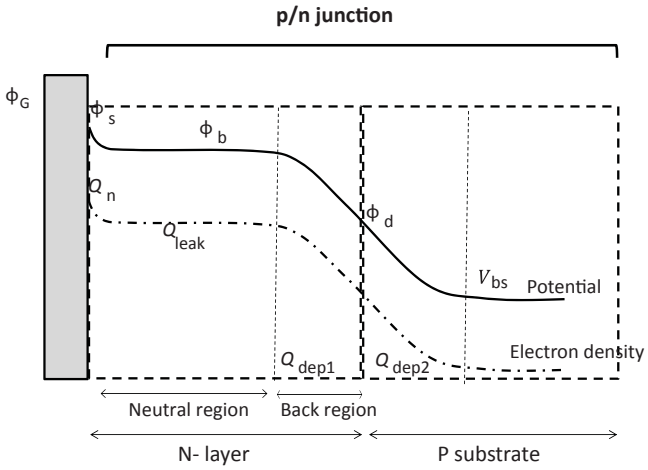

Fig. 30: Potential and electron carrier density distribution along the channel cross section of the depletion mode MOSFET.

25.1 DC current equation

The total drain current $I_{\rm ds}$ is written as follows

$$I_{\rm ds} = \frac{W_{\rm eff,nf}}{L_{\rm ch}} \cdot \frac{1}{\beta} \left(\mu \cdot I_{\rm dd}\right) + I_{\rm ds,resistor} + I_{\rm ds,back} \tag{286}$$

where,

$$I_{\rm dd} = -\beta \frac{(Q_{\rm n0} + Q_{\rm nl})}{2} \cdot \phi_{\rm ds} - Q_{\rm n0} + Q_{\rm nl} \tag{287}$$

$$I_{\rm ds,resistor} = W_{\rm eff,nf} \cdot Q_{\rm leak,resistor0} \cdot \mu_{\rm leak,resistor} \cdot \frac{V_{\rm ds,eff}}{L_{\rm ch}} \tag{288}$$

$$I_{\rm ds,back} = W_{\rm eff,nf} \cdot Q_{\rm leak,back0} \cdot \mu_{\rm leak,back} \cdot \frac{V_{\rm ds,eff}}{L_{\rm ch}} \tag{289}$$

$$Q_{\rm leak,resistor0} = -q \cdot N_{\rm depm} \cdot (T_{\rm ndep} - W_{\rm s} - W_{\rm b}) \tag{290}$$

$$Q_{\rm leak,back0} = -q \cdot N_{\rm depm} \cdot \exp\left\{\beta \left(\phi_{\rm b0} - V_{\rm ds,eff}\right)\right\} \cdot W_{\rm b} \tag{291}$$

$V_{\rm ds,eff}$ denotes the effective potential at the drain side in the resistor part and is defined as follows.

$$V_{\rm ds,eff} = \frac{DEP_{\rm vdsef2} \cdot V_{\rm ds}}{\left[1 + \left(\frac{V_{\rm ds}}{V_{\rm ds,sat}}\right)^{\Delta}\right]^{\frac{1}{\Delta}}} \tag{292}$$

where

$$V_{\rm ds,sat} = \Bigg[V_{\rm gp} + DEP_{\rm vdsef1} + \frac{qN_{\rm depm}\epsilon_{\rm Si}}{{C_{\rm ox}}^2}\Big\{1 - \sqrt{1 + 2\frac{{C_{\rm ox}}^2}{qN_{\rm depm}\epsilon_{\rm Si}}\Big\{V_{\rm gp} + DEP_{\rm vdsef1} - \frac{1}{\beta} - V_{\rm bs}\Big\}}\Big\}\Bigg] \tag{293}$$

$Q_{\rm n0}$ and $Q_{\rm nl}$ denote the accumlation charge in the N^- layor at the source side and the drain side, respectively. $Q_{\rm leak,resistor0}$ denotes the charge in the resistor part at the source side. Furthermore, $Q_{\rm leak,back0}$ denotes the charge in the back part(see Fig. 30) at the source side. $N_{\rm depm}$, $DEP_{\rm vdsef1}$ and $DEP_{\rm vdsef2}$ consider the gate length dependence of the impurity concentration as

$$N_{\rm depm} = \mathbf{NDEPM} \cdot \left(1 + \frac{\mathbf{NDEPML}}{(L_{\rm gate} \cdot 10^6)^{\mathbf{NDEPMLP}}}\right) \tag{294}$$

$$DEP_{\rm vdsef1} = \mathbf{DEPVDSEF1} \cdot \left(1 + \frac{\mathbf{DEPVDSEF1L}}{(L_{\rm gate} \cdot 10^6)^{\mathbf{DEPVDSEF1LP}}}\right) \tag{295}$$

$$DEP_{\rm vdsef2} = \mathbf{DEPVDSEF2} \cdot \left(1 + \frac{\mathbf{DEPVDSEF2L}}{(L_{\rm gate} \cdot 10^6)^{\mathbf{DEPVDSEF2LP}}}\right) \tag{296}$$

25.2 Mobility model

The mobility in each region is written with following equations.

a) Surface mobility:

$$\mu_{=} \frac{\mu_0}{\left(1 + \left(\frac{\mu_0 E_{\rm y}}{V_{\rm max}}\right)^{\mathbf{BB}}\right)^{\frac{1}{\mathbf{BB}}}} \tag{297}$$

where,

$$Q_{\rm iumue} = -Q_{\rm n0} \tag{298}$$
$$R_{\rm ns} = \frac{Q_{\rm iumue}}{q} \tag{299}$$
$$E_{\rm eff} = \frac{\left(\frac{\mathbf{NINV}}{\epsilon_{\rm Si}}\right) \cdot Q_{\rm iumue}}{1 + (\phi_{\rm sl} - \phi_{\rm s0}) \cdot N_{\rm invde}} \tag{300}$$
$$\mu_{\rm CB} = \mathbf{MUECB0} + \mathbf{MUECB1} \cdot \frac{R_{\rm ns}}{10^{11}} \tag{301}$$
$$\mu_{\rm PH} = \frac{M_{\rm uephonon}}{E_{\rm eff}{}^{\mathbf{MUEPH0}}} \tag{302}$$
$$\mu_{\rm SR} = \frac{\mathbf{MUESR1}}{E_{\rm eff}{}^{M_{\rm uesurface]}}} \tag{303}$$
$$\frac{1}{\mu_0} = \frac{1}{\mu_{\rm CB}} + \frac{1}{\mu_{\rm PH}} + \frac{1}{\mu_{\rm SR}} \tag{304}$$

b) Mobility of the resistor part:

$$\mu_{\rm leak,resistor} = \frac{\mu_0}{\left(1 + \left(\frac{\mu_0 E_{\rm y}}{DEP_{\rm vmax}}\right)^{\mathbf{DEPBB}}\right)^{\frac{1}{\mathbf{DEPBB}}}} \tag{305}$$
$$\tag{306}$$

where,

$$E_{\rm y} = \frac{V_{\rm ds,eff}}{L_{\rm ch}} \tag{307}$$
$$Q_{\rm iumue} = -Q_{\rm leak,resistor0} \tag{308}$$
$$R_{\rm ns} = \frac{Q_{\rm iumue}}{q} \tag{309}$$
$$E_{\rm eff} = \frac{Q_{\rm iumue}}{1 + (\phi_{\rm sl} - \phi_{\rm s0}) \cdot N_{\rm invde}} \tag{310}$$
$$\mu_{\rm CB} = DEP_{\rm mue0} + DEP_{\rm mue1} \cdot \frac{R_{\rm ns}}{10^{11}} \tag{311}$$
$$\mu_{\rm PH} = \frac{DEP_{\rm muephonon}}{E_{\rm eff}{}^{\mathbf{DEPMUEPH0}}} \tag{312}$$
$$\frac{1}{\mu_0} = \frac{1}{\mu_{\rm CB}} + \frac{1}{\mu_{\rm PH}} \tag{313}$$

c) Mobilty of the back part:

$$\mu_{\rm leak,back} = \frac{\mu_0}{\left(1 + \left(\frac{\mu_0 E_{\rm y}}{DEP_{\rm vmax}}\right)^{\mathbf{DEPBB}}\right)^{\frac{1}{\mathbf{DEPBB}}}} \tag{314}$$
$$\tag{315}$$

where,

$$E_{\rm y} = \frac{V_{\rm ds,eff}}{L_{\rm ch}} \tag{316}$$

$$Q_{\rm iumue} = -Q_{\rm leak,back0} \tag{317}$$

$$R_{\rm ns} = \frac{Q_{\rm iumue}}{q} \tag{318}$$

$$E_{\rm eff} = \frac{Q_{\rm iumue}}{1 + (\phi_{\rm sl} - \phi_{\rm s0}) \cdot N_{\rm invde}} \tag{319}$$

$$\mu_{\rm CB} = DEP_{\rm mueback} + DEP_{\rm mueback1} \cdot \frac{R_{\rm ns}}{10^{11}} \tag{320}$$

$$\mu_{\rm PH} = \frac{DEP_{\rm muephonon}}{E_{\rm eff}^{\mathbf{DEPMUEPH0}}} \tag{321}$$

$$\frac{1}{\mu_0} = \frac{1}{\mu_{\rm CB}} + \frac{1}{\mu_{\rm PH}} \tag{322}$$

where $DEP_{\rm mue0}$, $DEP_{\rm mue0}$, $DEP_{\rm mue1}$, $DEP_{\rm mueback}$, $DEP_{\rm mueback1}$, $N_{\rm invde}$ and $DEP_{\rm vmax}$ consider the gate length dependence as

$$DEP_{\rm mue0} = \mathbf{DEPMUE0} \cdot \left(1 + \frac{\mathbf{DEPMUE0L}}{(L_{\rm gate} \cdot 10^6)^{\mathbf{DEPMUE0LP}}}\right) \tag{323}$$

$$DEP_{\rm mue1} = \mathbf{DEPMUE1} \cdot \left(1 + \frac{\mathbf{DEPMUE1L}}{(L_{\rm gate} \cdot 10^6)^{\mathbf{DEPMUE1LP}}}\right) \tag{324}$$

$$DEP_{\rm mueback} = \mathbf{DEPMUEBACK0} \cdot \left(1 + \frac{\mathbf{DEPMUEBACK0L}}{(L_{\rm gate} \cdot 10^6)^{\mathbf{DEPMUEBACK0LP}}}\right) \tag{325}$$

$$DEP_{\rm mueback1} = \mathbf{DEPMUEBACK1} \cdot \left(1 + \frac{\mathbf{DEPMUEBACK1L}}{(L_{\rm gate} \cdot 10^6)^{\mathbf{DEPMUEBACK1LP}}}\right) \tag{326}$$

$$DEP_{\rm vmax} = \mathbf{DEPVMAX} \cdot \left(1 + \frac{\mathbf{DEPVMAXL}}{(L_{\rm gate} \cdot 10^6)^{\mathbf{DEPVMAXLP}}}\right) \tag{327}$$

$$N_{\rm invde} = \mathbf{NINVD} \cdot \left(1 + \frac{\mathbf{NINVDL}}{(L_{\rm gate} \cdot 10^6)^{\mathbf{NINVDLP}}}\right) \tag{328}$$

25.3 Quasi-Fermi potential model

In the depletion mode MOSFET model, the quasi-Fermi potential($V_{\rm ds,mod}$) at the drain side is written with following equation.

$$V_{\rm ds,mod} = \frac{V_{\rm ds}}{\left[1 + \left(\frac{V_{\rm ds}}{V_{\rm ds,sat}}\right)^{\Delta}\right]^{\frac{1}{\Delta}}} \tag{329}$$

where

$$V_{\rm ds,sat} = \Bigg[V_{\rm gp} + \frac{qN_{\rm depm}\epsilon_{\rm Si}}{{C_{\rm ox}}^2}\Big\{1 - \sqrt{1 + 2\frac{{C_{\rm ox}}^2}{qN_{\rm depm}\epsilon_{\rm Si}}\Big\{V_{\rm gp} - \frac{1}{\beta} - V_{\rm bs}\Big\}}\Big\}\Bigg] \tag{330}$$

The HiSIM model parameters introduced in section 25 are summarized in Table 25.

Table 25: HiSIM model parameters introduced in section 25 of this manual.

CODEP	model flag to select the depletion model
NDEPM	impurity concentration of the surface N^- layer
NDEPML	L_{gate} dependence of impurity concentration of the surface N^- layer
NDEPMLP	L_{gate} dependence of impurity concentration of the surface N^- layer
TNDEP	thickness of the surface N^- layer
DEPMUE0	Coulomb scattering in the resistor region
DEPMUE0L	L_{gate} dependence of the Coulomb scattering in the resistor region
DEPMUE0LP	L_{gate} dependence of the Coulomb scattering in the resistor region
DEPMUE1	Coulomb scattering in the resistor region
DEPMUE1L	L_{gate} dependence of the Phonon scattering in the resistor region
DEPMUE1LP	L_{gate} dependence of the Phonon scattering in the resistor region
DEPMUEBACK0	Coulomb scattering in the back region
DEPMUEBACK0L	L_{gate} dependence of the Coulomb scattering in the back region
DEPMUEBACK0LP	L_{gate} dependence of the Coulomb scattering in the back region
DEPMUEBACK1	Coulomb scattering in the back region
DEPMUEBACK1L	L_{gate} dependence of the Phonon scattering in the back region
DEPMUEBACK1LP	L_{gate} dependence of the Phonon scattering in the back region
DEPMUEPH0	Phonon scattering in the resistor region
DEPMUEPH1	Phonon scattering in the resistor region
DEPVMAX	saturation velocity in the resistor region
DEPVMAXL	L_{gate} dependence of the saturation velocity in the resistor region
DEPVMAXLP	L_{gate} dependence of the saturation velocity in the resistor region
DEPBB	high-field-mobility degradation in the resistor region
DEPLEAK	leakage current coefficient
DEPLEAKL	L_{gate} dependence of leakage current coefficient
DEPLEAKLP	L_{gate} dependence of leakage current coefficient
DEPETA	V_{ds} dependence of the threshold voltage shift
DEPVDSEF1	effetive drain potential coefficient-1 in the resistor region
DEPVDSEF1L	L_{gate} dependence of the effetive drain potential coefficient-1
DEPVDSEF1LP	L_{gate} dependence of the effetive drain potential coefficient-1
DEPVDSEF2	effetive drain potential coefficient-2 in the resistor region
DEPVDSEF2L	L_{gate} dependence of the effetive drain potential coefficient-2
DEPVDSEF2LP	L_{gate} dependence of the effetive drain potential coefficient-2
DEPMUETMP	temperature dependence of the phonon scatering in the resistor region

26 Binning Model

The binning option is introduced to secure enough accuracy of model calculation results, even though the effects observed are not modeled yet. The binning method is the same as that used in BSIM3/4

$$\mathit{Bin\_HiSIM\_model\_parameter} = \textbf{HiSIM\_model\_parameter} + \frac{\textbf{P1}}{L_{\rm bin}} + \frac{\textbf{P2}}{W_{\rm bin}} + \frac{\textbf{P3}}{L_{\rm bin}\,W_{\rm bin}} \tag{331}$$

where **P1**, **P2**, and **P3** are model parameters for **L HiSIM_model_parameter**, **W HiSIM_model_parameter**, and **L** $\cdot$ **W HiSIM_model_parameter**, respectively, and

$$L_{\rm bin} = \left(L_{\rm gate} \cdot 10^6\right)^{\textbf{LBINN}} \tag{332}$$

$$W_{\rm bin} = \left(W_{\rm gate} \cdot 10^6\right)^{\textbf{WBINN}} \tag{333}$$

The HiSIM model parameters introduced in section 26 are summarized in Table 26.

Table 26: HiSIM model parameters introduced in section 26 of this manual.

LBINN	power of $L_{\rm drawn}$ function
WBINN	power of $W_{\rm drawn}$ function
LMAX	maximum length of $L_{\rm drawn}$ valid
LMIN	minimum length of $L_{\rm drawn}$ valid
WMAX	maximum length of $W_{\rm drawn}$ valid
WMIN	minimum length of $W_{\rm drawn}$ valid

The model parameters which are effectively binned and which should not be used for binning are summarized in Table 27.

Table 27: HiSIM model parameters to be used for the binning option.

parameter	recommended	usable	not be used
basic	**NSUBC** **VFBC**		**TOX**, **KAPPA**, **XLD** **LL**, **LLD**, **LLN**, **XWD** **WL**, **WLD**, **WLN**, **VBI**
mobility	**MUECB0** **MUECB1** **MUEPH1** **MUESR1** **VMAX**	**NINV** **NDEP**	**MUEPH0**, **MUESR0** **MUEPHL**, **MUEPLP** **MUEPHS**, **MUEPSP** **MUESRL**, **MUESLP** **MUEPHW**, **MUEPWP** **MUESRW**, **MUESWP** **VOVER**, **VOVERP** **BB**
short-channel & pocket	**NSUBP**	**SC1**, **SC2**, **SC3** **SCP1**, **SCP2**, **SCP3**	**PARL2**, **LP** **NPEXT**, **LPEXT** **SCP21**, **SCP22**, **BS1**, **BS2**
poly-depletion		**PGD1**	**PGD2**, **PGD4**
CLM		**CLM1**, **CLM2**, **CLM3**	**CLM5**, **CLM6**
QME			**QME1**, **QME2**, **QME3**
resistance			**RS**, **RD**, **RSH**, **RSHG** **RSBPB**, **RBPD**, **RBPS** **RBDB**, **RBSB**
W_{gate} depnd.		**WFC**, **WVTH0**	**NSUBPW**, **NSUBPWP**
small size		**WL2**	**WL2P**
temperature		**EG0**	**TNOM**
		BGTMP1, **BGTMP2**	**EGIG**
		VTMP, **MUETMP**	**IGTEMP2**, **IGTEMP3**
		VDIFFJ	
STI	**WSTI**, **VTHSTI** **NSTI** **SCSTI1**, **SCSTI2**		**WL1**, **WL1P**
overlap	**LOVER**, **VFBOVER** **NOVER**	**CGSO**, **CGDO**	
I_{sub}	**SUB1**	**SUB2**, **SVDS** **SVBS**, **SVGS**	**SUB1L**, **SUB1LP**, **SUB2L** **SLG**, **SVGSL**, **SVGSLP** **SVGSW**, **SVGSWP**, **SLGL** **SLGLP**, **SVBSL**, **SVBSLP**
		IPBC1, **IPBC2**	
I_{gate}	**GLEAK1**, **GLEAK2** **GLEAK3**	**GLEAK6**	**GLEAK4**, **GLEAK5** **GLEAK7**
$I_{\text{gs}}/I_{\text{gd}}$	**GLKSD1**, **GLKSD2**		**GLKSD3**
I_{gb}	**GLKB1**, **GLKB2**		
I_{GIDL}		**GIDL1**, **GIDL2**	
junction		**JS0**, **JS0SW**, **NJ**, **CISBK**	
noise	**NFTRP**, **NFALP**		**CIT**
LOD	**NSUBCSTI1** **NSUMCSTI2** **NSUBCSTI3** **NSUBPSTI1** **NSUMPSTI2** **NSUBPSTI3** **MUESTI1** **MUESTI2** **MUESTI3**		

27 Bypass Treatment

Circuit simulator provides "BYPASS" options to enhance simulation speed. To select the option automatically the model parameter **BYPTOL** is introduced as summarized in Fig. 31. The range of the parameter is

$$0 \leq \mathbf{BYPTOL} \leq 1 \tag{334}$$

where default is set to zero without bypass.

	BYPASS=0	BYPASS=1 (default)
BYPTOL=0 (default)	off	off (default)
BYPTOL≠0	off	on

Fig. 31: Summary of bypass options.

The HiSIM model parameter introduced in section 27 is summarized in Table 28.

Table 28: HiSIM model parameter introduced in section 27 of this manual.

BYPTOL	for selection of bypass option

28 Summary of Important Model Equations

28.1 Physical Quantities

$$
\begin{aligned}
C_{\rm ox} &= \epsilon_0 \frac{\mathbf{KAPPA}}{T_{\rm ox}} \\
T_{\rm ox} &= \mathbf{TOX} + \Delta T_{\rm ox} \\
\Delta T_{\rm ox} &= \frac{\mathbf{QME1}}{V_{\rm gb} - V_{\rm th}(T_{\rm ox} = \mathbf{TOX}) + \mathbf{QME2}} + \mathbf{QME3} \\
V'_{\rm G} &= V_{\rm gb} - V_{\rm FB} + \Delta V_{\rm th} \\
\beta &= \frac{q}{kT} \\
V_{\rm th} &= V_{\rm FB} + 2\Phi_{\rm B} + \frac{\sqrt{2\epsilon_{\rm Si} q N_{\rm sub}}}{C_{\rm ox}} \sqrt{2\Phi_{\rm B}} \\
2\Phi_{\rm B} &= \frac{2}{\beta} \ln\left(\frac{N_{\rm sub}}{n_{\rm i}}\right)
\end{aligned}
$$

28.2 $L_{\rm eff}$ and $W_{\rm eff}$

$$
\begin{aligned}
L_{\rm gate} &= L_{\rm drawn} + \mathbf{XL} \\
W_{\rm gate} &= \frac{W_{\rm drawn}}{\mathbf{NF}} + \mathbf{XW} \\
L_{\rm poly} &= L_{\rm gate} - 2 \times \frac{\mathbf{LL}}{(L_{\rm gate} + \mathbf{LLD})^{\mathbf{LLN}}} \\
W_{\rm poly} &= W_{\rm gate} - 2 \times \frac{\mathbf{WL}}{(W_{\rm gate} + \mathbf{WLD})^{\mathbf{WLN}}} \\
L_{\rm eff} &= L_{\rm poly} - 2 \times \mathbf{XLD} \\
W_{\rm eff} &= W_{\rm poly} - 2 \times \mathbf{XWD}
\end{aligned}
$$

28.3 Temperature Dependence

$$
E_{\rm g} = E_{\rm g,TNOM} - \mathbf{BGTMP1} \cdot (T - \mathbf{TNOM}) - \mathbf{BGTMP2} \cdot (T^2 - \mathbf{TNOM}^2)
$$

$$
E_{\rm g,TNOM} = \mathbf{EG0} - 90.25 \times 10^{-6} \cdot \mathbf{TNOM} - 1.0 \times 10^{-7} \cdot \mathbf{TNOM}^2
$$

$$
n_{\rm i} = n_{\rm i0} \cdot T^{\frac{3}{2}} \cdot \exp\left(-\frac{E_{\rm g}}{2q}\beta\right)
$$

$$
\begin{aligned}
\mu_{\rm PH}({\rm phonon}) &= \frac{M_{\rm uephonon}}{(T/\mathbf{TNOM})^{\mathbf{MUETMP}} \times E_{\rm eff}^{\mathbf{MUEPH0}}} \\
V_{\rm max} &= \frac{\mathbf{VMAX}}{1.8 + 0.4(T/\mathbf{TNOM}) + 0.1(T/\mathbf{TNOM})^2 - \mathbf{VTMP} \times (1 - T/\mathbf{TNOM})} \\
\mu_{\rm PHdep}({\rm phonon}) &= \frac{DEP_{\rm muephonon}}{(T/\mathbf{TNOM})^{\mathbf{DEPMUETMP}} \times E_{\rm eff}^{\mathbf{DEPMUEPH0}}}
\end{aligned}
$$

$$
E_{\rm gp} = E_{\rm g,TNOM} + \mathbf{EGIG} + \mathbf{IGTEMP2}\left(\frac{1}{T} - \frac{1}{\mathbf{TNOM}}\right) + \mathbf{IGTEMP3}\left(\frac{1}{T^2} - \frac{1}{\mathbf{TNOM}^2}\right)
$$

28.4 Drain Current $I_{\rm ds}$

$$
\begin{aligned}
I_{\rm ds} &= \frac{W_{\rm eff}\cdot\mathbf{NF}}{L_{\rm eff}}\cdot\mu\cdot\frac{I_{\rm dd}}{\beta}\\
I_{\rm dd} &= C_{\rm ox}(\beta V'_{\rm G}+1)(\phi_{\rm SL}-\phi_{\rm S0})-\frac{\beta}{2}C_{\rm ox}(\phi_{\rm SL}^2-\phi_{\rm S0}^2)\\
&\quad -\frac{2}{3}const0\Big[\big\{\beta(\phi_{\rm SL}-V_{\rm bs})-1\big\}^{\frac{3}{2}}-\big\{\beta(\phi_{\rm S0}-V_{\rm bs})-1\big\}^{\frac{3}{2}}\Big]\\
&\quad +const0\Big[\big\{\beta(\phi_{\rm SL}-V_{\rm bs})-1\big\}^{\frac{1}{2}}-\big\{\beta(\phi_{\rm S0}-V_{\rm bs})-1\big\}^{\frac{1}{2}}\Big]\\
const0 &= qN_{\rm sub}L_{\rm D}\sqrt{2}
\end{aligned}
$$

$$
\begin{aligned}
I_{\rm ds} &= I_{\rm ds}+\frac{W_{\rm eff}\cdot\mathbf{NF}}{L_{\rm eff}}\frac{\mu}{\beta}\cdot(\phi_{\rm SL}-\phi_{\rm S0})\\
&\cdot\left\{C_{\rm ox}\cdot\beta\frac{\mathbf{PTL}}{(L_{\rm gate}\cdot10^6)^{\mathbf{PTLP}}}\cdot(\mathbf{VBI}-\phi_{\rm S0})^{\mathbf{PTP}}\cdot\left(1+\mathbf{PT2}\cdot V_{\rm ds}+\frac{\mathbf{PT4}\cdot(\phi_{\rm S0}-V_{\rm bs})}{(L_{\rm gate}\cdot10^6)^{\mathbf{PT4P}}}\right)\right\}\\
&+\frac{W_{\rm eff}\cdot\mathbf{NF}}{L_{\rm eff}}\frac{\mu}{\beta}\cdot(\phi_{\rm SL}-\phi_{\rm S0})\cdot C_{\rm ox}\cdot\beta\frac{\mathbf{GDL}}{(L_{\rm gate}\cdot10^6+\mathbf{GDLD}\cdot10^6)^{\mathbf{GDLP}}}\cdot V_{\rm ds}
\end{aligned}
$$

28.5 Substrate Impurity Concentration $\Delta N_{\rm sub}$

$$
\begin{aligned}
N_{\rm sub} &= \frac{\mathbf{NSUBC}(L_{\rm gate}-\mathbf{LP})+N_{\rm subp}\cdot\mathbf{LP}}{L_{\rm gate}}+\frac{N_{\rm PEXT}-\mathbf{NSUBC}}{\left(\frac{1}{\mathbf{xx}}+\frac{1}{\mathbf{LPEXT}}\right)L_{\rm gate}}\\
\mathbf{xx} &= 0.5\times L_{\rm gate}-\mathbf{LP}\\
N_{\rm pext} &= \mathbf{NPEXT}\cdot\left(1+\frac{\mathbf{NPEXTW}}{(W_{\rm gate}\cdot10^6)^{\mathbf{NPEXTWP}}}\right)\\
N_{\rm sub} &= \mathbf{NSUBC}\cdot\left(1+\frac{\mathbf{NSUBCW}}{(W_{\rm gate}\cdot10^6)^{\mathbf{NSUBCWP}}}\right)\cdot\left(1+\frac{\mathbf{NSUBCW2}}{(W_{\rm gate}\cdot10^6)^{\mathbf{NSUBCWP2}}}\right)\\
N_{\rm subc} &\le \mathbf{NSUBCMAX}\\
N_{\rm subb} &= \begin{cases}2\cdot N_{\rm subp}-\frac{(N_{\rm subp}-\mathbf{NSUBC})\cdot L_{\rm gate}}{\mathbf{LP}}-\mathbf{NSUBC} & (L_{\rm gate}\le 2\cdot\mathbf{LP})\\ 0 & (L_{\rm gate}>2\cdot\mathbf{LP})\end{cases}\\
N_{\rm subp,1} &= N_{\rm subp,0}\cdot\left(1+\frac{\mathbf{NSUBPW}}{(W_{\rm gate}\cdot10^6)^{\mathbf{NSUBPWP}}}\right)\\
N_{\rm subp,0} &= \mathbf{NSUBP}\cdot\left(\frac{2\cdot(1-\mathbf{NSUBPFAC})}{\mathbf{NSUBPL}}\cdot L_{\rm gate}\cdot10^6+2\cdot\mathbf{NSUBPFAC}-1\right)
\end{aligned}
$$

28.6 Threshold Voltage Shift $\Delta V_{\rm th}$

$$
\Delta V_{\rm th} = \Delta V_{\rm th,SC}+\Delta V_{\rm th,R}+\Delta V_{\rm th,P}+\Delta V_{\rm th,W}-\phi_{\rm Spg}
$$

$$
\begin{aligned}
\Delta V_{\rm th,SC} &= \frac{\epsilon_{\rm Si}}{C_{\rm ox}}\cdot W_{\rm d}\frac{2(\mathbf{VBI}-2\Phi_{\rm B})}{(L_{\rm gate}-\mathbf{PARL2})^2}\Big(\mathbf{SC1}+\mathbf{SC2}\cdot V_{\rm ds}+\mathbf{SC3}\cdot\frac{2\Phi_{\rm B}-V_{\rm bs}}{L_{\rm gate}}\\
&\quad \mathbf{SC4}\cdot V_{\rm ds}\cdot(2\Phi_{\rm B}-V_{\rm bs})\Big)
\end{aligned}
$$

$$
W_{\rm d} = \sqrt{\frac{2\epsilon_{\rm Si}(2\Phi_{\rm B}-V_{\rm bs})}{qN_{\rm sub}}}
$$

$$\Delta V_{\mathrm{th,P}} = (V_{\mathrm{th,R}} - V_{\mathrm{th0}}) \frac{\epsilon_{\mathrm{Si}}}{C_{\mathrm{ox}}} W_{\mathrm{d}} \frac{dE_{y,\mathrm{P}}}{dy} + dqb - \frac{\mathbf{SCP22}}{(\mathbf{SCP21} + V_{\mathrm{ds}})^2}$$

$$V_{\mathrm{th,R}} = V_{\mathrm{FB}} + 2\Phi_{\mathrm{B}} + \frac{Q_{\mathrm{B0}}}{C_{\mathrm{ox}}} + \log\left(\frac{N_{\mathrm{subb}}}{\mathbf{NSUBC}}\right)$$

$$Q_{\mathrm{B0}} = \sqrt{2q \cdot N_{\mathrm{sub}} \cdot \epsilon_{Si} \cdot (2\Phi_{\mathrm{B}} - V_{\mathrm{bs}})}$$

$$V_{\mathrm{th0}} = V_{\mathrm{FB}} + 2\Phi_{\mathrm{BC}} + \frac{\sqrt{2q\mathbf{NSUBC}\epsilon_{\mathrm{Si}}(2\Phi_{\mathrm{BC}} - V_{\mathrm{bs}})}}{C_{\mathrm{ox}}}$$

$$\Phi_{\mathrm{BC}} = \frac{2}{\beta} \ln\left(\frac{\mathbf{NSUBC}}{n_{\mathrm{i}}}\right)$$

$$\Phi_{\mathrm{B}} = \frac{2}{\beta} \ln\left(\frac{N_{\mathrm{sub}}}{n_{\mathrm{i}}}\right)$$

$$\frac{dE_{y,\mathrm{P}}}{dy} = \frac{2(\mathbf{VBI} - 2\Phi_{\mathrm{B}}^{'})}{\mathbf{LP}^2} \left(\mathbf{SCP1} + \mathbf{SCP2} \cdot V_{\mathrm{ds}} + \mathbf{SCP3} \cdot \frac{2\Phi_{\mathrm{B}}^{'} - V_{\mathrm{bs}}}{\mathbf{LP}}\right)$$

$$dqb = \frac{Q_{\mathrm{B0}} - Q_{\mathrm{Bmod}}}{C_{\mathrm{ox}}}$$

$$Q_{\mathrm{Bmod}} = \sqrt{2q \cdot N_{\mathrm{sub}} \cdot \epsilon_{Si} \cdot \left(2\Phi_{\mathrm{B}} - V_{\mathrm{bs}} - \frac{\mathbf{BS1}}{\mathbf{BS2} - V_{\mathrm{bs}}}\right)}$$

$$\Delta V_{\mathrm{th,W}} = \left(\frac{1}{C_{\mathrm{ox}}} - \frac{1}{C_{\mathrm{ox}} + 2C_{\mathrm{ef}}/(L_{\mathrm{eff}} W_{\mathrm{eff}})}\right) q N_{\mathrm{sub}} W_{\mathrm{d}} + \frac{\mathbf{WVTH0}}{W_{\mathrm{gate}} \times 10^6}$$

$$C_{\mathrm{ef}} = \frac{2\mathbf{KAPPA}}{\pi} L_{\mathrm{eff}} \ln\left(\frac{2T_{\mathrm{fox}}}{T_{\mathrm{ox}}}\right) = \frac{\mathbf{WFC}}{2} L_{\mathrm{eff}}$$

$$\phi_{\mathrm{Spg}} = \mathbf{PGD1} \left(\frac{N_{\mathrm{sub}}}{\mathbf{NSUBC}}\right)^{\mathbf{PGD4}} \exp\left(\frac{V_{\mathrm{gs}} - \mathbf{PGD2}}{V}\right)$$

28.7 Mobility Model

$$\mu = \frac{\mu_0}{\left(1 + \left(\frac{\mu_0 E_{\mathrm{y}}}{V_{\mathrm{max}}}\right)^{\mathbf{BB}}\right)^{\frac{1}{\mathbf{BB}}}}$$

$$V_{\mathrm{max}} = \mathbf{VMAX} \cdot \left(1 + \frac{\mathbf{VOVER}}{(L_{\mathrm{gate}} \times 10^6)^{\mathbf{VOVERP}}}\right) \cdot \left(1 + \frac{\mathbf{VOVERS}}{wl^{\mathbf{VOVERSP}}}\right)$$

$$\frac{1}{\mu_0} = \frac{1}{\mu_{\mathrm{CB}}} + \frac{1}{\mu_{\mathrm{PH}}} + \frac{1}{\mu_{\mathrm{SR}}}$$

$$\mu_{\mathrm{CB}}(\mathrm{Coulomb}) = M_{\mathrm{Coulomb0}} + M_{\mathrm{Coulomb1}} \frac{Q_{\mathrm{i}}}{q \times 10^{11}}$$

$$M_{\mathrm{Coulomb0}} = \mathbf{MUECB0} \cdot \left(\frac{L_{\mathrm{gate}} \cdot 10^6}{1\mu m} \right)^{\mathbf{MUECB0LP}}$$

$$M_{\mathrm{Coulomb1}} = \mathbf{MUECB1} \cdot \left(\frac{L_{\mathrm{gate}} \cdot 10^6}{1\mu m} \right)^{\mathbf{MUECB1LP}}$$

$$\mu_{\mathrm{PH}}(\mathrm{phonon}) = \frac{M_{\mathrm{uephonon}}}{E_{\mathrm{eff}}^{\mathbf{MUEPH0}}}$$

$$E_{\mathrm{eff}} = \frac{1}{\epsilon_{\mathrm{Si}}} \left(N_{\mathrm{dep}} \cdot Q_{\mathrm{b}} + \mathbf{NINV} \cdot Q_{\mathrm{i}} \right) \cdot f(\phi_{\mathrm{S}})$$

$$f(\phi_{\mathrm{S}}) = \frac{1}{1 + (\phi_{\mathrm{SL}} - \phi_{\mathrm{S0}}) \cdot \mathbf{NINVD}}$$

$$N_{\mathrm{dep}} = \mathbf{NDEP} \left(\frac{(L_{\mathrm{gate}} \cdot 10^6)^{\mathbf{NDEPLP}}}{\mathbf{NDEPL} + (L_{\mathrm{gate}} \times 10^6)^{\mathbf{NDEPLP}}} \right) \cdot \left(\frac{(W_{\mathrm{gate}} \cdot 10^6)^{\mathbf{NDEPWP}}}{\mathbf{NDEPW} + (W_{\mathrm{gate}} \times 10^6)^{\mathbf{NDEPWP}}} \right)$$

$$\begin{aligned} M_{\mathrm{uephonon}} &= \mathbf{MUEPH1} \cdot \left(1 + \frac{\mathbf{MUEPHL}}{(L_{\mathrm{gate}} \cdot 10^6 + \mathbf{MUEPLD} \cdot 10^6)^{\mathbf{MUEPLP}}} \right) \\ &\quad \cdot \left(1 + \frac{\mathbf{MUEPHL2}}{(L_{\mathrm{gate}} \cdot 10^6)^{\mathbf{MUEPLP2}}} \right) \\ M_{\mathrm{uephonon}} &= M_{\mathrm{uephonon}} \times \left(1 + \frac{\mathbf{MUEPHW}}{(W_{\mathrm{gate}} \cdot 10^6 + \mathbf{MUEPWD})^{\mathbf{MUEPWP}}} \right) \\ &\quad \cdot \left(1 + \frac{\mathbf{MUEPHW2}}{(W_{\mathrm{gate}} \cdot 10^6)^{\mathbf{MUEPWP2}}} \right) \end{aligned}$$

28.8 Channel-Length Modulation

$$L_{\mathrm{ch}} = L_{\mathrm{eff}} - \Delta L$$

$$\begin{aligned} \Delta L = \frac{1}{2} \Bigg[&- \frac{1}{L_{eff}} \left(2 \frac{I_{\mathrm{dd}}}{\beta Q_{\mathrm{i}}} z + 2 \frac{N_{\mathrm{sub}}}{\epsilon_{Si}} (\phi_S(\Delta L) - \phi_{SL}) z^2 + E_0 z^2 \right) \\ &+ \sqrt{\frac{1}{L_{eff}^2} \left(2 \frac{I_{\mathrm{dd}}}{\beta Q_{\mathrm{i}}} z + 2 \frac{N_{\mathrm{sub}}}{\epsilon_{Si}} (\phi_S(\Delta L) - \phi_{SL}) z^2 + E_0 z^2 \right)^2 - 4 \left(2 \frac{N_{\mathrm{sub}}}{\epsilon_{Si}} (\phi_S(\Delta L) - \phi_{SL}) z^2 + E_0 z^2 \right)} \Bigg] . \end{aligned}$$

$$\begin{aligned} \phi_{\mathrm{S}}(\Delta L) &= (1 - \mathbf{CLM1}) \cdot \phi_{\mathrm{SL}} + \mathbf{CLM1} \cdot (\phi_{\mathrm{S0}} + V_{\mathrm{ds}}) \\ z &= \frac{\epsilon_{Si}}{\mathbf{CLM2} \cdot Q_b + \mathbf{CLM3} \cdot Q_i} \\ E_0 &= 10^5 \end{aligned}$$

$$\Delta L = \Delta L (1 + \mathbf{CLM6} \times (L_{\mathrm{gate}} \times 10^6)^{\mathbf{CLM5}})$$

28.9 STI Effect

$$I_{\mathrm{ds,STI}} = 2 \frac{W_{\mathrm{STI}}}{L_{\mathrm{eff}} - \Delta L} \mu \frac{Q_{\mathrm{i,STI}}}{\beta} \left[1 - \exp(-\beta V_{\mathrm{ds}}) \right]$$

$$Q_{\mathrm{i,STI}} = N_{\mathrm{sub,STI}} L_{\mathrm{D,STI}} \sqrt{2} \Bigg[\exp\{-\beta(\phi_{\mathrm{S,STI}} - V_{\mathrm{bs}})\} + \beta(\phi_{\mathrm{S,STI}} - V_{\mathrm{bs}}) - 1 + \frac{n_{\mathrm{p0}}}{p_{\mathrm{p0}}} \Big\{ \exp\big(\beta(\phi_{\mathrm{S,STI}} - \phi_{\mathrm{f}})\big) - \exp\big(\beta(V_{\mathrm{bs}} - \phi_{\mathrm{f}})\big) \Big\} \Bigg]^{\frac{1}{2}} - q N_{\mathrm{sub,STI}} L_{\mathrm{D,STI}} \sqrt{2} \Bigg[\exp\{-\beta(\phi_{\mathrm{S,STI}} - V_{\mathrm{bs}})\} + \beta(\phi_{\mathrm{S,STI}} - V_{\mathrm{bs}}) - 1 \Bigg]^{\frac{1}{2}}$$

$$\begin{aligned}
V'_{\mathrm{gs,STI}} &= V_{\mathrm{gs}} - V_{\mathrm{FB}} + V_{\mathrm{thSTI}} + \Delta V_{\mathrm{th,SCSTI}} \\
V_{\mathrm{thSTI}} &= \mathbf{VTHSTI} - \mathbf{VDSTI} \cdot V_{\mathrm{ds}} \\
\Delta V_{\mathrm{th,SCSTI}} &= \frac{\epsilon_{\mathrm{Si}}}{C_{\mathrm{ox}}} \sqrt{\frac{2\epsilon_{\mathrm{Si}}(2\Phi_{\mathrm{B}} - V_{\mathrm{bs}})}{q\mathbf{NSTI}}} \frac{dE_y}{dy} \\
\frac{dE_y}{dy} &= \frac{2(\mathbf{VBI} - 2\Phi_{\mathrm{B}})}{(L_{\mathrm{gate,sm}} - \mathbf{PARL2})^2} (\mathbf{SCSTI1} + \mathbf{SCSTI2} \cdot V_{\mathrm{ds}}) \\
\phi_{\mathrm{S,STI}} &= V'_{\mathrm{gs,STI}} + \frac{\epsilon_{\mathrm{Si}} Q_{\mathrm{N,STI}}}{C'^{\,2}_{\mathrm{ox}}} \left[1 - \sqrt{1 + \frac{2C'^{\,2}_{\mathrm{ox}}}{\epsilon_{\mathrm{Si}} Q_{\mathrm{N,STI}}} \left(V'_{\mathrm{gs,STI}} - V_{\mathrm{bs}} - \frac{1}{\beta} \right)} \right] \\
Q_{\mathrm{N,STI}} &= q \cdot \mathbf{NSTI}
\end{aligned}$$

$$\begin{aligned}
Q_{\mathrm{N,STI}} &= q \cdot N_{\mathrm{STI}} \\
N_{\mathrm{STI}} &= \mathbf{NSTI} \cdot \left(1 + \frac{\mathbf{NSTIL}}{(L_{\mathrm{gate}} \cdot 10^6)^{\mathbf{NSTILP}}} \right)
\end{aligned}$$

$$\begin{aligned}
W_{\mathrm{d,STI}} &= \sqrt{\frac{2\epsilon_{\mathrm{Si}}(2\Phi_{\mathrm{B,STI}} - V_{\mathrm{bs}})}{q\mathbf{NSTI}}} \\
W_{\mathrm{STI}} &= \mathbf{WSTI} \left(1 + \frac{\mathbf{WSTIL}}{(L_{\mathrm{gate,sm}} \times 10^6)^{\mathbf{WSTILP}}} \right) \left(1 + \frac{\mathbf{WSTIW}}{(W_{\mathrm{gate}} \times 10^6)^{\mathbf{WSTIWP}}} \right)
\end{aligned}$$

$$L_{\mathrm{gate,sm}} = L_{\mathrm{gate}} + \frac{\mathbf{WL1}}{wl^{\mathbf{WL1P}}}$$

29 Exclusion of Modeled Effects and Model Flags

1. To exclude specific modeled effects, following parameter settings should be chosen:

Short-Channel Effect	**SC1** = **SC2** = **SC3** = 0
Reverse-Short-Channel Effect	**LP** = 0
Quantum-Mechanical Effect	**QME1** = **QME3** = 0
Poly-Depletion Effect	**PGD1** = **PGD2** = 0
Channel-Length Modulation	**CLM1** = 0
Narrow-Channel Effect	**WFC** = **MUEPHW** = **WL1** = 0
Small-Size Effect	**WVTH0** = **WL2** = 0

Following flags are prepared to select required model options.

2. Contact resistances $R_{\rm s}$ and $R_{\rm d}$ are included:

   CORSRD = 0: no (default)

   CORSRD = 1 & **RS**/**RD** $\neq$ 0: yes, as internal resistances of HiSIM

   CORSRD = 2 & **RD** $\neq$ 0: yes, simple analytical formulation

   CORSRD = -1 & **RS**/**RD** $\neq$ 0: yes, as external resistances of HiSIM

3. Overlap capacitance model is selected as:

   COOVLP = 1: bias dependent overlap capacitance (default)

   COOVLP = 0: constant overlap capacitance

   either given **LOVER** plus **CGSO**/**CGDO** or **LOVER** only

   COOVLP = 1: yes

   selecting a model either by defining **NOVER** value or not

4. Overlap capacitance for **COOVLP** = 1 and **NOVER** $\neq$ 0 is solved in different ways:

   COQOVSM = 0: analytically solved without inversion condition

   COQOVSM = 1: iteratively solved (default)

   COQOVSM = 2: analytically solved with inversion condition

5. Substrate current $I_{\rm sub}$ is calculated:

   COISUB = 0: no (default)

   COISUB = 1: yes

6. Gate current $I_{\rm gate}$ is calculated:

   COIIGS = 0: no (default)

   COIIGS = 1: yes

7. GIDL current $I_{\rm GIDL}$ is calculated:

   COGIDL = 0: no (default)

   COGIDL = 1: yes

8. STI leakage current $I_{\rm ds,STI}$ is calculated:

   COISTI = 0: no (default)

   COISTI = 1: yes

9. Lateral field induced and overlap charges/capacitances are added to intrinsic ones:

   COADOV = 0: no

   COADOV = 1: yes (default)

10. Non-quasi-static mode is invoked:

    CONQS = 0: no (default)

    CONQS = 1: yes

11. Gate-contact resistance is included (This flag can also be given as an instance parameter.):

    CORG = 0: no (default)

    CORG = 1: yes

12. Substrate resistance network is invoked (This flag can also be given as an instance parameter.):

    CORBNET = 0: no (default)

    CORBNET = 1: yes

13. $1/f$ noise is calculated:

    COFLICK = 0: no (default)

    COFLICK = 1: yes

14. Thermal noise is calculated:

    COTHRML = 0: no (default)

    COTHRML = 1: yes

15. Induced gate and cross correlation noise are calculated:

    COIGN = 0 $\|$ **COTHRML** = 0: no (default)

    COIGN = 1 & **COTHRML** = 1: yes

16. Previous Ids is used as an initial value for calculating source/drain resistance effect ($R_{\rm s}$ and/or $R_{\rm d} \neq 0$):

    COIPRV = 0: no

    COIPRV = 1: yes (default)

17. Previous $\phi_{\rm S}$ is used as an initial value for the iteration:

    COPPRV = 0: no

    COPPRV = 1: yes (default)

18. Parameter variations for the DFM support are considered:

    CODFM = 0: no (default)

    CODFM = 1: yes

19. Accurate calculation of the capacitance reciprocity is performed:

    CORECIP = 0: no

    CORECIP = 1: yes (default)

20. Lateral-Field-Induced Charge is considered:

    COQY = 0: no (default)

    COQY = 1: yes

21. Selection for the depletion mode model:

CODEP = 0: conventional MOSFET model (default).

CODEP = 1: depletion mode MOSFET model.

22. Selection for the $V_{\mathrm{ds,eff}}$ model:

CODDLT = 0: previous $V_{\mathrm{ds,sat}}$ model.

CODDLT = 1: new $V_{\mathrm{ds,sat}}$ model (default).

30 Summary of Model Parameters and Physical Values

(* indicates minor parameters, and ** indicates minor parameters for special cases.)

Basic Device Parameters

TOX	physical oxide thickness
XL	difference between real and drawn gate length
XW	difference between real and drawn gate width
XLD	gate-overlap length
XWD	gate-overlap width
TPOLY	height of the gate poly-Si for fringing capacitance
LL	coefficient of gate length modification
LLD	coefficient of gate length modification
LLN	coefficient of gate length modification
WL	coefficient of gate width modification
WLD	coefficient of gate width modification
WLN	coefficient of gate width modification
NSUBC	substrate-impurity concentration
NSUBP	maximum pocket concentration
LP	pocket penetration length
∗**NPEXT**	maximum concentration of pocket tail
∗**LPEXT**	extension length of pocket tail
VFBC	flat-band voltage
VFBCL	channel length dependence of flat-band voltage
VFBCLP	channel length dependence of flat-band voltage
VBI	built-in potential
KAPPA	dielectric constant for gate dielectric
EG0	bandgap
BGTMP1	temperature dependence of bandgap
BGTMP2	temperature dependence of bandgap
TNOM	temperature selected as a nominal temperature value

Velocity

VMAX	saturation velocity
VOVER	velocity overshoot effect
VOVERP	$L_{\rm eff}$ dependence of velocity overshoot
∗**VTMP**	temperature dependence of the saturation velocity

Quantum Mechanical Effect

QME1	$V_{\rm gs}$ dependence of quantum mechanical effect
QME2	$V_{\rm gs}$ dependence of quantum mechanical effect
QME3	minimum $T_{\rm ox}$ modification

Poly-Silicon Gate Depletion Effect

PGD1	strength of poly-depletion effect
PGD2	threshold voltage of poly-depletion effect
∗**PGD4**	$L_{\rm gate}$ dependence of poly-depletion effect

Short Channel Effect

PARL2	depletion width of channel/contact junction
SC1	magnitude of short-channel effect
SC2	V_{ds} dependence of short-channel effect
∗**SC3**	V_{bs} dependence of short-channel effect
∗**SC3VBS**	for diminishing of impurity gradient
∗∗ **SC4**	coupling of V_{ds} and V_{bs} dependence
SCP1	magnitude of short-channel effect due to pocket
SCP2	V_{ds} dependence of short-channel due to pocket
∗**SCP3**	V_{bs} dependence of short-channel effect due to pocket
∗**SCP21**	short-channel-effect modification for small V_{ds}
∗**SCP22**	short-channel-effect modification for small V_{ds}
∗**BS1**	body-coefficient modification by impurity profile
∗**BS2**	body-coefficient modification by impurity profile
∗**PTL**	strength of punchthrough effect
∗**PTLP**	channel-length dependence of punchthrough effect
∗**PTP**	strength of punchthrough effect
∗**PT2**	V_{ds} dependence of punchthrough effect
∗**PT4**	V_{bs} dependence of punchthrough effect
∗**PT4P**	V_{bs} dependence of punchthrough effect
∗**GDL**	strength of high-field effect
∗**GDLP**	channel-length dependence of high-field effect
∗**GDLD**	channel-length dependence of high-field effect
∗**NSUBPL**	starting channel lenght of **NSUBP** reduction
∗**NSUBPFAC**	minimum factor of reduction
∗**NSUBPDLT**	delta for smoothness of the **NSUBPFAC** model

Mobility

MUECB0	Coulomb scattering
MUECB0LP	length dependence of Coulomb scattering
MUECB1	Coulomb scattering
MUECB1LP	length dependence of Coulomb scattering
MUEPH0	phonon scattering
MUEPH1	phonon scattering
MUETMP	temperature dependence of phonon scattering
∗**MUEPHL**	length dependence of phonon mobility reduction
∗**MUEPLP**	length dependence of phonon mobility reduction
∗**MUEPLD**	length dependence of phonon mobility reduction
∗∗ **MUEPHL2**	length dependence of phonon mobility reduction
∗∗ **MUEPLP2**	length dependence of phonon mobility reduction
MUESR0	surface-roughness scattering
MUESR1	surface-roughness scattering
∗**MUESRL**	length dependence of surface roughness mobility reduction
∗**MUESLP**	length dependence of surface roughness mobility reduction
∗**MUEPHS**	mobility modification due to small size
∗**MUEPSP**	mobility modification due to small size
NDEP	depletion charge contribution on effective-electric field
∗**NDEPL**	modification of Q_B contribution for short-channel case
∗**NDEPLP**	modification of Q_B contribution for short-channel case
NINV	inversion charge contribution on effective-electric field
∗**NINVD**	reduced resistance effect for small V_{ds}
∗**NINVDL**	L_{gate} dependence of reduced resistance effect for small V_{ds}
∗**NINVDLP**	L_{gate} dependence of reduced resistance effect for small V_{ds}
BB	high-field-mobility degradation

Channel-Length Modulation

CLM1	hardness coefficient of channel/contact junction
CLM2	coefficient for Q_B contribution
CLM3	coefficient for Q_I contribution
∗**CLM4**	no more used
∗**CLM5**	effect of pocket implantation
∗**CLM6**	effect of pocket implantation

Narrow Channel Effect

WFC	threshold voltage change due to capacitance change
∗**WVTH0**	threshold voltage shift
∗∗**NSUBCW**	modification of substrate concentration for narrow width
∗∗**NSUBCWP**	modification of substrate concentration for narrow width
∗∗**NSUBCW2**	modification of substrate concentration for narrow width
∗∗**NSUBCWP2**	modification of substrate concentration for narrow width
∗∗**NSUBCMAX**	upper limit of substrate concentration for narrow width
∗**NSUBPW**	modification of pocket concentration for narrow width
∗**NSUBPWP**	modification of pocket concentration for narrow width
∗**NPEXTW**	modification of expension concentration for narrow width
∗**NPEXTWP**	modification of expension concentration for narrow width
∗**MUEPHW**	width dependence of phonon mobility reduction
∗**MUEPWP**	width dependence of phonon mobility reduction
∗**MUEPWD**	width dependence of phonon mobility reduction
∗∗**MUEPHW2**	phonon related mobility reduction
∗∗**MUEPWP2**	phonon related mobility reduction
∗**MUESRW**	change of surface roughness related mobility
∗**MUESWP**	change of surface roughness related mobility
∗**NDEPW**	modification of universal mobility for narrow width
∗**NDEPWP**	modification of universal mobility for narrow width
∗**VTHSTI**	threshold voltage shift due to STI
∗**VDSTI**	$V_{\rm ds}$ dependence of STI subthreshold
∗**SCSTI1**	the same effect as **SC1** but at STI edge
∗**SCSTI2**	the same effect as **SC2** but at STI edge
NSTI	substrate-impurity concentration at the STI edge
∗∗**NSTIL**	length dependence of STI impurity concentration
∗∗**NSTILP**	length dependence of STI impurity concentration
WSTI	width of the high-field region at STI edge
∗**WSTIL**	channel-length dependence of **WSTI**
∗**WSTILP**	channel-length dependence of **WSTI**
∗**WSTIW**	channel-width dependence of **WSTI**
∗**WSTIWP**	channel-width dependence of **WSTI**
WL1	threshold voltage shift of STI leakage due to small size effect
WL1P	threshold voltage shift of STI leakage due to small size effect
NSUCPSTI1	channel concentration change due to diffusion-region length between gate and STI
NSUBCSTI2	channel concentration change due to diffusion-region length between gate and STI
NSUBCSTI3	channel concentration change due to diffusion-region length between gate and STI
NSUBPSTI1	pocket concentration change due to diffusion-region length between gate and STI
NSUBPSTI2	pocket concentration change due to diffusion-region length between gate and STI
NSUBPSTI3	pocket concentration change due to diffusion-region length between gate and STI
MUESTI1	mobility change due to diffusion-region length between gate and STI
MUESTI2	mobility change due to diffusion-region length between gate and STI
MUESTI3	mobility change due to diffusion-region length between gate and STI
SAREF	reference length of diffusion between gate and STI
SBREF	reference length of diffusion between gate and STI

Small Size Effect

WL2	threshold voltage shift due to small size effect
WL2P	threshold voltage shift due to small size effect
∗**MUEPHS**	mobility modification due to small size
∗**MUEPSP**	mobility modification due to small size
∗**VOVERS**	modification of maximum velocity due to small size
∗**VOVERSP**	modification of maximum velocity due to small size

Substrate Current

SUB1	substrate current coefficient of magnitude
SUB1L	L_{gate} dependence **SUB1**
SUB1LP	L_{gate} dependence **SUB1**
SUB2	substrate current coefficient of exponential term
SUB2L	L_{gate} dependence of **SUB2**
SVDS	substrate current dependence on V_{ds}
SLG	substrate current dependence on L_{gate}
SLGL	substrate current dependence on L_{gate}
SLGLP	substrate current dependence on L_{gate}
SVBS	substrate current dependence on V_{bs}
SVBSL	L_{gate} dependence of **SVBS**
SVBSLP	L_{gate} dependence of **SVBS**
SVGS	substrate current dependence on V_{gs}
SVGSL	L_{gate} dependence of **SVGS**
SVGSLP	L_{gate} dependence of **SVGS**
SVGSW	W_{gate} dependence of **SVGS**
SVGSWP	W_{gate} dependence of **SVGS**

Impact-ionization induced Bulk Potential Change

IBPC1	impact-ionization induced bulk potential change
IBPC2	impact-ionization induced bulk potential change

Gate Leakage Current

GLEAK1	gate to channel current coefficient
GLEAK2	gate to channel current coefficient
GLEAK3	gate to channel current coefficient
GLEAK4	gate to channel current coefficient
∗**GLEAK5**	gate to channel current coefficient (short channel correction)
∗**GLEAK6**	gate to channel current coefficient (V_{ds} dependence correction)
∗**GLEAK7**	gate to channel current coefficient (gate length and width dependence correction)
EGIG	temperature dependence of gate leakage
IGTEMP2	temperature dependence of gate leakage
IGTEMP3	temperature dependence of gate leakage
GLKSD1	gate to source/drain current coefficient
GLKSD2	gate to source/drain current coefficient
GLKSD3	gate to source/drain current coefficient
GLKB1	gate to bulk current coefficient
GLKB2	gate to bulk current coefficient
GLKB3	flat-bans shift for gate to bulk current

GIDL Current

GIDL1	magnitude of GIDL
GIDL2	field dependence of GIDL
GIDL3	V_{ds} dependence of GIDL
∗**GIDL4**	threshold of V_{ds} dependence
∗**GIDL5**	correction of high-field contribution
∗**GIDL6**	V_{bs} dependence of GIDL
∗**GIDL7**	correction of high-field contribution

Conservation of the Symmetry at $V_{ds} = 0$ for Short-Channel MOSFETs

VZADD0	symmetry conservation coefficient
PZADD0	symmetry conservation coefficient

Smoothing coefficient between linear and saturation region

***DDLTMAX**	smoothing coefficient for V_{ds}
***DDLTSLP**	L_{gate} dependence of smoothing coefficient
***DDLTICT**	L_{gate} dependence of smoothing coefficient

Source/Bulk and Drain/Bulk Diodes

JS0	saturation current density
JS0SW	sidewall saturation current density
NJ	emission coefficient
NJSW	sidewall emission coefficient
XTI	temperature coefficient for forward current densities
XTI2	temperature coefficient for reverse current densities
DIVX	reverse current coefficient
CTEMP	temperature coefficient of reverse currents
CISB	reverse biased saturation current
CISBK	reverse biased saturation current (at low temperature)
CVB	bias dependence coefficient of **CISB**
CVBK	bias dependence coefficient of **CISB** (at low temperature)
CJ	bottom junction capacitance per unit area at zero bias
CJSW	source/drain sidewall junction cap. grading coefficient per unit length at zero bias
CJSWG	source/drain sidewall junction capacitance per unit length at zero bias
MJ	bottom junction capacitance grading coefficient
MJSW	source/drain sidewall junction capacitance grading coefficient
MJSWG	source/drain gate sidewall junction capacitance grading coefficient
PB	bottom junction build-in potential
PBSW	source/drain sidewall junction build-in potential
PBSWG	source/drain gate sidewall junction build-in potential
VDIFFJ	diode threshold voltage between source/drain and substrate
TCJBD	temperature dependence of drain-side diode capacitance
TCJBDSW	temperature dependence of drain-side diode capacitance
TCJBDSWG	temperature dependence of drain-side diode capacitance
TCJBS	temperature dependence of source-side diode capacitance
TCJBSSW	temperature dependence of source-side diode capacitance
TCJBSSWG	temperature dependence of source-side diode capacitance

1/f Noise

NFALP	contribution of the mobility fluctuation
NFTRP	ratio of trap density to attenuation coefficient
∗**CIT**	capacitance caused by the interface trapped carriers
FALPH	power of f describing deviation of 1/f

DFM Support

MPHDFM	mobility dependence on **NSUBC** due to $\mu_{\rm phonon}$

Depletion Mode Model

CODEP	model flag to select the depletion model
NDEPM	impurity concentration of the surface N^- layer
NDEPML	$L_{\rm gate}$ dependence of impurity concentration of the surface N^- layer
NDEPMLP	$L_{\rm gate}$ dependence of impurity concentration of the surface N^- layer
TNDEP	thickness of the surface N^- layer
DEPMUE0	Coulomb scattering in the resistor region
DEPMUE0L	$L_{\rm gate}$ dependence of the Coulomb scattering in the resistor region
DEPMUE0LP	$L_{\rm gate}$ dependence of the Coulomb scattering in the resistor region
DEPMUE1	Coulomb scattering in the resistor region
DEPMUE1L	$L_{\rm gate}$ dependence of the Phonon scattering in the resistor region
DEPMUE1LP	$L_{\rm gate}$ dependence of the Phonon scattering in the resistor region
DEPMUEBACK0	Coulomb scattering in the back region
DEPMUEBACK0L	$L_{\rm gate}$ dependence of the Coulomb scattering in the back region
DEPMUEBACK0LP	$L_{\rm gate}$ dependence of the Coulomb scattering in the back region
DEPMUEBACK1	Coulomb scattering in the back region
DEPMUEBACK1L	$L_{\rm gate}$ dependence of the Phonon scattering in the back region
DEPMUEBACK1LP	$L_{\rm gate}$ dependence of the Phonon scattering in the back region
DEPMUEPH0	Phonon scattering in the resistor region
DEPMUEPH1	Phonon scattering in the resistor region
DEPVMAX	saturation velocity in the resistor region
DEPVMAXL	$L_{\rm gate}$ dependence of the saturation velocity in the resistor region
DEPVMAXLP	$L_{\rm gate}$ dependence of the saturation velocity in the resistor region
DEPBB	high-field-mobility degradation in the resistor region
DEPLEAK	leakage current coefficient
DEPLEAKL	$L_{\rm gate}$ dependence of leakage current coefficient
DEPLEAKLP	$L_{\rm gate}$ dependence of leakage current coefficient
DEPETA	$V_{\rm ds}$ dependence of the threshold voltage shift
DEPVDSEF1	effetive drain potential coefficient-1 in the resistor region
DEPVDSEF1L	$L_{\rm gate}$ dependence of the effetive drain potential coefficient-1
DEPVDSEF1LP	$L_{\rm gate}$ dependence of the effetive drain potential coefficient-1
DEPVDSEF2	effetive drain potential coefficient-2 in the resistor region
DEPVDSEF2L	$L_{\rm gate}$ dependence of the effetive drain potential coefficient-2
DEPVDSEF2LP	$L_{\rm gate}$ dependence of the effetive drain potential coefficient-2
DEPMUETMP	temperature dependence of the phonon scatering in the resistor region

Non-Quasi-Static Model

DLY1	coefficient for delay due to diffusion of carriers
DLY2	coefficient for delay due to conduction of carriers
DLY3	coefficient for RC delay of bulk carriers

Capacitance

XQY	distance from drain junction to maximum electric field point
∗**XQY1**	$V_{\rm bs}$ dependence of $Q_{\rm y}$
∗**XQY2**	$L_{\rm gate}$ dependence of $Q_{\rm y}$
QYRAT	partitioning ratio of $Q_{\rm y}$ between source and drain
LOVER	overlap length
NOVER	impurity concentration in overlap region
VFBOVER	flat-band voltage in overlap region
OVSLP	coefficient for overlap capacitance
OVMAG	coefficient for overlap capacitance
CGSO	gate-to-source overlap capacitance
CGDO	gate-to-drain overlap capacitance

Parasitic Resistances

RS	source-contact resistance in LDD region
RD	drain-contact resistance in LDD region
RSH	source/drain sheet resistance
RSHG	gate sheet resistance
GBMIN	substrate resistance network
RBPB	substrate resistance network
RBPD	substrate resistance network
RBPS	substrate resistance network
RBDB	substrate resistance network
RBSB	substrate resistance network

Binning Model

LBINN	power of L_{drawn} dependence
WBINN	power of W_{drawn} dependence
LMAX	maximum length of L_{drawn} valid
LMIN	minimum length of L_{drawn} valid
WMAX	maximum length of W_{drawn} valid
WMIN	minimum length of W_{drawn} valid

Bypass Option

BYPTOL	for selection of bypass option

31 List of Model Parameters in Alphabetic Order

(* indicates minor parameters)

BB	high-field-mobility degradation
BGTMP1	temperature dependence of bandgap
BGTMP2	temperature dependence of bandgap
∗**BS1**	body-coefficient modification by impurity profile
∗**BS2**	body-coefficient modification by impurity profile
BYPTOL	for selection of bypass option
CGBO	gate-to-bulk overlap capacitance
CGDO	gate-to-drain overlap capacitance
CGSO	gate-to-source overlap capacitance
CISB	reverse biased saturation current
CISBK	reverse biased saturation current (at low temperature)
∗**CIT**	capacitance caused by the interface trapped carriers
CJ	bottom junction capacitance per unit area at zero bias
CJSW	source/drain sidewall junction cap. grading coefficient per unit length at zero bias
CJSWG	source/drain sidewall junction capacitance per unit length at zero bias
CLM1	hardness coefficient of channel/contact junction
CLM2	coefficient for $Q_{\rm B}$ contribution
CLM3	coefficient for $Q_{\rm I}$ contribution
∗**CLM4**	no more used
∗**CLM5**	effect of pocket implantation
∗**CLM6**	effect of pocket implantation
CTEMP	temperature coefficient of reverse currents
CVB	bias dependence coefficient of **CISB**
CVBK	bias dependence coefficient of **CISB** (at low temperature)
DDLTMAX	smoothing coefficient
DDLTSLP	$L_{\rm gate}$ dependence of smoothing coefficient
DDLTICT	$L_{\rm gate}$ dependence of smoothing coefficient
DIVX	reverse current coefficient
DLY1	coefficient for delay due to diffusion of carriers
DLY2	coefficient for delay due to conduction of carriers
DLY3	coefficient for RC delay of bulk carriers
EGIG	bandgap of gate current
EG0	bandgap
FALPH	power of f describing deviation of $1/f$
∗**GDL**	strength of high-field effect
∗**GDLP**	channel-length dependence of high-field effect
∗**GDLD**	channel-length dependence of high-field effect
GIDL1	magnitude of GIDL
GIDL2	field dependence of GIDL
GIDL3	$V_{\rm ds}$ dependence of GIDL
∗**GIDL4**	threshold of $V_{\rm ds}$ dependence
∗**GIDL5**	correction of high-field contribution
∗**GIDL6**	threshold of $V_{\rm bs}$ dependence
∗**GIDL7**	correction of high-field contribution
GLEAK1	gate to channel current coefficient
GLEAK2	gate to channel current coefficient
GLEAK3	gate to channel current coefficient
GLEAK4	gate to channel current coefficient
∗**GLEAK5**	gate to channel current coefficient (short channel correction)
∗**GLEAK6**	gate to channel current coefficient ($V_{\rm ds}$ dependence correction)
∗**GLEAK7**	gate to channel current coefficient (gate length and width dependence correction)

GLKB1	gate to bulk current coefficient
GLKB2	gate to bulk current coefficient
GLKB3	flat-bans shift for gate to bulk current
GLKSD1	gate to source/drain current coefficient
GLKSD2	gate to source/drain current coefficient
GLKSD3	gate to source/drain current coefficient
IBPC1	impact-ionization induced bulk potential change
IBPC2	impact-ionization induced bulk potential change
IGTEMP2	temperature dependence of gate current
IGTEMP3	temperature dependence of gate current
JS0	saturation current density
JS0SW	sidewall saturation current density
KAPPA	dielectric constant for gate oxide
LBINN	power of L_{drawn} dependence
LL	coefficient of gate length modification
LLD	coefficient of gate length modification
LLN	coefficient of gate length modification
LMAX	maximum length of L_{drawn} valid
LMIN	minimum length of L_{drawn} valid
LOVER	overlap length
LP	pocket penetration length
∗**LPEXT**	extension length of pocket tail
MJ	bottom junction capacitance grading coefficient
MJSW	source/drain sidewall junction capacitance grading coefficient
MJSWG	source/drain gate sidewall junction capacitance grading coefficient
MPHDFM	N_{sub} dependence of μ_{phonon}
MUECB0	Coulomb scattering
MUECB0LP	length dependence of Coulomb scattering
MUECB1	Coulomb scattering
MUECB1LP	length dependence of Coulomb scattering
MUEPH0	phonon scattering
MUEPH1	phonon scattering
∗**MUEPHL**	length dependence of phonon mobility reduction
∗∗**MUEPHL2**	length dependence of phonon mobility reduction
∗**MUEPHS**	mobility modification due to small size
∗**MUEPHW**	width dependence of phonon mobility reduction
∗∗**MUEPHW2**	phonon related mobility reduction
∗**MUEPLD**	length dependence of phonon mobility reduction
∗**MUEPLP**	length dependence of phonon mobility reduction
∗∗**MUEPLP2**	length dependence of phonon mobility reduction
∗**MUEPSP**	mobility modification due to small size
∗**MUEPWD**	width dependence of phonon mobility reduction
∗**MUEPWP**	width dependence of phonon mobility reduction
∗∗**MUEPWP2**	phonon related mobility reduction
∗**MUESLP**	length dependence of surface roughness mobility reduction
MUESR0	surface-roughness scattering
MUESR1	surface-roughness scattering
∗**MUESRL**	length dependence of surface roughness mobility reduction
∗**MUESRW**	change of surface roughness related mobility
MUESTI1	mobility change due to diffusion-region length between gate and STI
MUESTI2	mobility change due to diffusion-region length between gate and STI
MUESTI3	mobility change due to diffusion-region length between gate and STI
∗**MUESWP**	change of surface roughness related mobility
MUETMP	temperature dependence of phonon scattering

NDEP	depletion charge contribution on effective-electric field
*__NDEPL__	modification of Q_B contribution for short-channel case
*__NDEPLP__	modification of Q_B contribution for short-channel case
∗__NDEPW__	modification of universal mobility for narrow width
∗__NDEPWP__	modification of universal mobility for narrow width
NFALP	contribution of the mobility fluctuation
NFTRP	ratio of trap density to attenuation coefficient
NINV	inversion charge contribution on effective-electric field
∗__NINVD__	reduced resistance effect for small V_{ds}
NJ	emission coefficient
NJSW	sidewall emission coefficient
NOVER	impurity concentration in overlap region
∗__NPEXT__	maximum concentration of pocket tail
∗__NPEXTW__	modification of expension concentration for narrow width
∗__NPEXTWP__	modification of expension concentration for narrow width
NPEXTWPE	pocket-tail concentration change due to WPE
NSTI	substrate-impurity concentration at the STI edge
**__NSTIL__	length dependence of STI impurity concentration
**__NSTILP__	length dependence of STI impurity concentration
NSUBC	substrate-impurity concentration
∗∗ **NSUBCMAX**	upper limit of substrate concentration for narrow width
NSUBCSTI1	channel concentration change due to diffusion-region length between gate and STI
NSUBCSTI2	channel concentration change due to diffusion-region length between gate and STI
NSUBCSTI3	channel concentration change due to diffusion-region length between gate and STI
∗∗ **NSUBCW**	modification of substrate concentration for narrow width
∗∗ **NSUBCW2**	modification of substrate concentration for narrow width
∗∗ **NSUBCWP**	modification of substrate concentration for narrow width
∗∗ **NSUBCWP2**	modification of substrate concentration for narrow width
NSUBCWPE	channel concentration change due to WPE
NSUBP	maximum pocket concentration
∗__NSUBPFAC__	minimum factor of reduction
∗__NSUBPDLT__	delta for smoothness of the **NSUBPFAC** model
∗__NSUBPL__	starting channel length of **NSUBP** reduction
∗__NSUBPW__	modification of pocket concentration for narrow width
NSUBPWPE	pocket concentration change due to WPE
NSUBPSTI1	pocket concentration change due to diffusion-region length between gate and STI
NSUBPSTI2	pocket concentration change due to diffusion-region length between gate and STI
NSUBPSTI3	pocket concentration change due to diffusion-region length between gate and STI
∗__NSUBPWP__	modification of pocket concentration for narrow width
OVMAG	coefficient for overlap capacitance
OVSLP	coefficient for overlap capacitance
PARL2	depletion width of channel/contact junction
PB	bottom junction build-in potential
PBSW	source/drain sidewall junction build-in potential
PBSWG	source/drain gate sidewall junction build-in potential
PGD1	strength of poly depletion
PGD2	threshold voltage of poly depletion
∗__PGD4__	L_{gate} dependence of poly depletion
∗__PT2__	V_{ds} dependence of punchthrough effect
∗__PT4__	V_{bs} dependence of punchthrough effect
∗__PT4P__	V_{bs} dependence of punchthrough effect
∗__PTL__	strength of punchthrough effect
∗__PTLP__	channel-length dependence of punchthrough effect
∗__PTP__	strength of punchthrough effect
PZADD0	symmetry conservation coefficient
QME1	V_{gs} dependence
QME2	V_{gs} dependence
QME3	minimum T_{ox} modification
QYRAT	partitioning ratio of Q_y between source and drain

RBDB	substrate resistance network
RBPB	substrate resistance network
RBPD	substrate resistance network
RBPS	substrate resistance network
RBSB	substrate resistance network
RD	drain-contact resistance in LDD region
RS	source-contact resistance in LDD region
RSH	source/drain sheet resistance
RSHG	gate sheet resistance
SAREF	reference length of diffusion between gate and STI
SBREF	reference length of diffusion between gate and STI
SC1	magnitude of short-channel effect
SC2	$V_{\rm ds}$ dependence of short-channel effect
∗**SC3**	$V_{\rm bs}$ dependence of short-channel effect
∗**SC3VBS**	for diminishing of impurity gradient
∗∗**SC4**	coupling of $V_{\rm ds}$ and $V_{\rm bs}$ dependence
SCP1	magnitude of short-channel effect due to pocket
SCP2	$V_{\rm ds}$ dependence of short-channel due to pocket
∗**SCP21**	short-channel-effect modification for small $V_{\rm ds}$
∗**SCP22**	short-channel-effect modification for small $V_{\rm ds}$
∗**SCP3**	$V_{\rm bs}$ dependence of short-channel effect due to pocket
***SCSTI1**	the same effect as **SC1** but at STI edge
***SCSTI2**	the same effect as **SC2** but at STI edge
SLG	substrate current dependence on $L_{\rm gate}$
SLGL	substrate current dependence on $L_{\rm gate}$
SLGLP	substrate current dependence on $L_{\rm gate}$
SUB1	substrate current coefficient of magnitude
SUB1L	$L_{\rm gate}$ dependence **SUB1**
SUB1LP	$L_{\rm gate}$ dependence **SUB1**
SUB2	substrate current coefficient of exponential term
SUB2L	$L_{\rm gate}$ dependence of **SUB2**
SVBS	substrate current dependence on $V_{\rm bs}$
SVBSL	$L_{\rm gate}$ dependence of **SVBS**
SVBSLP	$L_{\rm gate}$ dependence of **SVBS**
SVDS	substrate current dependence on $V_{\rm ds}$
SVGS	substrate current dependence on $V_{\rm gs}$
SVGSL	$L_{\rm gate}$ dependence of **SVGS**
SVGSLP	$L_{\rm gate}$ dependence of **SVGS**
SVGSW	$W_{\rm gate}$ dependence of **SVGS**
SVGSWP	$W_{\rm gate}$ dependence of **SVGS**
TCJBD	temperature dependence of drain-side diode capacitance
TCJBDSW	temperature dependence of drain-side diode capacitance
TCJBDSWG	temperature dependence of drain-side diode capacitance
TCJBS	temperature dependence of source-side diode capacitance
TCJBSSW	temperature dependence of source-side diode capacitance
TCJBSSWG	temperature dependence of source-side diode capacitance
TNOM	temperature selected as a nominal temperature value
TOX	physical oxide thickness
TPOLY	height of the gate poly-Si
VBI	built-in potential
VDIFFJ	diode threshold voltage between source/drain and substrate
VDSTI	$V_{\rm ds}$ dependence of STI subthreshold
VFBC	flat-band voltage
VFBCL	channel length dependence of flat-band voltage
VFBCLP	channel length dependence of flat-band voltage
VFBOVER	flat-band voltage in overlap region
VMAX	saturation velocity

VOVER	velocity overshoot effect
VOVERP	L_{eff} dependence of velocity overshoot
∗**VOVERS**	modification of maximum velocity due to small size
∗**VOVERSP**	modification of maximum velocity due to small size
∗**VTHSTI**	threshold voltage shift due to STI
∗**VTMP**	temperature dependence of the saturation velocity
VZADD0	symmetry conservation coefficient
WBINN	power of W_{drawn} dependence
WEB	modification of layout characterization factor
WEC	modification of layout characterization factor
WFC	threshold voltage change due to capacitance change
WL	coefficient of gate width modification
WL1	threshold voltage shift of STI leakage due to small size effect
WL1P	threshold voltage shift of STI leakage due to small size effect
WL2	threshold voltage shift due to small size effect
WL2P	threshold voltage shift due to small size effect
WLD	coefficient of gate width modification
WLN	coefficient of gate width modification
WLP	magnitude of small-size effect on L_{eff}
WMAX	maximum length of W_{drawn} valid
WMIN	minimum length of W_{drawn} valid
WSTI	width of the high-field region at STI edge
∗**WSTIL**	channel-length dependence of **WSTI**
∗**WSTILP**	channel-length dependence of **WSTI**
∗**WSTIW**	channel-width dependence of **WSTI**
∗**WSTIWP**	channel-width dependence of **WSTI**
∗**WVTH0**	threshold voltage shift
XL	difference between real and drawn gate length
XLD	gate-overlap length
XQY	distance from drain junction to maximum electric field point
∗**XQY1**	V_{bs} dependence of Q_{y}
∗**XQY2**	L_{gate} dependence of Q_{y}
XTI	temperature coefficient for forward current densities
XTI2	temperature coefficient for reverse current densities
XW	difference between real and drawn gate width
XWD	gate-overlap width

32 List of Instance Parameters

Partly the same instance-parameter names and their definitions as in the BSIM3/4 models are adopted for the convenience of HiSIM users. The HiSIM Research Group wishes to acknowledge the UC Berkeley BSIM Research Group for the introduction of these instance parameters.

L	gate length (L_{gate})
W	gate width (W_{gate})
	** Diode **
AD	area of drain junction
AS	area of source junction
PD	perimeter of drain junction
PS	perimeter of source junction
	** Source/Drain Resistance **
NRS	number of source squares
NRD	number of drain squares
	** Gate Resistance **
XGW	distance from the gate contact to the channel edge
XGL	offset of the gate length
NF	number of gate fingers
M	multiplication factor
NGCON	number of gate contacts
	** Substrate Network **
RBPB	substrate resistance network
RBPD	substrate resistance network
RBPS	substrate resistance network
RBDB	substrate resistance network
RBSB	substrate resistance network
	** Length of Diffusion **
SA	length of diffusion between gate and STI
SB	length of diffusion between gate and STI
SD	length of diffusion between gate and gate
	** Temperature **
TEMP	device temperature (T)
DTEMP	device temperature change
	** Design for Manufacturability **
NSUBCDFM	substrate impurity concentration
MPHDFM	substratemobility dependence of **NSUBC** due to μ_{phonon}
SCA	layout characterization factor
SCB	layout characterization factor
SCC	layout characterization factor

33 Default Parameters and Limits of the Parameter Values

The maximum and minimum limits of the model parameter are recommended values. These values may be violated in some specific cases.

parameter	unit	min	max	default	remarks
TOX	[m]			3n	
XL	[m]			0	
XW	[m]			0	
XLD	[m]	0	50n	0	
XWD	[m]	-10n	100n	0	
TPOLY	[m]			200×10^{-9}	
LL	[$\mathrm{m}^{\mathbf{LLN+1}}$]			0	
LLD	[m]			0	
LLN	[—]			0	
WL	[$\mathrm{m}^{\mathbf{WLN+1}}$]			0	
WLD	[m]			0	
WLN	[—]			0	
NSUBC	[cm^{-3}]	1×10^{16}	1×10^{19}	5×10^{17}	**CODEP**=0
	[cm^{-3}]	1×10^{16}	1×10^{19}	5×10^{16}	**CODEP**=1
NSUBP	[cm^{-3}]	1×10^{16}	1×10^{19}	1×10^{18}	**CODEP**=0
		1×10^{16}	1×10^{19}	1×10^{17}	**CODEP**=1
LP	[m]	0	300n	15n	**CODEP**=0
		0	300n	0n	**CODEP**=1
∗**NPEXT**	[cm^{-3}]	1×10^{16}	1×10^{18}	5×10^{17}	
∗**LPEXT**	[m]	1×10^{-50}	1×10^{-5}	1×10^{-50}	
VFBC	[V]	-1.2	0.0	-1.0	**CODEP**=0
		-1.2	0.8	-0.2	**CODEP**=1
VFBCL	[$\mu\mathrm{m}^{\mathbf{VFBCLP}}$]	–		0	
VFBCLP	[—]			1.0	
VBI	[V]	1.0	1.2	1.1	
KAPPA	[—]			3.9	
EG0	[eV]	1.0	1.3	1.1785	
BGTMP1	[$\mathrm{eV\,K}^{-1}$]	50μ	1000μ	90.25μ	
BGTMP2	[$\mathrm{eV\,K}^{-2}$]	-1μ	1μ	0.1μ	
TNOM	[°C]	22	32	27	
VMAX	[$\mathrm{cm\,s}^{-1}$]	0.1MEG	20MEG	10MEG	
VOVER	[cm^{VOVERP}]	0	50	0.3	
VOVERP	[—]	0	2.0	0.3	
∗**VTMP**	[$\mathrm{cm\,s}^{-1}$]	-5.0	1.0	0	
QME1	[Vm]	0	1n	0	
QME2	[V]	1.0	3.0	2.0	
QME3	[m]	0	500p	0	
PGD1	[V]	0	50m	0	
PGD2	[V]	0	0.3	0.3	
∗**PGD4**	[—]	0	3.0	0	

parameter	unit	min	max	default	remarks
PARL2	[m]	0	50n	10n	
SC1	[—]	0	20	1.0	
SC2	[V^{-1}]	0	2	0	
∗**SC3**	[$V^{-1}m$]	0	100n	0	
∗**SC3VBS**	[—]	-3	0	0	
∗∗**SC4**	[1/V]	0		0	
SCP1	[—]	0	20	1.0	
SCP2	[V^{-1}]	0	2	0	
∗**SCP3**	[$V^{-1}m$]	0	100n	0	
∗**SCP21**	[V]	0	5.0	0	
∗**SCP22**	[V^4]	0	0	0	fixed
∗**BS1**	[V^2]	-1	50m	0	
∗**BS2**	[V]	0.5	1.0	0.9	
∗**PTL**	[$V^{\mathbf{PTP}-1}m^{\mathbf{PTLP}}$]	0		0	
∗**PTLP**	[—]			1.0	
∗**PTP**	[—]	3.0	4.0	3.5	
∗**PT2**	[V^{-1}]	0		0	
∗**PT4**	[V^{-2}]	0		0	
∗**PT4P**	[—]	0		1	
∗**GDL**	[$m^{\mathbf{GDLP}}$]	0	220m	0	
∗**GDLP**	[—]			0	
∗**GDLD**	[m]			0	
∗**NSUBPL**	[m]	0.001	10.0	0.001	
∗**NSUBPFAC**	[—]	0.2	1.0	1.0	◇
∗**NSUBPDLT**	[—]	1×10^{-50}	0.1	0.01	◇
MUECB0	[$cm^2V^{-1}s^{-1}$]	100	100k	1k	
MUECB0LP	[—]	0	2	0	
MUECB1	[$cm^2V^{-1}s^{-1}$]	5	10k	100	
MUECB1LP	[—]	0	2	0	
MUEPH0	[—]	0.25	0.35	0.3	fixed
MUEPH1	[$cm^2/V/s(V/cm)^{\mathbf{MUEPH0}}$]	2k	30k	25k(nMOS),9k(pMOS)	
MUETMP	[—]	0.5	2.0	1.5	
∗**MUEPHL**	[$\mu m^{\mathbf{MUEPLP}}$]			0	
∗**MUEPLP**	[—]			1.0	
∗∗**MUEPHL2**	[$\mu m^{\mathbf{MUEPLP2}}$]			0	
∗∗**MUEPLP2**	[—]			1.0	
∗**MUEPLD**	[μm]			0	
MUESR0	[—]	1.8	2.2	2.0	
MUESR1	[$cm^2/V/s(V/cm)^{\mathbf{MUESR0}}$]	1×10^{13}	1×10^{16}	1×10^{15}	**CODEP**=0
	[$cm^2/V/s(V/cm)^{\mathbf{MUESR0}}$]	1×10^{13}	1×10^{16}	5×10^{15}	**CODEP**=1
∗**MUESRL**	[$\mu m^{\mathbf{MUESLP}}$]			0	
∗**MUESLP**	[—]			1.0	
NDEP	[—]	0	1.0	1.0	
∗**NDEPL**	[$\mu m^{\mathbf{NDEPLP}}$]			0	
∗**NDEPLP**	[—]			1.0	
NINV	[—]	0	1.0	0.5	
∗**NINVD**	[1/V]	0		0	
∗**NINVDL**	[$m^{\mathbf{NINVDLP}}$]			0	
∗**NINVDLP**	[—]			1	
BB	[—]			2.0(nMOS),1.0(pMOS)	fixed

◇ reset within the range

parameter	unit	min	max	default	remarks
WFC	[F m^{-1}]	-5.0×10^{-15}	1×10^{-6}	0	
∗**WVTH0**	[V·μm]			0	
∗∗**NSUBCW**	[μm$^{\mathbf{NSUBCWP}}$]			0	
∗∗**NSUBCWP**	[—]			1	
∗∗**NSUBCW2**	[μm$^{\mathbf{NSUBCWP2}}$]			0	
∗∗**NSUBCWP2**	[—]			1	
∗∗**NSUBCMAX**	[cm^{-3}]			5×10^{18}	
∗**NSUBPW**	[μm$^{\mathbf{NSUBPWP}}$]			0	
∗**NSUBPWP**	[—]			1.0	
∗**NPEXTW**	[—]			0	
∗**NPEXTWP**	[—]			1.0	
∗**MUEPHW**	[μm$^{\mathbf{MUEPHW}}$]			0	
∗**MUEPWP**	[—]			1.0	
∗**MUEPWD**	[μm]			0	
∗∗**MUEPHW2**	[μm$^{\mathbf{MUEPHW2}}$]			0	
∗∗**MUEPWP2**	[—]			1.0	
∗**MUESRW**	[μm$^{\mathbf{MUESRW}}$]			0	
∗**MUESWP**	[—]			1.0	
∗**NDEPW**	[—]			0	
∗**NDEPWP**	[—]			1.0	
∗**VTHSTI**	[V]			0	
∗**VDSTI**	[—]			0	
∗**SCSTI1**	[—]			0	
∗**SCSTI2**	[V^{-1}]			0	
∗**NSTI**	[cm^{-3}]	1 ×10^{16}	1×10^{19}	5×10^{17}	
∗∗**NSTIL**	[μm^{NSTILP}]			0	
∗∗**NSTILP**	[—]			1.0	
WSTI	[m]			0	
∗**WSTIL**	[μm$^{\mathbf{WSTILP}}$]			0	
∗**WSTILP**	[—]			1.0	
∗**WSTIW**	[μm$^{\mathbf{WSTIWP}}$]			0	
∗**WSTIWP**	[—]			1.0	
WL1	[μm$^{\mathbf{2WL1P+1}}$]			0	
WL1P	[—]			1.0	
NSUBCSTI1	[m]			0	
NSUBCSTI2	[—]			0	
NSUBCSTI3	[—]			1.0	
NSUBPSTI1	[m]			0	
NSUBPSTI2	[—]			0	
NSUBPSTI3	[—]			1.0	
MUESTI1	[m]			0	
MUESTI2	[—]			0	
MUESTI3	[—]			1.0	
NSUBCWPE	[cm^{-3}]			0	
NSUBPWPE	[cm^{-3}]			0	
NPEXTWPE	[cm^{-3}]			0	
WEB	[—]			0	
WEC	[—]			0	

parameter	unit	min	max	default	remarks
WL2	[V μm$^{\mathbf{2WL2P}}$]			0	
WL2P	[—]			1.0	
∗**MUEPHS**	[μm$^{\mathbf{2MUEPSP}}$]			0	
∗**MUEPSP**	[—]			1.0	
∗**VOVERS**	[—]			0	
∗**VOVERSP**	[—]			0	
CLM1	[—]	0.5	1.0	0.7	
CLM2	[—]	1.0	4.0	2.0	
CLM3	[—]	0.5	5.0	1.0	
∗**CLM5**	[—]	0	2.0	1.0	
∗**CLM6**	[μm$^{-\mathbf{CLM5}}$]	0	20.0	0	
SUB1	[V^{-1}]			10	
SUB1L	[m$^{\mathbf{2WL1P+1}}$]			2.5×10^{-3}	
SUB1LP	[—]			1.0	
SUB2	[V]			25.0	
SUB2L	[m]	0	1.0	2×10^{-6}	
SVDS	[—]			0.8	
SLG	[m]			3×10^{-8}	
SLGL	[m$^{\mathbf{SLGLP}}$]			0	
SLGLP	[—]			1.0	
SVBS	[—]			0.5	
SVBSL	[m$^{\mathbf{SVBSLP}}$]			0	
SVBSLP	[—]			1.0	
SVGS	[—]			0.8	
SVGSL	[m$^{\mathbf{SVGSLP}}$]			0	
SVGSLP	[—]			1.0	
SVGSW	[m$^{\mathbf{SVGSWP}}$]			0	
SVGSWP	[—]			1.0	
IBPC1	[VA^{-1}]	0	1.0×10^{12}	0	
IBPC2	[V^{-1}]	0	1.0×10^{12}	0	
MPHDFM	[—]	-3	3	-0.3	
SAREF	[m]			1.0×10^{-6}	
SBREF	[m]			1.0×10^{-6}	
GIDL1	[V$^{-3/2}$s^{-1}m]			2.0	
GIDL2	[V$^{-0.5}$m^{-1}]			3×10^{7}	
GIDL3	[—]			0.9	
∗**GIDL4**	[V]			0	
∗**GIDL5**	[—]			0.2	
∗**GIDL6**	[—]			0	
∗**GIDL7**	[—]			1.0	

parameter	unit	min	max	default	remarks
GLEAK1	$[V^{-3/2}s^{-1}]$			50	
GLEAK2	$[V^{-1/2}m^{-1}]$			10MEG	
GLEAK3	[—]			60×10^{-3}	
GLEAK4	$[m^{-1}]$			4.0	
∗**GLEAK5**	$[V\,m^{-1}]$			7.5×10^{3}	
∗**GLEAK6**	[V]			250×10^{-3}	
∗**GLEAK7**	$[m^2]$			1×10^{-6}	
EGIG	[V]			0.0	
IGTEMP2	[V K]			0	
IGTEMP3	$[V\,K^2]$			0	
GLKSD1	$[A\,m\,V^{-2}]$			1f	
GLKSD2	$[V^{-1}m^{-1}]$			5MEG	
GLKSD3	$[m^{-1}]$			-5MEG	
GLKB1	$[A\,V^{-2}m^{-2}]$			5×10^{-16}	
GLKB2	$[m\,V^{-1}]$			1.0	
GLKB3	[V]			0	
∗**DDLTMAX**	[—]	1	20	10	
∗**DDLTSLP**	$[\mu m^{-1}]$	0	20	10	**CODDLT**=1
	$[\mu m^{-1}]$	0	20	0	**CODDLT**=0
∗**DDLTICT**	[—]	-3	20	0	**CODDLT**=1
	[—]	-3	20	10	**CODDLT**=0
JS0	$[A\,m^{-2}]$			0.5×10^{-6}	
JS0SW	$[A\,m^{-1}]$			0	
NJ	[—]			1.0	
NJSW	[—]			1.0	
XTI	[—]			2.0	
XTI2	[—]			0	
DIVX	$[V^{-1}]$			0	
CTEMP	[—]			0	
CISB	[—]			0	
CISBK	[A]			0	
CVB	[—]	-0.1	0.2	0	
CVBK	[—]	-0.1	0.2	0	
CJ	$[F\,m^{-2}]$			5×10^{-4}	
CJSW	$[F\,m^{-1}]$			5×10^{-10}	
CJSWG	$[F\,m^{-1}]$			5×10^{-10}	
MJ	[—]			0.5	
MJSW	[—]			0.33	
MJSWG	[—]			0.33	
PB	[V]			1.0	
PBSW	[V]			1.0	
PBSWG	[V]			1.0	
VDIFFJ	[V]			0.6×10^{-3}	
TCJBD	$[K^{-1}]$			0	
TCJBDSW	$[K^{-1}]$			0	
TCJBDSWG	$[K^{-1}]$			0	
TCJBS	$[K^{-1}]$			0	
TCJBSSW	$[K^{-1}]$			0	
TCJBSSWG	$[K^{-1}]$			0	

parameter	unit	min	max	default	remarks
NFALP	[cm s]			1×10^{-19}	
NFTRP	[V^{-1}]			10G	
∗**CIT**	[F m^{-2}]			0	
FALPH	[s m^3]			1.0	
DLY1	[s]			100×10^{-12}	
DLY2	[m^2]			0.7	
DLY3	[Ω m^2]			0.8×10^{-6}	
∗**XQY**	[m]	10n	50n	10n	
∗**XQY1**	[F·$\mu m^{\mathbf{XQY2}-1}$]	0		0	
∗**XQY2**	[—]	0		2	
QYRAT	[—]			0.5	
LOVER	[m]			30n	
NOVER	[cm^{-3}]			1×10^{19}	
VFBOVER	[V]	-0.2	0.2	0	
OVSLP	[m V^{-1}]			2.1×10^{-7}	
OVMAG	[V]			0.6	
CGSO	[F m^{-1}]	0	100nm ×C_{ox}		to be set by user
CGDO	[F m^{-1}]	0	100nm ×C_{ox}		to be set by user
CGBO	[F m^{-1}]	0		0	
RS	[Ωm]	0	10m	0	
RD	[Ωm]	0	100m	0	
RSH	[V A^{-1}square]	0	200	0	
RSHG	[V A^{-1}square]	0	100	0	
GBMIN	[—]			1×10^{-12}	used in circuit sim.
RBPB	[Ω]			50	treated as instance
RBPD	[Ω]			50	treated as instance
RBPS	[Ω]			50	treated as instance
RBDB	[Ω]			50	treated as instance
RBSB	[Ω]			50	treated as instance
VZADD0	[V]			20m	
PZADD0	[V]			20m	
LBINN	[-]			1	
WBINN	[-]			1	
LMAX	[μm]				
LMIN	[μm]				
WMAX	[μm]				
WMIN	[μm]				
BYPTOL	[-]	0	1	0	

parameter	unit	min	max	default	remarks
NDEPM	[cm^{-3}]	5×10^{15}	2×10^{17}	1×10^{17}	**CODEP**=1
NDEPML	[$m^{\mathbf{NDEPMLP}}$]			0	**CODEP**=1
NDEPMLP	[—]			1	**CODEP**=1
TNDEP	[m]	100n	1000n	200n	**CODEP**=1
DEPMUE0	[$\mathrm{cm}^2\mathrm{V}^{-1}\mathrm{s}^{-1}$]			1K	**CODEP**=1
DEPMUE0L	[$m^{\mathbf{DEPMUE0LP}}$]			0	**CODEP**=1
DEPMUE0LP	[—]			1	**CODEP**=1
DEPMUE1	[$\mathrm{cm}^2\mathrm{V}^{-1}\mathrm{s}^{-1}$]			0	**CODEP**=1
DEPMUE1L	[$m^{\mathbf{DEPMUE1LP}}$]			0	**CODEP**=1
DEPMUE1LP	[—]			1	**CODEP**=1
DEPMUEBACK0	[$\mathrm{cm}^2\mathrm{V}^{-1}\mathrm{s}^{-1}$]			100	**CODEP**=1
DEPMUEBACK0L	[$m^{\mathbf{DEPMUEBACK0LP}}$]			0	**CODEP**=1
DEPMUEBACK0LP	[—]			1	**CODEP**=1
DEPMUEBACK1	[$\mathrm{cm}^2\mathrm{V}^{-1}\mathrm{s}^{-1}$]			0	**CODEP**=1
DEPMUEBACK1L	[$m^{\mathbf{DEPMUEBACK1LP}}$]			0	**CODEP**=1
DEPMUEBACK1LP	[—]			1	**CODEP**=1
DEPMUEPH0	[—]			0.3	**CODEP**=1
DEPMUEPH1	[—]	1	1.0e5	5e3	**CODEP**=1
DEPVMAX	[$\mathrm{cm}\,\mathrm{s}^{-1}$]			3e7	**CODEP**=1
DEPVMAXL	[$m^{\mathbf{DEPLEAKLP}}$]			0	**CODEP**=1
DEPVMAXLP	[—]			1	**CODEP**=1
DEPLEAK	[—]			0.5	**CODEP**=1
DEPLEAKL	[$m^{\mathbf{DEPLEAKLP}}$]			0	**CODEP**=1
DEPLEAKLP	[—]			1	**CODEP**=1
DEPETA	[V^{-1}]			0	**CODEP**=1
DEPBB	[—]			1	**CODEP**=1
DEPVDSEF1	[V]			2.0	**CODEP**=1
DEPVDSEF1L	[$m^{\mathbf{DEPVDSEF1LP}}$]			0	**CODEP**=1
DEPVDSEF1LP	[—]			1	**CODEP**=1
DEPVDSEF2	[—]	0.1	2.0	0.5	**CODEP**=1
DEPVDSEF2L	[$m^{\mathbf{DEPVDSEF1LP}}$]			0	**CODEP**=1
DEPVDSEF2LP	[—]			1	**CODEP**=1
DEPMUETMP	[—]			1.5	**CODEP**=1

34 Default Instance Parameters and Limits of these Values

The maximum and minimum limits of the instance parameters are recommended values. These values may be violated in individual cases.

parameter	unit	min	max	default	remarks
L	[m]			5μ	
W	[m]			5μ	
AD	[m^2]			0	
AS	[m^2]			0	
PD	[m]			0	
PS	[m]			0	
NRS	[m]			0	
NRD	[m]			0	
XGW	[m]			0	
XGL	[m]			0	
NF	[—]			1	
NGCON	[m]			1	
SA	[m]			0	
SB	[m]			0	
SD	[m]			0	
TEMP	[°C]			27	
DTEMP	[°C]			0	
RBPB	[Ω]			50	treated also as a model parameter
RBPD	[Ω]			50	treated also as a model parameter
RBPS	[Ω]			50	treated also as a model parameter
RBDB	[Ω]			50	treated also as a model parameter
RBSB	[Ω]			50	treated also as a model parameter
NSUBCDFM	[cm^{-3}]	1.0×10^{16}	1.0×10^{19}		
SCA	[—]			0	
SCB	[—]			0	
SCC	[—]			0	

35 Overview of the Parameter-Extraction Procedure

In HiSIM, device characteristics are strongly dependent on basic device parameter values, such as the impurity concentration and the oxide thickness. Therefore, the parameter-value extraction has to be repeated with measured characteristics of different devices in a specific sequence until extracted parameter values reproduce all device characteristics consistently and reliably. To achieve reliable results, it is recommended to start with initial parameter values according to the recommendations listed in the table below. Since some of the model parameters such as T_{ox} are difficult to extract, they are expected to be determined directly by dedicated measurements. Threshold voltage measurements allow to derive a rough extraction for the model parameters referred to as "basic device parameters". The parameters identified with the symbol "*" in the Model Parameter Table are initially fixed to zero.

Determined by dedicated measurements (not changed during extraction procedure)	Default values listed in the section 33 are used initially for the groups of parameters listed below
TOX	basic device parameters (not listed on left side)
XPOLYD	velocity
XDIFFD	quantum effect
LL	poly depletion effects
LLD	short channel
LLN	mobility
WL	narrow channel
WLD	small size
WLN	channel-length modulation
KAPPA	substrate current
	gate leakage
	GIDL
	source/bulk and drain/bulk diodes
	noise
	subthreshold swing
	non-quasi-static model
	overlap capacitances

The sequence of device selection for the parameter extraction is recommended in 4 steps

1. Long-Channel Devices
2. Short-Channel Devices
3. Long-Narrow Devices
4. Short-Narrow Devices

References

[1] H. C. Pao and C. T. Sah, "Effects of diffusion current on characteristics of metal-oxide (insulator)-semiconductor transistors," *Solid-State Electron.*, vol. 9, pp. 927–937, Oct. 1966.

[2] J. D. Bude, "MOSFET modeling into the ballistic regime," *Proc. SISPAD*, pp. 23–26, 2000.

[3] J. R. Brews, "A charge-sheet model of the MOSFET," *Solid-State Electron.*, vol. 21, pp. 345–355, Feb. 1978.

[4] M. Miura-Mattausch, Hans Juergen Mattausch, and T. Ezaki, "The physics and modeling of MOSFETs," World Scientific, 2008.

[5] M. Miura-Mattausch, U. Feldmann, A. Rahm, M. Bollu, and D. Savignac, "Unified complete MOSFET model for analysis of digital and analog circuits," *IEEE Trans. CAD/ICAS*, vol. 15, pp. 1–7, Jan. 1996.

[6] M. Miura-Mattausch and H. Jacobs, "Analytical model for circuit simulation with quarter micron metal oxide semiconductor field effect transistors: Subthreshold characteristics," *Jpn. J. Appl. Phys.*, vol. 29, pp. L2279–L2282, Dec. 1990.

[7] S.-Y. Oh, D. E. Ward, and R. W. Dutton, "Transient Analysis of MOS Transistors," *IEEE J. Solid-State Circ.*, vol. SC–15, pp. 636–643, Aug. 1980.

[8] Y. P. Tsividis, "Operation and Modeling of the MOS Transistor," *McGraw-Hill*, 1999.

[9] C. T. Sah, "Characteristics of the metal-oxide-semiconductor transistors," *IEEE Electron Devices*, vol. ED-11, pp. 324–345, 1964.

[10] *BSIM3, version3.0 manual*, Department of Electrical Engineering and Computer Science, University of California, Berkeley CA, 1996.

[11] *BSIM4.0.0 MOSFET Model, User's Manual*, Department of Electrical Engineering and Computer Science, University of California, Berkeley CA, 2000.

[12] P. M. Rousseau, S. W. Crowder, P. B. Griffin, and J. D. Plummer, "Arsenic deactivation enhanced diffusion and the reverse short-channel effect," *IEEE Electron Device Lett.*, vol. 18, pp. 42–44, 1997.

[13] M. Suetake, M. Miura-Mattausch, H. J. Mattausch, S. Kumashiro, N. Shigyo, S. Odanaka, and N. Nakayama, "Precise physical modeling of the reverse-short-channel effect for circuit simulation," in *Proc. SISPAD*, pp. 207–210, Sep. 1999.

[14] M. Miura-Mattausch, M. Suetake, H. J. Mattausch, S. Kumashiro, N. Shigyo, S. Odanaka, and N. Nakayama, "Physical modeling of the reverse-short-channel effect for circuit simulation," *IEEE Electron Devices*, vol. 48, pp. 2449-2452, Oct., 2001.

[15] S. Kumashiro, H. Sakamoto, and K. Takeuchi, "Modeling of channel boron distribution deep sub-0.1μm n-MOSFETs," *IEICE Trans. Electro.*, vol. E82-C, June 1999.

[16] D. Buss, "Device issues in the integration of analog/RF functions in deep submicron digital CMOS," *Tech. Digest IEDM*, pp. 423–426, 1999.

[17] D. Kitamaru, H. Ueno, K. Morikawa, M. Tanaka, M. Miura-Mattausch, H. J. Mattausch, S. Kumashiro, T. Yamaguchi, K. Yamashita, and N. Nakayama, "$V_{\rm th}$ model of pocket-implanted MOSFETs for circuit simulation," *Proc. SISPAD*, pp. 392–395, 2001.

[18] H. Ueno, D. Kitamaru, K. Morikawa, M. Tanaka, M. Miura-Mattausch, H. J. Mattausch, S. Kumashiro, T. Yamaguchi, K. Yamashita, and N. Nakayama, "Impurity-Profile-Based Threshold-Voltage Model of Pocket-Implanted MOSFETs for Circuit Simulation," *IEEE Electron Devices*, vol. 49, pp. 1783–1789, Oct 2002.

[19] M. Suetake, K. Suematsu, H. Nagakura, M. Miura-Mattausch, H. J. Mattausch, S. Kumashiro, T. Yamaguchi, S. Odanaka, and N. Nakayama, "HiSIM: A drift-diffusion-based advanced MOSFET model for circuit simulation with easy parameter extraction," *Proc. SISPAD*, pp. 261–264, 2000.

[20] F. Stern and W. E. Howard, "Properties of semiconductor surface inversion layers in the electric quantum limit," *Phys. Rev.*, vol. 163, No. 3, pp. 816–835, 1967.

[21] Z. Yu, R. W. Dutton, and R. A. Kiehl, "Circuit device modeling at the quantum level," *Proc. IWCE-6*, pp. 222–229, 1998.

[22] T. Ando, A. B. Fowler, and F. Stern, "Electronic properties of two-dimensional systems," *Rev. Modern Phys.*, vol. 54, pp. 437–621, 1982.

[23] Y. Matsumoto and Y. Uemura, "Scattering mechanism and low temperature mobility of MOS inversion layers," *Jpn. J. Appl. Phys. Suppl.*, vol. 2, Pt 2, pp. 367–370, 1974.

[24] S. Takagi, M. Iwase, and A. Toriumi, "On the universality of inversion-layer mobility in n- and p-channel MOSFETs," *Tech. Digest IEDM*, pp. 398–401, 1988.

[25] S. Matsumoto, K. Hisamitsu, M. Tanaka, H. Ueno, M. Miura-Mattausch, H. J. Mattausch, S. Kumashiro, T. Yamaguchi, S. Odanaka, and N. Nakayama, "Validity of the Mobility Universality for Scaled Metal-Oxide-Semiconductor Field-Effect Transistors down to 100nm Gate Length," *J. Appl. Phys.*, vol. 92, pp. 5228–5232, 2002.

[26] D. M. Caughey and R. E. Thomas, "Carrier mobilities in Silicon empirically related to doping and field," *Proc. IEEE*, vol. 55, pp. 2192–2193, 1967.

[27] K. Joardar, K. K. Gullapalli, C. C. McAndrew, M. E. Burnham, and A. Wild, "An improved MOSFET model for circuit simulation," *IEEE Trans. Electron Devices*, vol. 45, pp. 134–148, Jan. 1998.

[28] Y. A. El-Mansy and A. R. Boothroyd, "A simple two-dimensional model of IGFET operation in the saturation region," *IEEE Trans. Electron Devices*, vol. ED-24, pp. 241–253, 1977.

[29] D. Navarro, T. Mizoguchi, M. Suetake, K. Hisamitsu, H. Ueno, M. Miura-Mattausch, H. J. Mattausch, S. Kumashiro, T. Yamaguchi, K. Yamashita, and N. Nakayama, "A compact model of the pinch-off region of 100nm MOSFETs based on the surface potential," *IEICE Trans. Electron.*, vol. E88-C, No. 5, pp. 1079-1086, 2005.

[30] G. Scott, J. Lutze, M. Rubin, F. Nouri, and M. Manley, "NMOS drive current reduction caused by transistor layout and trench isolation induced stress," *Tech. Digest IEDM*, pp. 827–830, 1999.

[31] M. Miura-Mattausch, "Analytical MOSFET model for quarter micron technologies," *IEEE Trans. CAD/ICAS*, vol. 13, pp. 610–615, 1994.

[32] *BSIM4.6.0 MOSFET Model, User's Manual*, Department of Electrical Engineering and Computer Science, University of California, Berkeley CA, 2006.

[33] F. H. Gaensslen and R. C. Jaeger, "Temperature dependent threshold behavior of depletion mode MOSFETs." *Solid-State Electron.*, vol. 22, pp. 423–430, 1979.

[34] D. Navarro, K. Hisamitsu, T. Yamaoka, M. Tanaka, H. Kawano, H. Ueno, M. Miura-Mattausch, H. J. Mattausch, S. Kumashiro, T. Yamaguchi, K. Yamashita, and N. Nakayama, "Circuit-Simulation Model of Gate-Drain- Capacitance Changes in Small-Size MOSFETs Due to High Channel-Field Gradients," Proc. SISPAD, pp. 51-54, 2002.

[35] B. J. Sheu and P.-K. Ko, "Measurement and modeling of short-channel MOS transistor gate capacitances," *IEEE J. Solid-State Circuits*, vol. SC-22, pp. 464–472, 1987.

[36] R. Shrivastava and K. Fitzpatrik, "A simple model for the overlap capacitance of a VLSI MOS device," *Proc. IEEE*, vol. ED-29, pp. 1870–1875, 1982.

[37] N. Arora, "MOSFET models for VLSI circuit simulation: theory and practice," *Springer-Verlag*, 1993.

[38] E. O. Kane, "Zener Tunneling in Semiconductors," *J. Phys. Chem. Solids*, vol. 12, pp. 181–188, 1959.

[39] Q. Ngo, D. Navarro, T. Mizoguchi, S. Hosokawa, H. Ueno, M. Miura-Mattausch, and C. Y. Yang, "Gate Current Partitioning in MOSFET Models for Circuit Simulation," *Proc. Modeling and Simulation of Microsystems*, vol. 1.2, pp. 322–325, 2003.

[40] R. Inagaki, K. Konno, N. Sadachika, D. Navarro, K. Machida, Q. Ngo, C. Y. Yang, T. Ezaki, H. J. Mattausch, M. Miura-Mattausch, and Y. Inoue, "A Gate–Current Model for Advanced MOSFET Technologies Implemented into HiSIM2," *Proc. Int. 3rd Workshop on Compact Modeling*, Yokohama, Jan. 2006.

[41] T. Yoshida, M. Miura-Mattausch, H. Ueno, H. J. Mattausch, S. Kumashiro, T. Yamaguchi, K. Yamashita, and N. Nakayama, "Conservation of symmetry at $V_{\rm ds} = 0$ for reliable analog simulations," to be submitted for publication.

[42] S. Matsumoto, H. Ueno, S. Hosokawa, T. Kitamura, M. Miura-Mattausch, H. J. Mattausch, T. Ohguro, S. Kumashiro, T. Yamaguchi, K. Yamashita, and N. Nakayama, "$1/f$ noise characteristics in 100nm-MOSFETs and its modeling for circuit simulation," *IEICE Trans. Electron.*, vol. E88-C, pp. 247–254, 2005.

[43] A. van der Ziel, "Noise in solid state devices and circuits," New York, John Wiley

[44] S. Hosokawa, Y. Shiraga, H. Ueno, M. Miura-Mattausch, H. J. Mattausch, T. Ohguro, S. Kumashiro, M. Taguchi, H. Masuda, and S. Miyamoto, "Origin of enhanced thermal noise for 100nm-MOSFETs," Ext. Abs. SSDM, pp. 20–22, 2003.

[45] S. Hosokawa, D. Navarro, M. Miura-Mattausch, H. J. Mattausch, T. Ohguro, T. Iizuka, M. Taguchi, S. Kumashiro, and S. Miyamoto, "Gate-length and drain-voltage dependence of thermal drain noise in advanced metal-oxide-semiconductor field-effect transistors," Appl. Phys. Lett. 87, 092104, 2005.

[46] M. Miura-Mattausch, H. Ueno, H. J. Mattausch, K. Morikawa, S. Itoh, A. Kobayashi, and H. Masuda, "100nm-MOSFET model for circuit simulation: Challenges and solutions," *IEICE Trans. Electron.*, vol. E86-C, pp. 1009–1021, 2003.

[47] T. Warabino, M. Miyake, N. Sadachika, D. Navarro, Y. Takeda, G. Suzuki, T. Ezaki, M. Miura-Mattausch, H. J. Mattausch, T. Ohguro, T. Iizuka, M. Taguchi, S. Kumashiro, and S. Miyamoto, "Analysis and compact modeling of MOSFET high-frequency noise,"Proc. SISPAD, pp. 158-161, 2006.

[48] N. Nakayama, D. Navarro, M. Tanaka, H. Ueno, M. Miura-Mattausch, H. J. Mattausch, T. Ohguro, S. Kumashiro, M. Taguchi, and S. Miyamoto, "Non-quasi-static model for MOSFET based on carrier-transit delay," *Electronics Letters*, vol. 40, pp. 276–278, 2004.

[49] D. Navarro, N. Nakayama, K. Machida, Y. Takeda, H. Ueno, H. J. Mattausch, M. Miura-Mattausch, T. Ohguro, T. Iizuka, M. Taguchi, T. Kage, and S. Miyamoto,"Modeling of carrier transport dynamics at GHz-frequencies for RF circuit simulation," Proc. SISPAD, pp. 259-262, 2004.

[50] D. Navarro, Y. Takeda, M. Miyake, N. Nakayama, K. Machida, T. Ezaki, H. J. Mattausch, M. Miura-Mattausch, "A carrier-tansit-delay-based non-quasi-static MOSFET model for circuit simulation and its application to harmonic distortion analysis," IEEE T. Electron Devices, vol. 53, pp. 2025–2034, 2006.

[51] D. Navarro, Y. Takeda, M. Miura-Mattausch, H. J. Mattausch, T. Ohguro, T. Iizuka, M. Taguchi, T. Kage, and S. Miyamoto,"On the validity of conventional MOSFET nonlinearity characterization at RF switching," IEEE Microwave and Wireless Components Lett., pp. 125-127, 2006.

[52] K. Machida, D. Navarro, M. Miyake, R. Inagaki, N. Sadachika, G. Suzuki, Y. Takeda, T. Ezaki, H. J. Mattausch, M. Miura-Mattausch, "Efficient NQS MOSFET Model for both Time-Domain and Frequency-Domain Analysis," Proc. SiRF, pp. 73-76, 2006.